A Micro Surgical Instrument for Age Related Macular Degeneration

By:

Aashini Gulati

Student Number: 4046587

Supervisor: Prof. Dr. Ir. R. Dekker (Philips Research Eindhoven/TU Delft)

MSc Thesis Report: Electrical Engineering (Microelectronics)

Delft University of Technology

Philips Research Eindhoven

August, 2011

Abstract

Age-Related Macular Degeneration (AMD) is a degenerative condition of the macula, which results in a loss of vision. AMD is a common contributor to vision loss in adults over the age of 50. In Western countries, AMD affects nearly 30% of the individuals over the age of 75. In the Rotterdam Eye Hospital an experimental surgical procedure has been developed to treat patients suffering from this disease. However there are still various problems associated with this procedure, some of which are related to the manipulation of delicate tissue grafts. This thesis presents an instrument prototype, to be used in this surgical procedure, which would overcome these shortcomings.

The working principle of the instrument presented is the "Indirect Heat Induced Attachment and Detachment (HIAD)" principle which has been developed at the BioMedical Engineering Department, at the Faculty of 3mE, TU Delft. It is a heat based principle in which short heat pulses are used to attach/detach a tissue graft during the surgical procedure.

During the course of this thesis, the feasibility of a micro machined device (based on the HIAD Principle) is tested. Numerical simulations have been used to understand what happens when heat pulses are given by a heater placed on the instrument to penetrate into the tissue. Tissue damage due to heat is a major concern and is studied in further detail through these simulations.

A prototype of the instrument is fabricated using a modified Flex-to-Rigid (F2R) foil technology. Polymer foils fabricated by the F2R technology are extremely thin and hence require reinforcement to be suitable to handle the tissue grafts. Two methods to provide reinforcement are suggested: inclusion of polyimide beams in various patterns and free standing silicon beams inside polyimide columns. The idea of having polyimide beams to reinforce the foils has been successfully demonstrated by fabricating a number of samples. Tests have been done to verify the effectiveness of this method. The idea of including silicon beams inside the polyimide beams could not be realized successfully. Suggestions are given as to how this can be proceeded with.

Table of Contents

Chapter 1: Introduction

Age-Related Macular Degeneration (AMD) is a degenerative condition of the macula, which results in a loss of vision. AMD is a common contributor to vision loss in adults over the age of 50. In Western countries, AMD affects nearly 30% of the individuals over the age of 75. There are a number of contributing factors to AMD, including age, quality of nutrition, sunlight exposure, smoking and genetics. It is a direct consequence of the growth of new blood vessels in or around the macula**.** In the Rotterdam Eye Hospital an experimental surgical procedure has been developed to cure patients suffering from this disease. However there are still various problems associated with it. During the tenure of this thesis, it was aimed to make a prototype of an instrument to be used in this surgical procedure, which would overcome these shortcomings.

1.1 The Human Eye:

The structure of the human eye is shown in Fig. 1.1 (a).

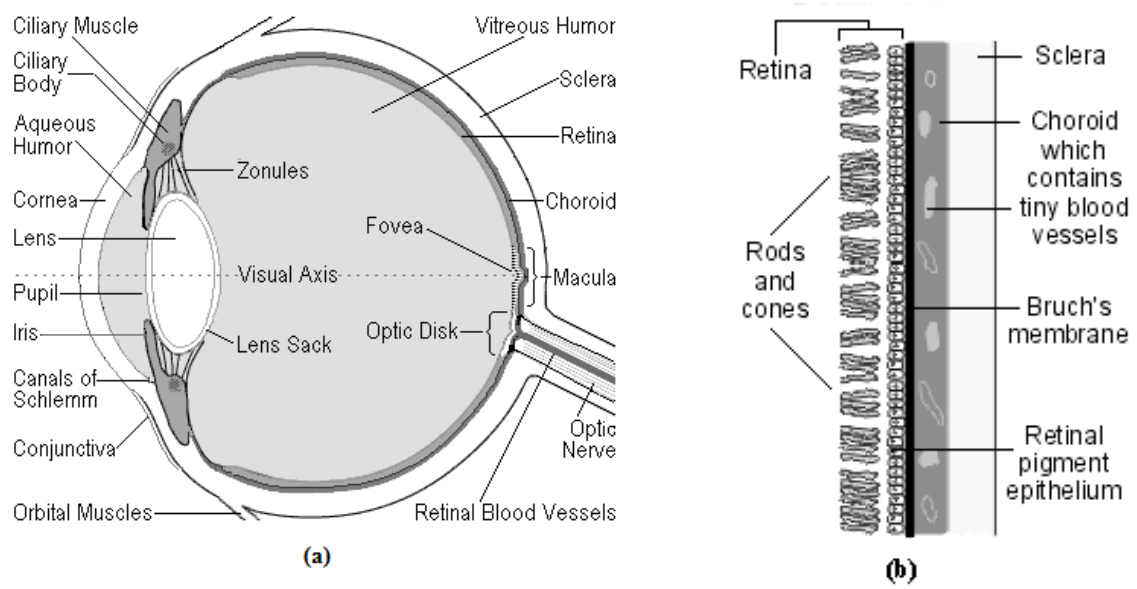

Figure 1.1: (a) Structure of the human eye (b) Structure of the macula

The retina is made up of two main layers (Fig. 1.1b). There is an inner layer of 'seeing cells' called rods and cones. These cells react to light and send electrical signals down tiny nerve fibres (which collect into the optic nerve) to the brain. The outer layer, the retinal pigment epithelium (RPE), is a layer of cells behind the rods and cones. The RPE is an insulating layer between the retina and the choroid (the layer of tissue behind the retina containing

many blood vessels). These cells help to nourish and support the rods and cones. They pass nutrients from the blood vessels in the choroid to the rods and cones. They also take waste materials from the rods and cones to the blood vessels in the choroid. The RPE can be thought of as a filter, determining what substances reach the retina. Many components of the blood are harmful to the retina and are kept away from it by a normally functioning RPE. The rods and cones are responsible for vision under different conditions. The cone cells ('cones') help us to see in the daylight, providing the basis for colour vision. The rod cells ('rods') help us to see in the dark, enabling night vision.

The macula is a small but vital area of the retina at the back of the eye (Fig. 1.1 (b)). It is about 5 mm in diameter. It is the part of the retina that is the most densely packed with rods and cones. The macula is essential for central vision. In the middle of the macula, there exists the fovea. It is an indentation in the center of the macula with a diameter of 1.5mm. This small part of the retina is responsible for our highest visual acuity and is the center of our central vision. Only cones are present here. These help to take oxygen and nutrients to the retina. Bruch's membrane is a thin membrane which helps to form a barrier between the choroid and the delicate retina. The sclera is the outer thick, white layer of the eye. When one looks at an object, light from the object passes through the cornea, then the lens, and then hits the retina at the back of the eye. The light from the object focuses on the macula. A healthy macula is essential for a detailed central vision.

1.2 Age-Related Macular Degeneration:

Age-Related Macular Degeneration (AMD) is a degenerative condition of the macula, which results in a loss of vision. Figure 1.2 shows the difference between normal vision and the typical vision of a person suffering from AMD. AMD is a common contributor to vision loss in adults over the age of 50. In Western countries, AMD affects nearly 30% of individuals over the age of 75. There are a number of contributing factors to AMD, including age, quality of nutrition, sunlight exposure, smoking and genetics. It is a direct consequence of the growth of new blood vessels behind the retina, under the macula. These new blood vessels tend to be very fragile and often leak blood and fluid. The blood and fluid raise the macula from its normal place at the back of the eye. Damage to the macula occurs rapidly. The cause for the growth of extra blood vessels is a lack of oxygen in the cells in the eye. The body tries to deliver more oxygen to these cells by growing extra blood vessels. The patient may suffer from a blurred or distorted central vision (wherein objects appear to be of an unusual size or

shape), blank patches or dark spots may appear in the central vision, may have difficulty seeing details or identifying people's faces, have sensitivity to light or may be able to see inexistent lights.

Figure 1.2: Normal vision vs. typical vision of a patient suffering from AMD

In the Rotterdam Eye Hospital a promising experimental surgical treatment to restore the patient's vision has been developed. This procedure is called a "Free RPE-Choroid Graft Translocation" and involves transplanting a vulnerable healthy tissue graft from a donor location in the eye to the diseased location. It is vital that the very thin and fragile tissue graft is not damaged during this procedure.

1.3 Free RPE-Choroid Graft Translocation:

The "free RPE-Choroid Graft Translocation" is schematically represented Fig. 1.3 [1, 2]:

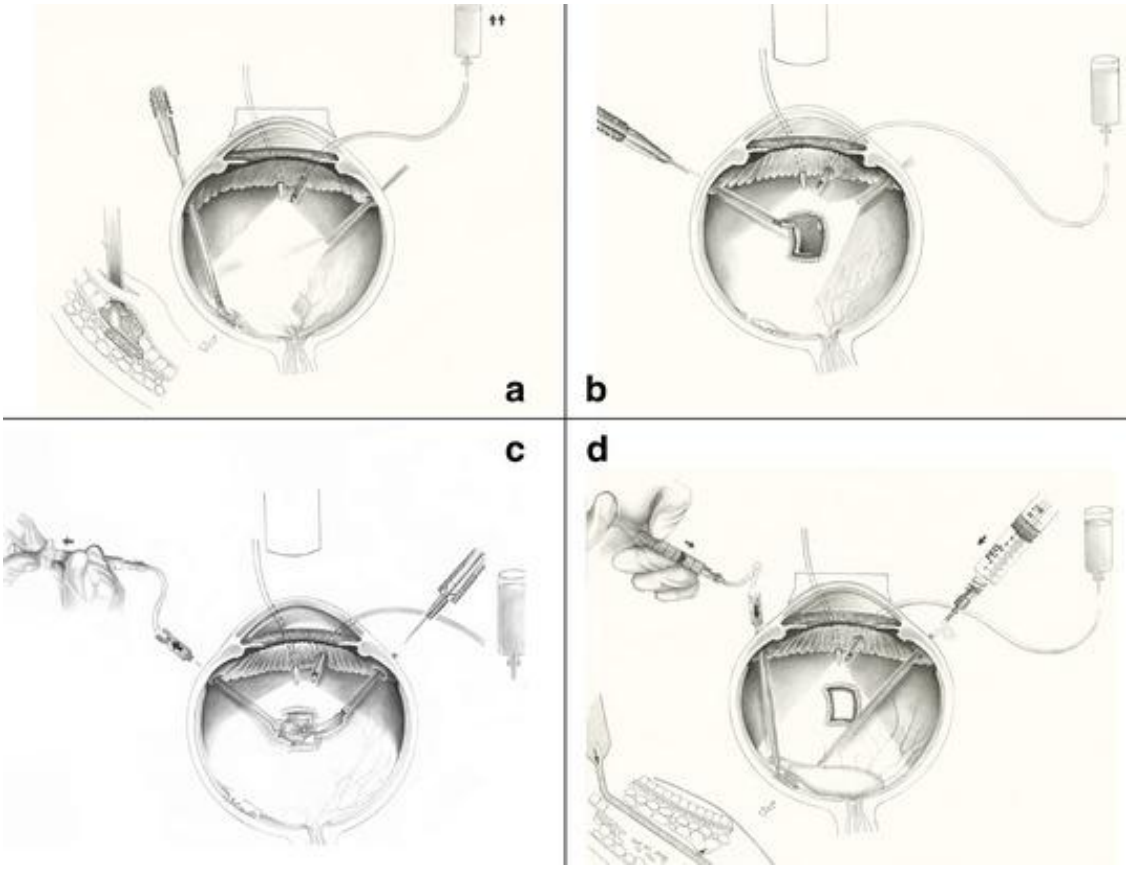

Figure 1.3: (a) Removal of CNV affected tissue (b) Cutting the patch (c) Loading the patch on the instrument (d) Placement of the patch under the fovea [2]

During the procedure, the patient is fully anesthetized. Small, minimally invasive instruments and a light source are inserted through incisions in the anterior sclera (Fig. 1.1. (a)). The vitreous is replaced with silicone oil to keep the eyeball's shape and create enough workspace. A small incision is made in the retina at about 5.5 mm from the macula to remove the CNV (Choroidal Neo Vascularization) affected tissue behind the macula (Fig. 1.3 (a)). Next, a diathermia tool is used to coagulate the choroidal vessels of approximately 5 x 6 mm square in the mid periphery of the retina (Fig. 1.3 (b)). From within these diathermia boundaries, a 3 x 3 mm patch is cut from the retina with a pair of scissors. The patch is loaded on a spatula or forceps before the retina is removed from the patch (Fig. 1.3 (c)). The 3 x 3 mm patch without the retina, consisting of the RPE layer and the choroid, is placed in the sub macular region via the incision (Fig. 1.3 (d)). After the patch is placed, the silicone oil is replaced with fresh silicone oil. Finally the scleral incisions are sutured. Bleeding during the removal of CNV affected tissue is prevented by raising the intra ocular pressure from

normal 2.00- 2.67 kPa (15-20 mmHg) to 16.00-18.67 kPa (120-140 mmHg) and slowly decreasing it afterwards. During the intervention, pressure is only raised at the first sign of bleeding.

1.3.1 Problems Faced in the Procedure:

Handling the 3mm x 3mm tissue patch while transferring it from a donor location in the eye to the diseased location, without causing tissue damage, is quite a cumbersome task. The tissue graft is about 0.5mm thick and weighs a few nanograms [5, 6]. Manipulating this tissue by the current method is problematic. Two main problems occur during the procedure: patch folding and patch sticking.

Patch Folding:

The tissue patch tends to curl up once the retina is separated from it (Fig. 1.4 (d)). The folding happens in such a way that the choroid layer is on the inside, and the RPE layer is on the outside. The patch needs to be flattened manually before insertion into the sub macular space [3]. The tissue handling required, damages the RPE layer immensely (Fig. 1.4 (f)).

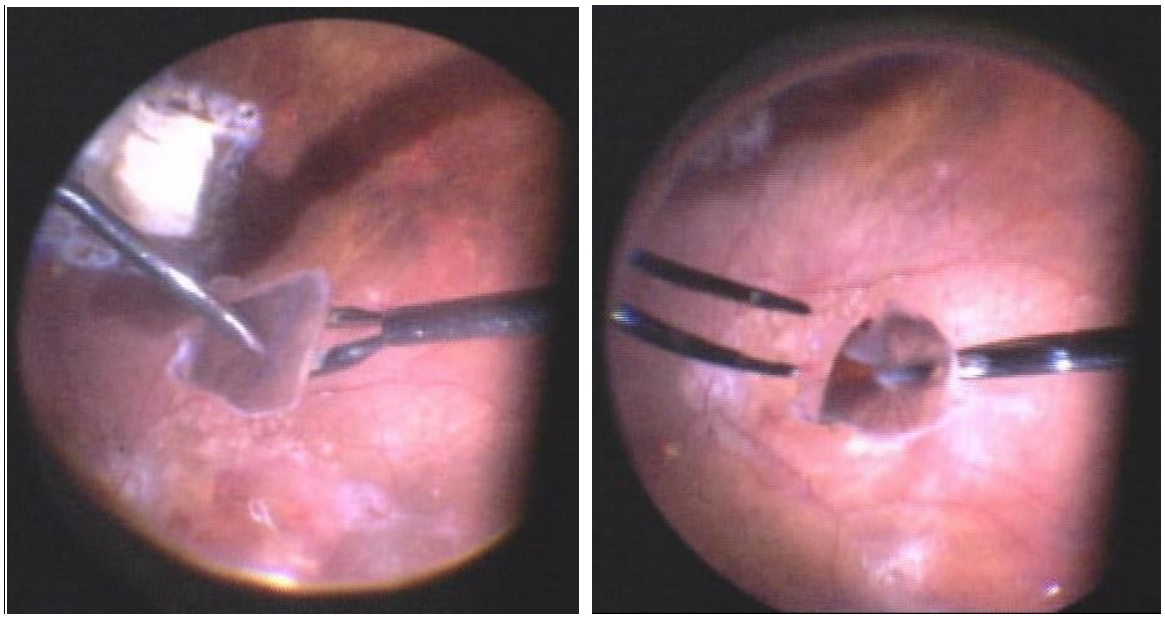

(a) **(b)**

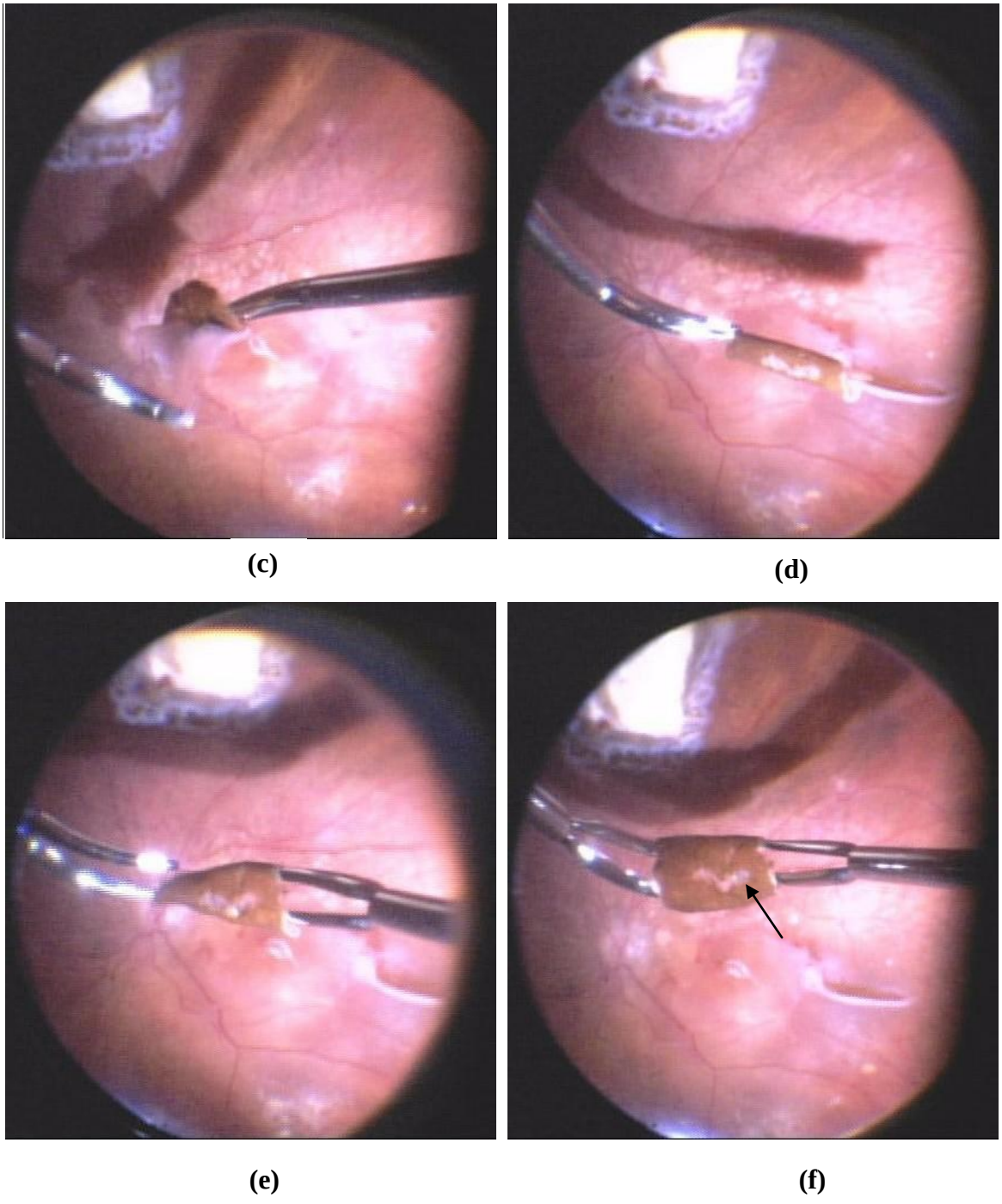

Figure 1.4: (a) A flat patch cut out (b) Flat patch squeezed in the centre by forceps for handling (c) Removal of retina (d) Immediate curling up of patch (e) Extra handling for flattening of patch (f) Damage seen as discoloured portion on the patch

Two possible causes for the patch to curl up have been suggested [1]. In the first place, the blood pressure in the parallel choroidal vessels decreases when the patch is cut. Due to the elastic properties of choroidal tissue, the patch shrinks on the choroidal side while the RPE side keeps the same volume, making the patch curl up. In the second place, the pressure drop in the vessels being cut, results in less stress in the choroidal tissue. The tissue and vessel

musculature try to compensate for the reduced stress, resulting in the patch folding due to a volume decrease on the choroidal side of the patch.

Patch Sticking:

When the instrument that is used to hold the tissue is retracted from the sub macular space, the graft tends to stick to the instrument and is folded, moved or withdrawn along with it (Fig. 1.5 (b)). As a consequence the graft needs to be flattened and reinserted into the sub macular space. Again these additional manipulations can easily damage the fragile tissue graft. The mechanism behind the sticking behavior [1] is the adhesion at atomic and molecular level between the tissue and the forceps. The choroidal side of the patch has a rough structure with loose tissue fibers that can entangle with the instrument.

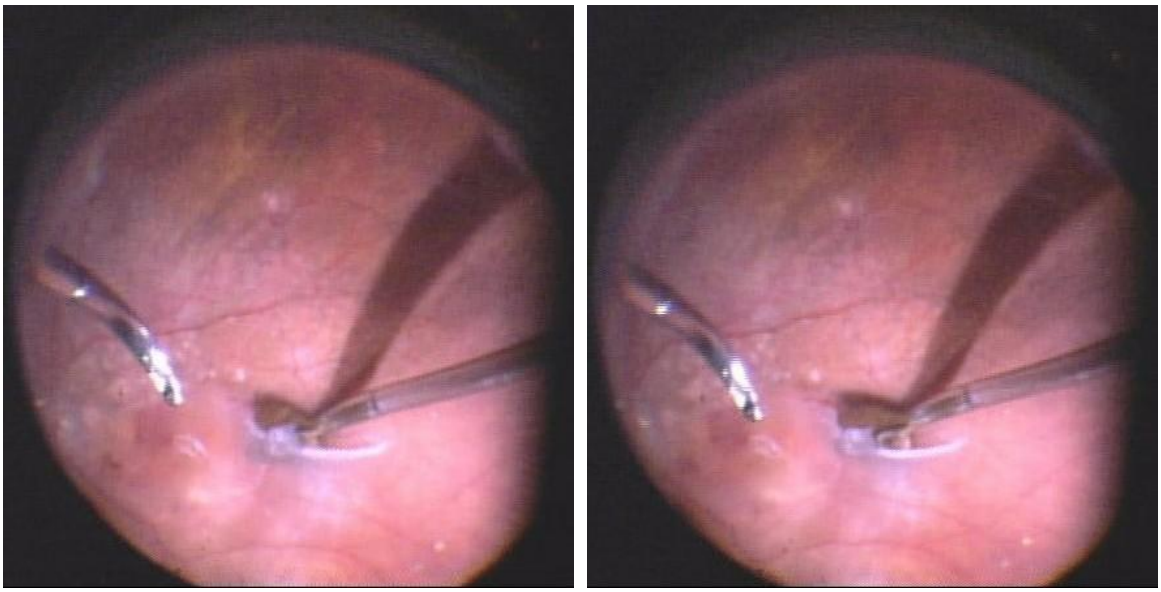

(a) **(b)**

Figure 5: (a) Insertion of the patch (b) Problematic removal of instrument [3]

Students at the Department of BioMedical Engineering, Faculty of Mechanical, Maritime and Materials Engineering at TU Delft came up with an ingenious solution to solve the problems associated with this surgery. They recommended the use of an instrument designed on the Heat Induced Attachment/ Detachment (HIAD) Principle to grasp delicate tissue instead of traditional forceps [1]. This is discussed in further detail in the next chapter. To test this principle, a resistively heated metal wire was used to successfully attach and detach tissue samples. The instrument heating properties, adhesion forces, attachment and detachment success and thermal damage were studied. However, the implementation of indirect HIAD in

a handheld ophthalmic device required major downscaling of the prototype and the electronics involved. This provided an excellent platform for the start of a new micro fabrication project. During the course of this thesis, the feasibility of a micro machined device (based on the HIAD Principle) will be tested. Tissue damage due to heat is a major concern and will be studied in further detail through thermal simulations done on a basic instrument idea. The instrument will be designed based on the requirements provided (discussed in the following chapter) and will be fabricated on true scale. The applicability and usefulness of the fabricated device will be tested.

Chapter 2: Underlying Concepts

Before the design and fabrication of the instrument prototype is explained, it is important to understand certain basic principles upon which the instrument is based.

2.1 Heat Induced Attachment and Detachment:

To improve the post-operative results for the Free RPE-Choroid Graft Translocation procedure, it is important that the damage induced to the delicate tissue graft is minimized. It is the aim of this project to achieve this by developing a specially designed surgical tool. The tissue is unfortunately so thin and fragile that any form of mechanical "grabbing" or restriction can easily damage it. However, the recently developed "Indirect Heat Induced Attachment and Detachment (HIAD)" principle at the BioMedical Engineering Department, at Faculty of 3mE, TU Delft, holds great potential to grab and release these ultra thin tissue grafts with minimal damage [1]. In experiments, a resistively heated metal wire was used to successfully attach and detach tissue samples. The heater made from the metal wire was very small resulting in a small heat capacitance. This makes it possible to quickly increase and decrease the temperature of the heater. First the heater is brought into contact with the tissue and a short heat pulse is given resulting in a surface temperature increase to 70°C. Since the temperature pulse is very short, it only affects the top surface of the tissue. This first pulse causes the tissue to attach to the heater. The attachment is probably caused by protein denaturation and is therefore dependent on tissue temperature, time for which the heat is applied and the tissue type [1]. Only a short heat pulse is required for continuous attachment, presumably since denaturation is an irreversible reorganization of protein structures. To release the tissue a second heat pulse is given resulting in a surface temperature increase to 100°C. Detachment is probably caused by vaporizing cell fluids due to quick rises in temperature and is thus dependent on heat transfer, time duration of heat application and tissue type. An "everyday" analogy of the principle can be found in the sticking behavior of meat on a barbecue. When a piece of meat is placed on a hot barbeque it initially sticks to the grid. However, when the temperature at the interface of the grid with the meat has reached such a temperature that the water starts to boil, the meat detaches itself from the cooking grid.

This principle was successfully tested (Fig. 2.1) on a piece of chicken fillet [1]. However, a real surgical instrument based on this principle has to fulfill a number of requirements which are discussed at length in the next section.

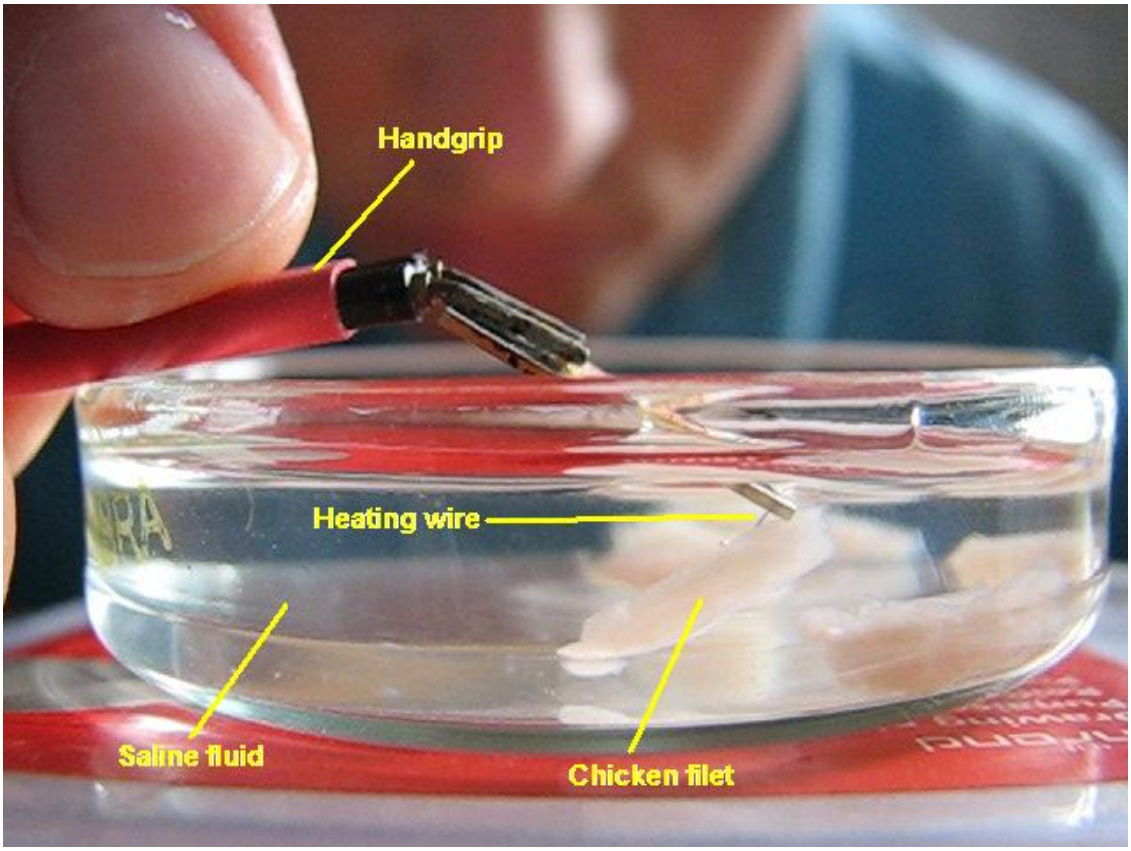

Figure 2.1: Testing the HIAD principle on chicken fillet

2.2 Design Requirements and First Design

As per the standard norms of minimally invasive eye surgeries, the instrument should have a maximum width of 0.6mm at the point of entry into the eye. Once inside, it can open up to a width of 2mm. Heater/s have to be placed to allow for tissue manipulation by applying heat pulses. It must be able to hold, support and manipulate a 3 x 3mm, fragile tissue patch. It should have a low heat capacity to allow the required temperatures for attachment and detachment to be reached with short pulses of heat, thereby minimising the heat penetration and subsequent damage due to heat. The materials used must be safe to be inserted into the eye apart from being bio compatible. The design should be such that the heat affects only the target tissue and does not bother the surrounding tissue layers. As per these requirements, it was desired for the design of the instrument to be such that there is considerable mechanical stiffness in the vertical direction while leaving it flexible enough in the horizontal plane. This would allow a folding out of the instrument once inserted into the eye but will not compromise on its structural strength. It was decided to try out a design wherein the instrument was made of polyimide foils strengthened by polyimide beams running vertically and spreading out over the surface to lend stability. Pizza plate like shapes were envisioned

where the instrument would be folded inside a tube and opened out once pushed out from it. This instrument should also be strong enough to hold the heaters. It was decided to add a minimum of 4 heaters (placed to be at the corners of the tissue patch). It is essential that the instrument be designed and fabricated such that the heaters would remain unharmed during the folding in and out mechanism. The idea of the design is depicted in Fig. 2.2.

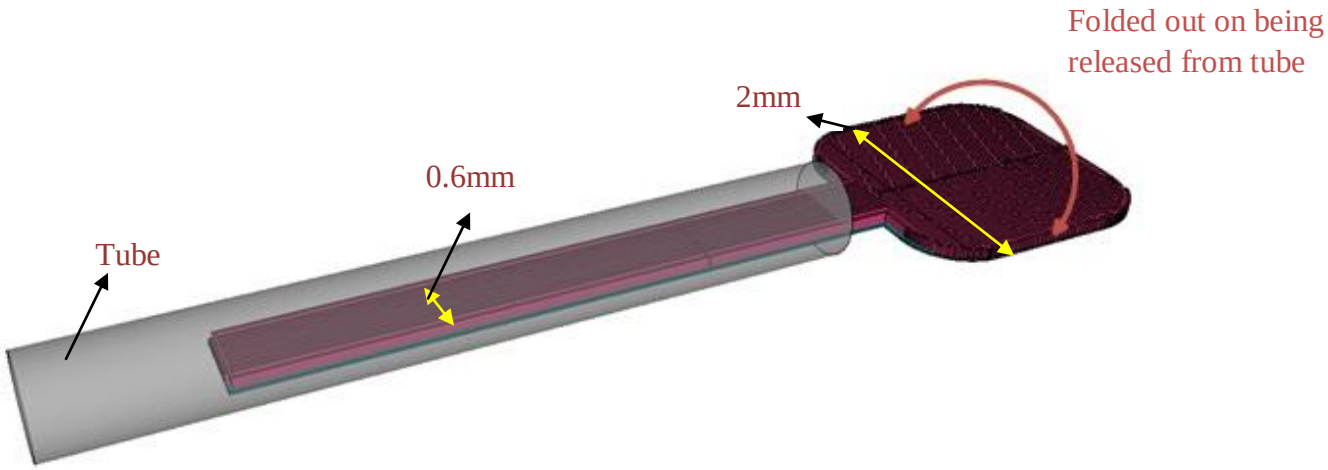

(a)

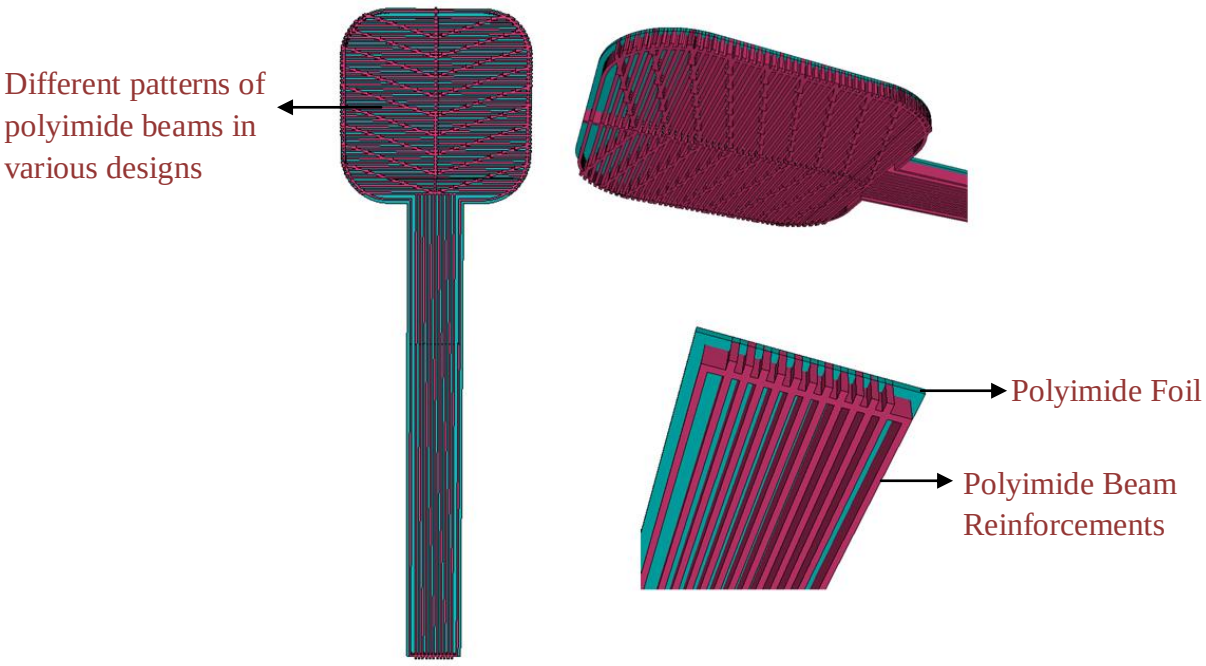

(b)

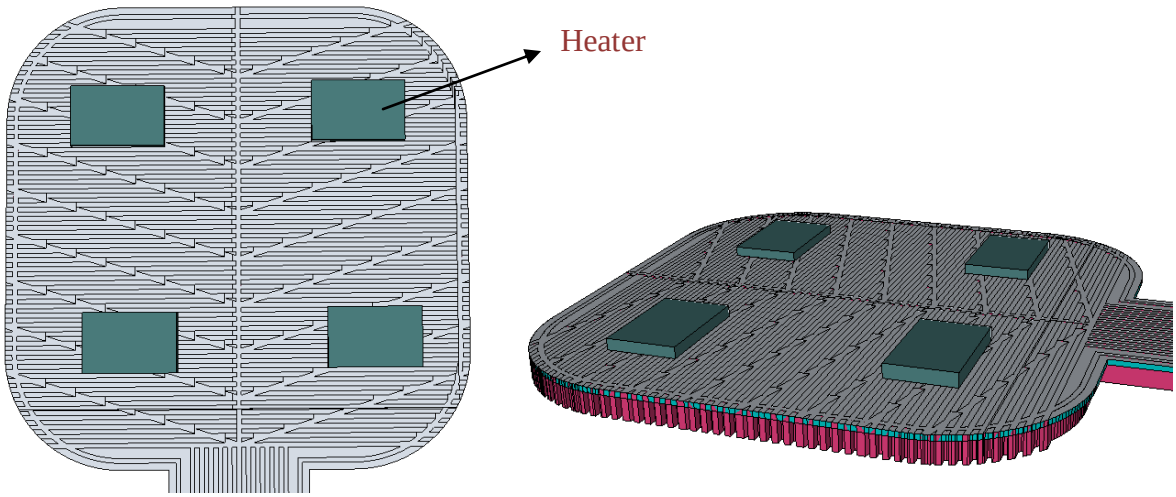

(c)

Figure 2.2: Models to understand the design of the Instrument (a) The instrument envisioned as being inside a tube while folded, pushed out to open up (b) Made up of a polyimide foil (blue) which is reinforced with polyimide beams (pink) (c) Heaters placed on the flat side of the foil

In addition to this, it was decided to leave free standing beams of silicon inside the polyimide beams of some designs to add to the stiffness. This idea is depicted in Fig. 2.3.

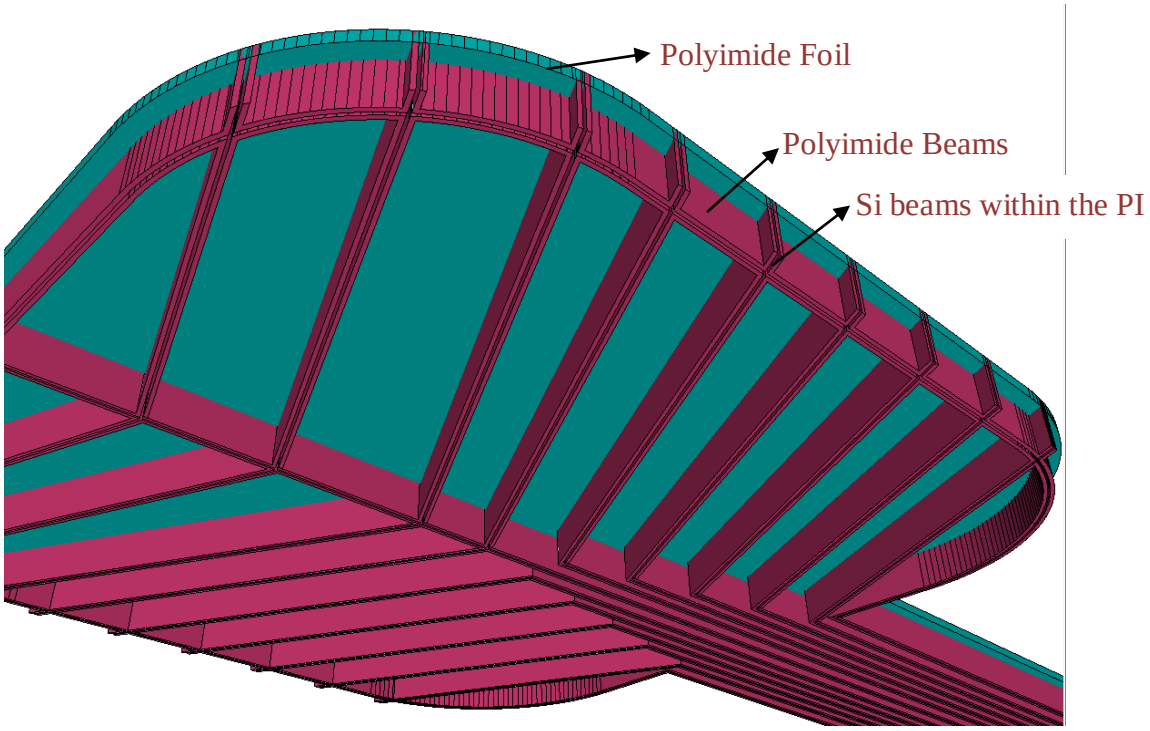

Figure 2.3: Addition of Si beams inside PI beams

2.3 F2R- Flex to Rigid Foil Technology:

Minimally invasive diagnosis and therapy techniques like endoscopy and catheterization are typically used for detecting and/or treating blockages caused due to the deposition of fatty tissue, coagulated blood or calcium along the walls of blood vessels. The affected area is reached by making a small incision in a main artery or vessel, usually in the groin. Through this opening, a thin flexible wire (guide wire) is inserted and pushed along the blood vessels to the destination. The guide wire usually does not contain any sensing functionality. A hollow tube with transducing functionality (a catheter) is then pushed over the guide wire. The diameter of a catheter can vary from 1 to 3mm while that of the guide wire can be as small as 300μm. The further the instrument needs to penetrate into the smaller blood vessels, the thinner it needs to be. Pressure sensing, flow sensing and imaging, alone or combined, are a few functionalities that have been incorporated into these instruments and a few compliant devices have been presented [7, 8]. Flex-to-Rigid (F2R) foil technology is an innovative technology that is used for the fabrication of partially flexible miniature components of any shape and thickness, attached by extremely flexible, high density interconnects [4]. The use of conventionally shaped (square or rectangle) chips is problematic for use in cylindrical and hollow catheters. Also, depending on the type of sensing functionality to be added, the location of the sensing system can differ. The transducing chip of a forward looking catheter will have to be placed at the tip of the instrument while in the case of a ring shaped catheter, the sensors may be bent around it. The F2R method is ideal for such requirements since it has the advantage of enabling the fabrication of chips of any arbitrary shape and thickness. Rigid Si chips are still present in the system and thus standard wire bonding and flip-chipping technologies are possible. The presence of rigid parts facilitates the handling and the mounting of the whole system.

2.3.1 F2R- Fabrication Process:

For the purpose of demonstration of this technology, two demonstrators were designed in [4]. One included ring shaped silicon (Si) chips which would allow an instrument like a probe to go through one or more (stacked) chips, avoiding the need of through wafer vias but having extra functionality (Fig. 2.4 (a)). The second demonstrator had a polyimide based flexible foil attached to a Si chip, which could be bent around a catheter or a guide wire while the rigid chips could be placed inside to connect the flexible sensor to the wires running through the

instrument (Fig. 2.4 (b)). Polyimide hinges were used to keep the foil attached to the wafer. The structures were removed by cutting the hinges.

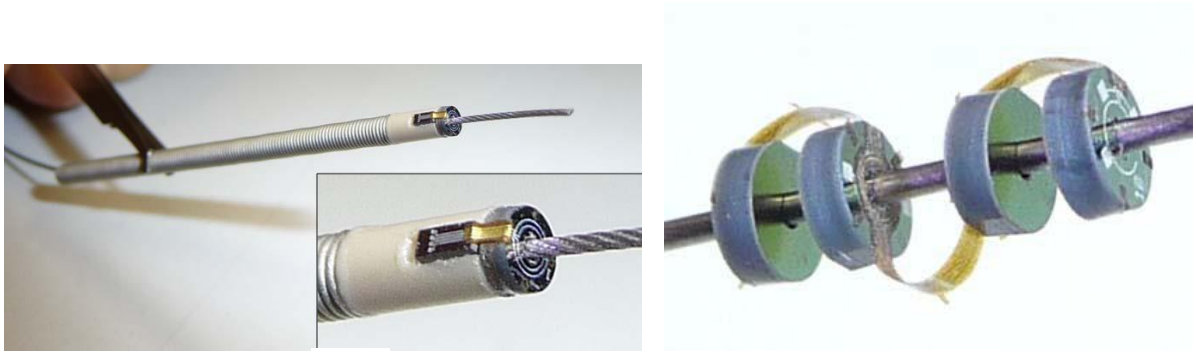

(a) **(b)**

Figure 2.4: (a) Demonstrator 1 with a 2mm diameter sensor chip and flexible interconnect mounted on the tip of a catheter (b) Demonstrator 2 with 2mm diameter sensor chips folded and stacked on a wire of diameter 0.5mm

To fabricate these, a 1µm thick thermal silicon oxide (SiO_2) layer was first grown on both sides of the wafer (150mm, p type, <100>, 400µm thick) at 1000 ºC. The front side was sputtered with 200 nm of aluminum and patterned, followed by a deposition of a 300 nm thick layer of PECVD SiO_2 at 400ºC. After the patterning of the PECVD SiO_2 layer, polyimide was spun on the front side of the wafer and subsequently patterned. The PI layer was then cured for 2 hours at 400 ºC in a nitrogen environment. A 1µm thick Al routing layer was deposited by sputter coating and patterned, followed by spinning and curing of a second PI layer. The 1µm backside thermal oxide layer was patterned using RIE dry etching and HPR504 resist as a masking layer. 200nm of Al was then sputtered and patterned on the front side of the wafer, on top of the PI layer. This layer was later used in the process as a masking layer for the etching of the Polyimide layer. A 12µm thick resist (AZ9260) was then patterned on the backside of the wafer. A two step anisotropic DRIE of the silicon wafer backside using the Bosh process was done to define and reduce the thickness of the Si chips to 50µm. First, 50µm was etched using both the thick resist and the thermal oxide as a masking layer, followed by the selective etching (toward Al) of the exposed backside thermal SiO_2, using the thick resist as masking layer. After the second anisotropic DRIE of 350µm, the thick resist was removed from the backside using acetone. The 1µm layer of thermal oxide was then removed from the backside together with the thermal oxide exposed from the front side, still using an etchant selective toward Al. Finally, the top PI layer was patterned in

oxygen plasma using the thin Al layer as a hard etch mask, after which the hard etch mask was removed using a PES-type etchant. Figure 2.5 describes the fabrication process.

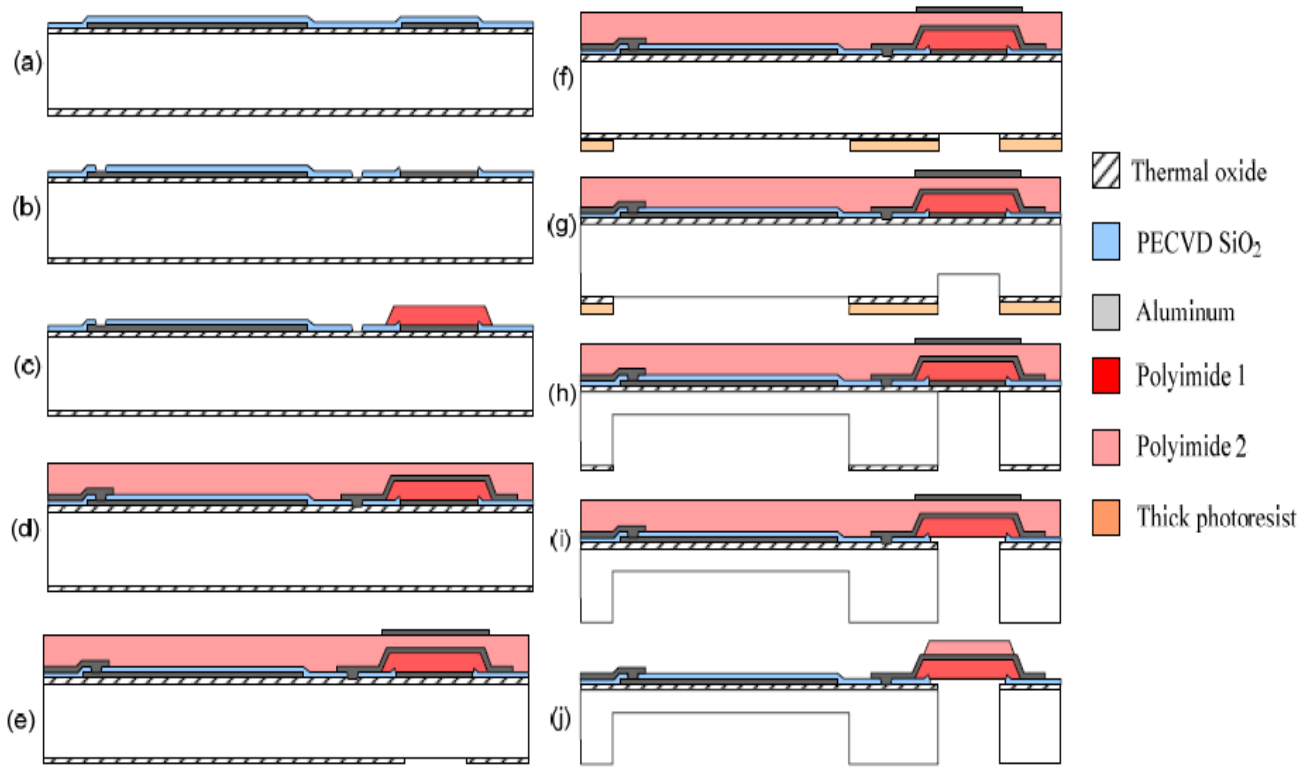

Figure 2.5: Fabrication sequence of the F2R process

The F2R technology would be the perfect choice to fabricate an instrument for the surgical procedure described earlier because of the following main reasons:

- This technology enables us to fabricate Si chips of arbitrary shapes and sizes. The instrument design requires that it be a maximum thickness of 0.6mm for insertion into the eye and can have a width of 2mm once inside. It must also be strong enough to hold a piece of tissue (along with the heaters) and transfer it. Such design requirements would call for shapes other than the traditional rectangular shapes that chips are made in.
- The instrument is to be designed as being inside a tube (maximum thickness 0.6mm). Once inserted into the eye, it will be pushed out and opened up to a width of 2mm. It is thus vital for the instrument to be highly flexible. The folding should not cause damage to the mechanical strength of the instrument or to the electronic features present on it. Interconnects made of such foils have been tested and bent up to a

radius of 50µm without causing any harm to its electrical continuity [4]. Figure 2.6 shows the test setup.

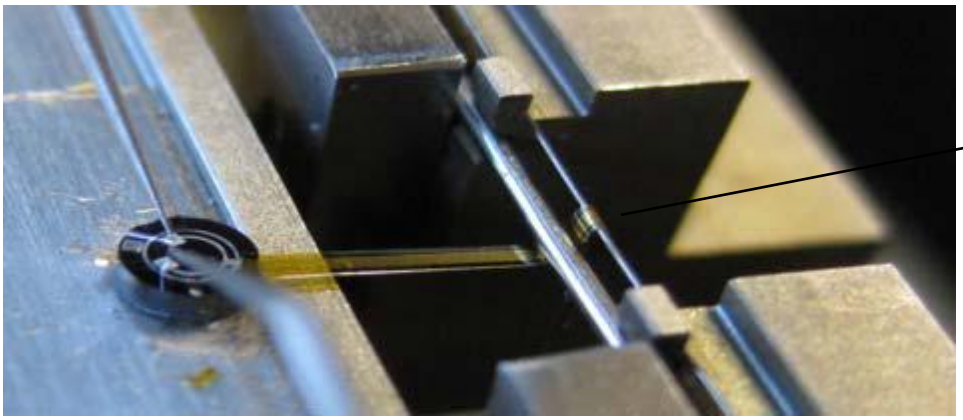

Figure 2.6: Electrical continuity testing of the interconnect when bent

- Sensor systems and heaters can be incorporated onto the instrument by means of this technology.

This technology would need some alterations in order to be adapted for the purposes of this thesis. Apart from having the heater embedded into the polymer (metal wires in case of the demonstrators), it is also required to provide reinforcements to the foil with additional polymer beams. The heaters must be on the flat side of the polymer as shown in Fig. 2.2 (c). To accomplish this, it would be necessary to make the polyimide beams first and then deposit the metal layer and finish with the second layer of the polymer. This process is explained in detail in chapter 5 which deals with the fabrication process. The following chapters deal with the simulations, design, fabrication and testing of the device.

Chapter 3: Simulations

Before commencing with the fabrication, it was important to understand if such a device could be made on a small scale using the F2R foil technology, based on the HIAD principle. Various questions needed to be answered. Simulations were done to understand what would happen if heat pulses were given by a heater placed on the instrument to penetrate into the tissue. It was important to see if the required temperatures could be achieved with reasonable amount of power and sufficiently low heat penetration into the tissue (which would cause further tissue damage). How thick must the sandwiching layers of polyimide be? Would the heat affect the surrounding tissue which is not targeted? How would the placement, size and number of the heaters affect the spread of the heat?

3.1 Simulation Model

Simulations were carried out using COMSOL which is well suited for thermal simulations. The initial simulations were carried out in 2D and then repeated in 3D to get a better understanding of the heat flow. The heater was assumed to be a uniform layer of aluminium with a thickness of 1.5 µm and a width of 200 µm (Fig. 3.1). Note that in reality the heater (most likely) will have the shape of a meander. In the 2D simulations the 3rd dimension of the structure is assumed to be 1mm (which is also used in the 3D simulations). The heater was sandwiched between two layers of a polymer as in the real instrument. The surrounding environment was chosen as water since human eye tissue is 78% water and it is a reasonable approximation to make.

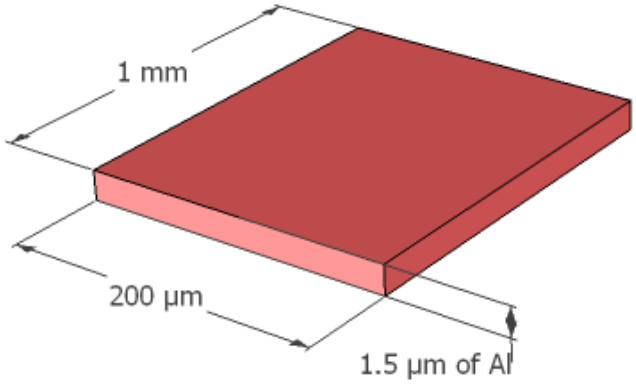

Figure 3.1: Heater dimensions used for simulations

The material chosen to sandwich the heater must have a low heat capacity. Polyimide (with a specific heat capacity of 1.15 $kJkg^{-1}K^{-1}$) and parylene (with a specific heat capacity of 711.7 $Jkg^{-1}K^{-1}$) were considered [11]. The specific heat capacity of parylene is less than that of water (1100 $Jkg^{-1}K^{-1}$). As a result, if parylene was selected, even though the heat would transfer quickly to the target tissue, it would also affect the surrounding tissue which should have been left unharmed. The heat applied would be conducted quickly in all directions. Due to this reason, polyimide was chosen as the material to be used. The specific heat capacity of polyimide is reasonably low to allow the surface temperature of the target tissue rise quickly but it is higher than that of water and hence it isolates the surrounding tissue from the heat much better than parylene would.

In a previous work it has been demonstrated that a short pulse of heat taking the surface temperature to 70°C is required to cause the tissue proteins to denature and subsequently adhere to the instrument while a heat pulse causing the temperature to rise to 100°C is required to detach the tissue [1]. In the FEM simulations it was investigated how these temperatures could be achieved with short pulses of heat. What would be the optimum pulse duration, the required power and how far would the heat penetrate into the tissue? The width of the heater and its placement in the whole device also needed to be determined such that the heat would be provided sharply on the bottom of the device while limiting the heating on the other side to temperatures comfortably below 70°C to prevent damage to the surrounding tissues. Different combinations of all factors were simulated. The thickness of the heater was kept to a low value of 1.5 μm. This value was chosen for ease of fabrication. A thicker layer of aluminium would be hard to sputter during the fabrication stages while a thinner layer would require a higher voltage to deliver the same energy. The thickness of the layer of polyimide between the heater and the target tissue was kept to a low value of 1 μm to help the heat travel quickly to the tissue. A thicker layer of polyimide was required on the other side of the heater in order to isolate the surrounding tissue. This value had to be chosen such that when a heat pulse is applied and the surface temperature of the target tissue rises to 100°C, the temperature of the surrounding tissue remains comfortably below 70°C (to avoid any attachment on this side). When a heat pulse at a certain power is applied, the surface temperature of the target tissue rises to 100°C. The graph in Fig. 3.2 depicts this. The Y-axis shows the temperature and the X-axis represents a line along the cross section of the model. The point ‘0’ is the point of contact between the thinner polyimide layer and the tissue surface to be heated. It can be seen that in order to keep the temperatures of the surrounding

tissue below 70°C, the polyimide layer must end beyond the red line. Since the lower polyimide layer and the heater have a combined thickness of 2.5 µm, the thickness of the polyimide layer on the top must be a minimum of 14 µm. It was decided to keep this thickness to 16 µm to be on the safe side. Figure 3.3 shows the final model.

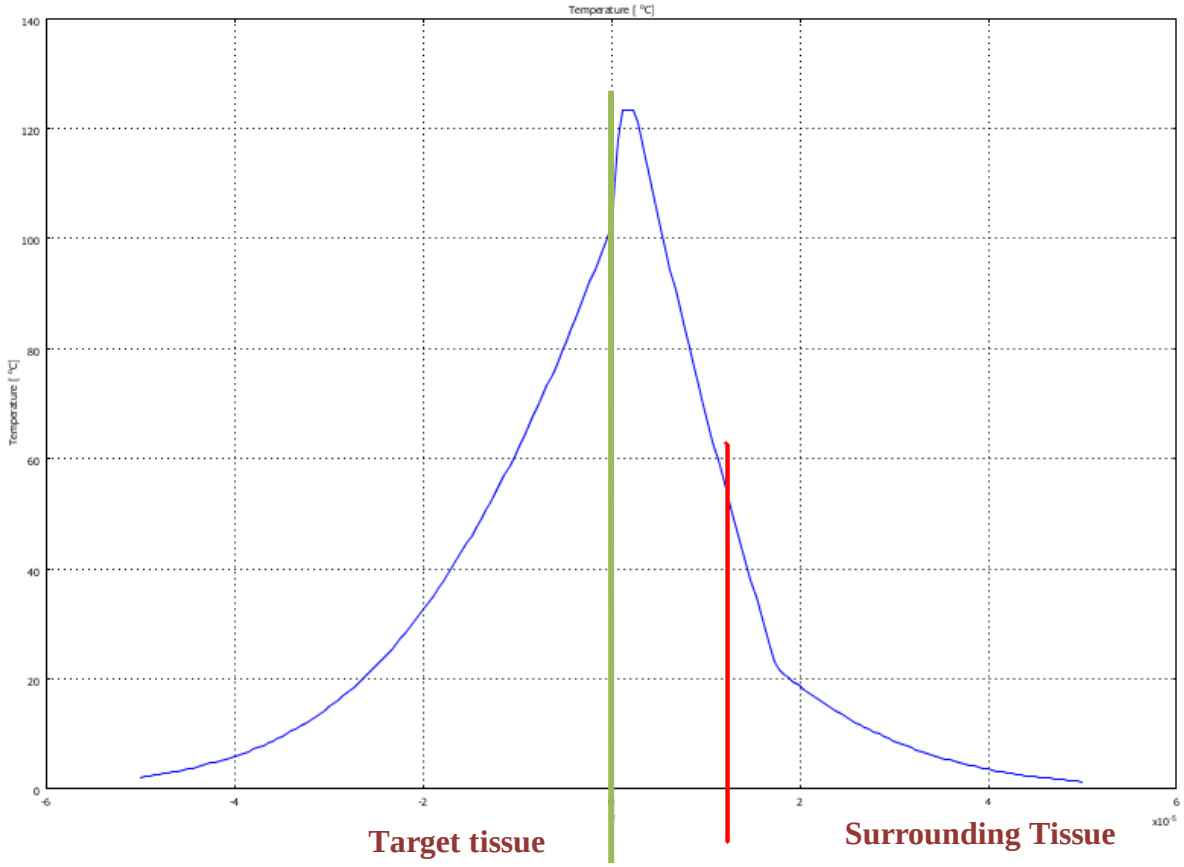

Figure 3.2: Appropriate thickness of the polyimide layers

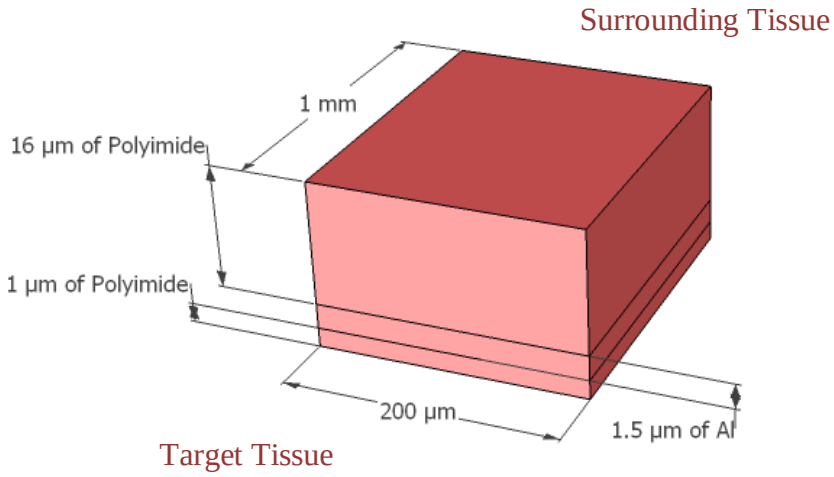

Figure 3.3: Instrument model for simulations

3.2 Simulations in COMSOL

Simulations using the device configuration shown in Fig. 3.3 were performed for different powers and different time durations of the heat pulses. The required temperatures could be achieved for various combinations. Table 3.1 lists a few possibilities.

		Power (W)	Time (ms)	Penetration Depth (μm)
70°C	1.	1.5	0.9	4
	2.	1	1.8	5
	3.	0.9	2.1	8
	4.	0.5	5	18
100°C	1.	1.5	1.8	7.5
	2.	1	3.7	8.5
	3.	0.9	4.1	12
	4.	0.5	12.5	25

Table 3.1: Power-Pulse duration combinations to achieve fixed temperatures

It can be seen that by increasing the power, the pulse length needed to reach the required surface temperature decreases. The penetration depth also decreases with the pulse length. Appropriate values can be chosen to get the needed temperatures, keeping the penetration depths within a safe limit of about 15 μm (the damage due to the heat below this penetration depth is minimum, as informed by Dr. Jan van Meurs, Rotterdam eye Centre). A power of 1 W was used for further analysis since the required temperatures could be achieved with low penetration depths of heat. The detailed results of the simulations for this case are discussed in the next sub section.

3.2.1 Graft Attachment

It was found that a heat pulse of 1 W applied for duration of 1.8 ms resulted in a temperature of 73.5°C at the surface of the target tissue. The simulation showed a heat distribution as shown in Fig. 3.4 at the moment of time where the highest temperature is obtained.

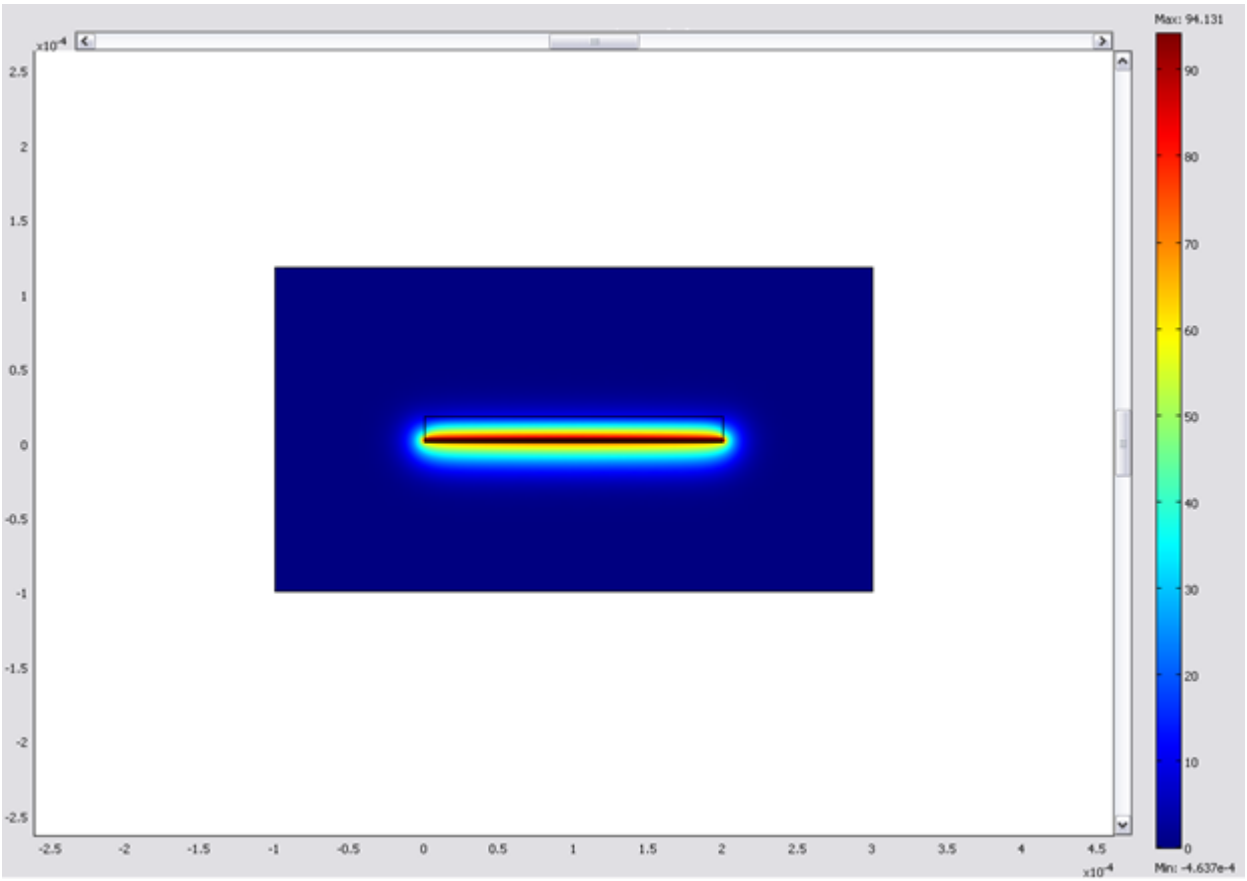

Figure 3.4: Heat distribution

Figure 3.5 shows a plot of the temperatures versus along the cross section of the model. The point '0' is the point of contact between the thinner polyimide layer and the tissue surface to be heated and thus, the temperatures at this point are of concern to us. The maximum temperature is reached at the location of the heater. It should also be noted that the temperature on the point of contact of the thicker polyimide layer and the surrounding tissue (wrong side of the instrument from point 2.5 μm to 18.5 μm) is much lower than 70°C (since it has dropped below that value even at a distance of 4 μm).

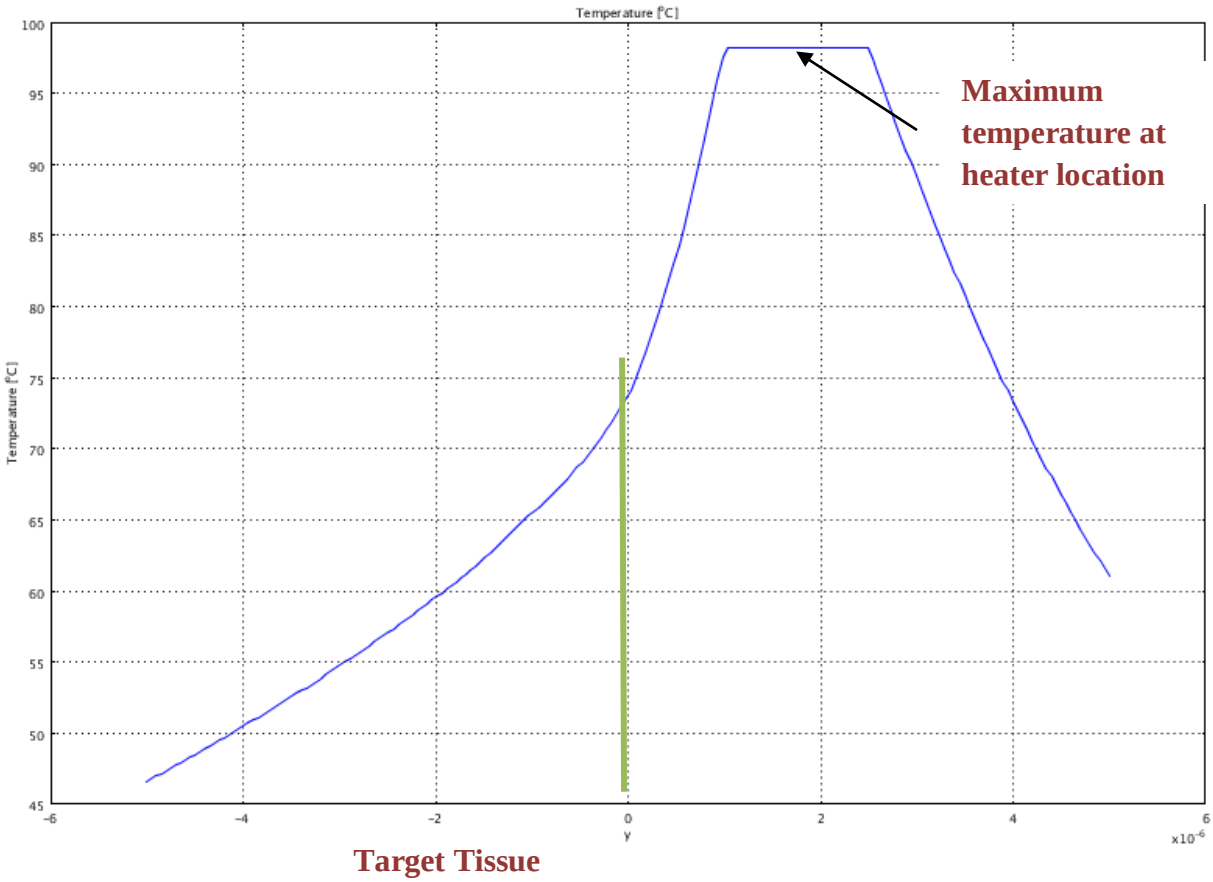

Figure 3.5: Plot showing the temperatures along the cross section of the model

Before the heat pulse is applied, the system is at room temperature. On application of heat, the temperature rises sharply, reaches a maximum and then decreases (as can be seen in Fig. 3.6).

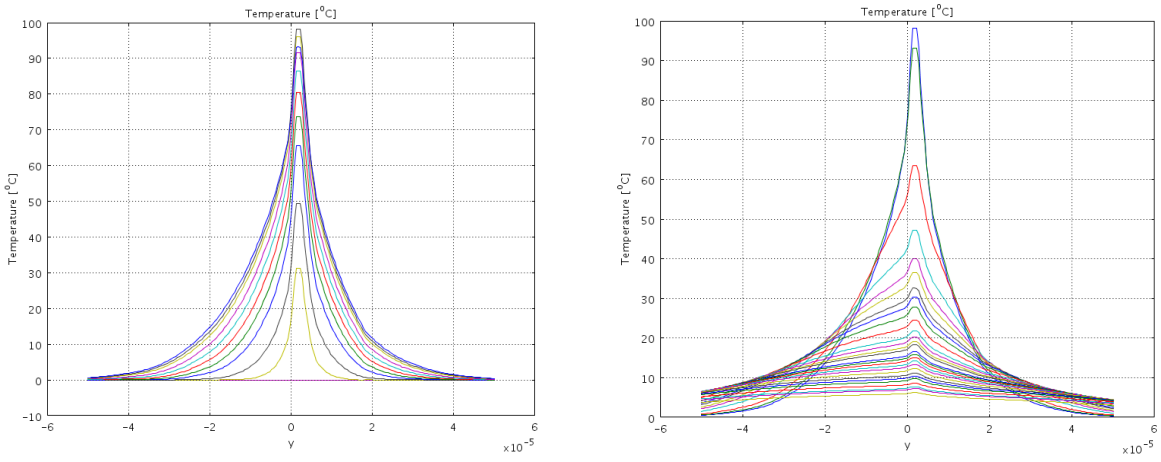

(a) **(b)**

Figure 3.6: Plot showing the changes in temperature with time (with respect to the surface being heated) (a) During the Heat pulse application (b) After switch off

Figure 3.7 shows the penetration depth of the heat at the moment of time when the maximum temperature is attained. We can measure the distance at the point where the temperature is 60% of the maximum value. For this case, the penetration depth is about 5 μm into the tissue. This is an acceptable value. The damage done to the tissue due to this is negligible.

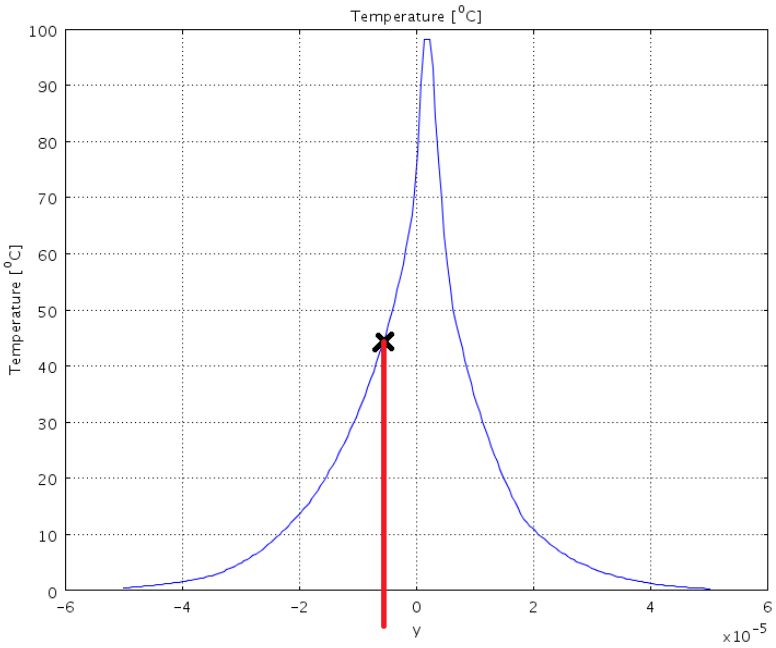

Figure 3.7: Plot showing the penetration depth of heat

3.2.2 Graft Detachment

A heat pulse of 1W applied for 3.7 ms resulted in a temperature of 101°C. The corresponding plots and figures (as in the previous sub section) are shown below.

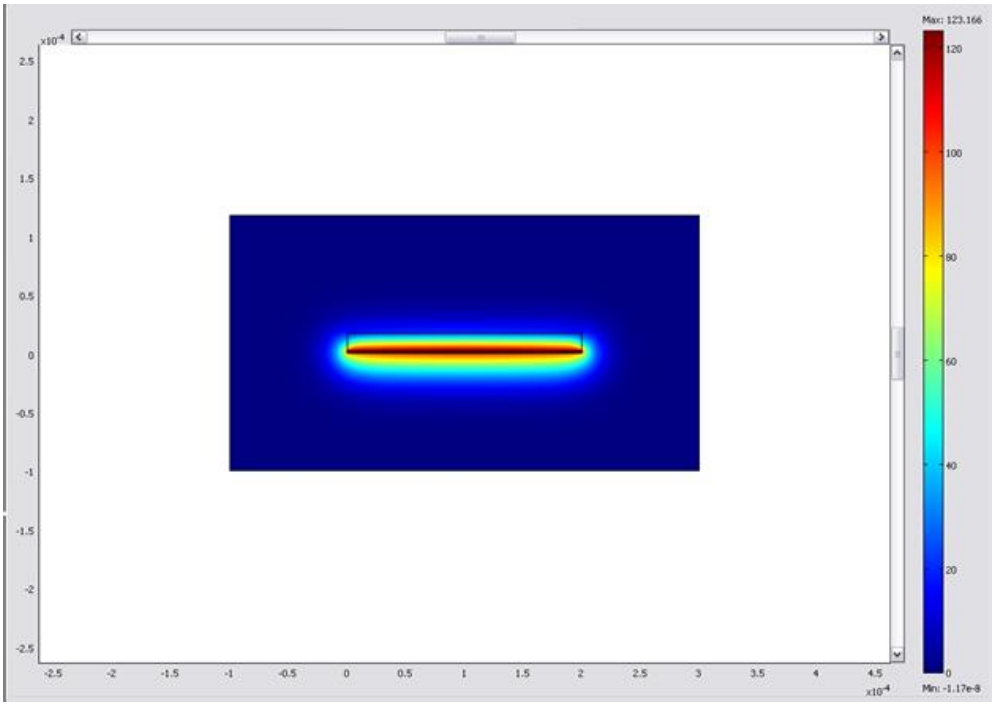

Figure 3.8: Heat distribution

A temperature of 101°C is observed at point '0' in fig. 3.9. The temperature at point 18.5µm is also below 70°C.

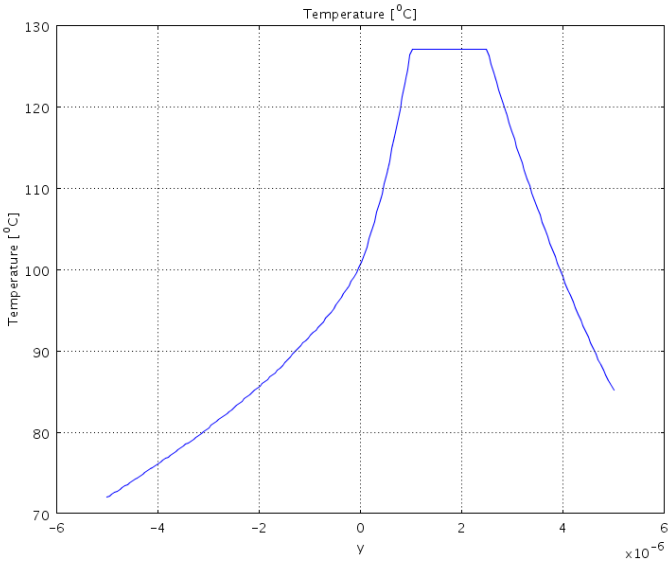

Figure 3.9: Plot showing the temperatures along the cross section of the model

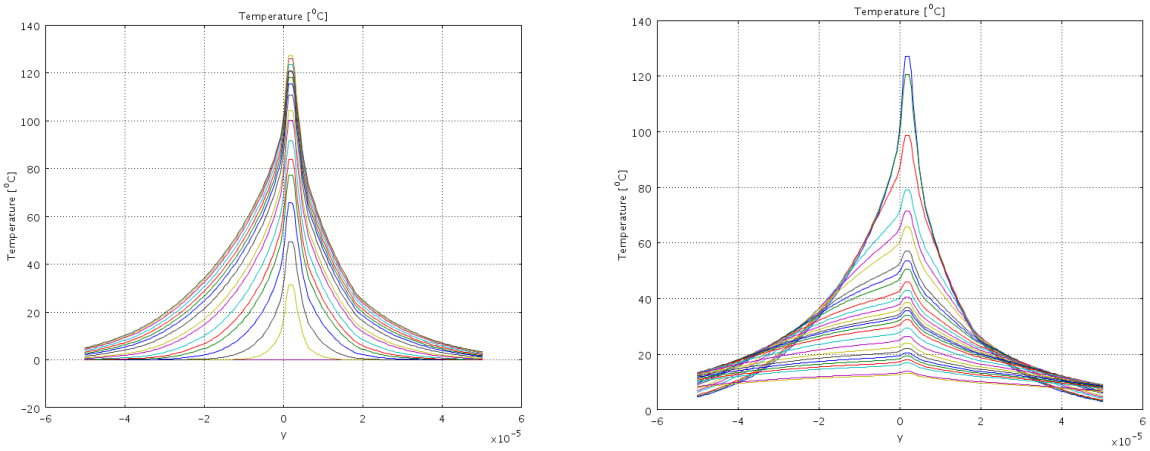

(a) **(b)**

Figure 3.10: Plot showing the changes in temperature with time (with respect to the surface being heated) (a) As the heat pulse is applied (b) After switch off

The penetration depth is about 8.5μm which is also in the acceptable limit.

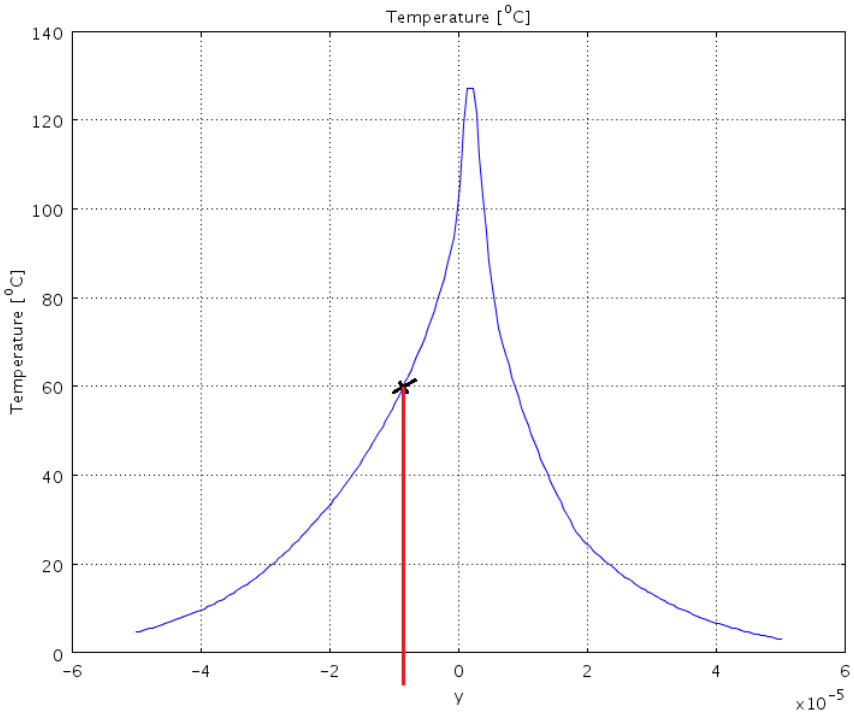

Figure 3.11: Plot showing the penetration depth of heat

3.2.3 Splitting the Heater

In the real device, a set of heaters distributed over the surface of the instrument will be used (instead of just one). It is therefore interesting to see what happens when the single heater is split into a number of heaters. Figure 3.12 shows the simulation model used for this purpose. The length and thickness of the heater are kept the same as in the model used before and the width is reduced by a factor of 4.

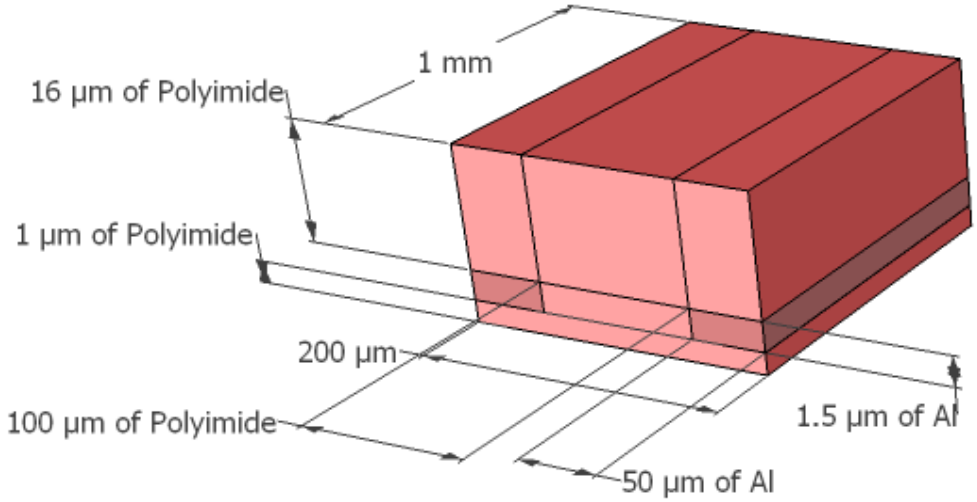

Figure 3.12: Simulation Model to see the effect of splitting the heaters

Figure 3.13 shows the heat distribution at the moment of time where the maximum temperature is attained for a power of 0.25W and a heat pulse of 3.7 ms applied at each heater.

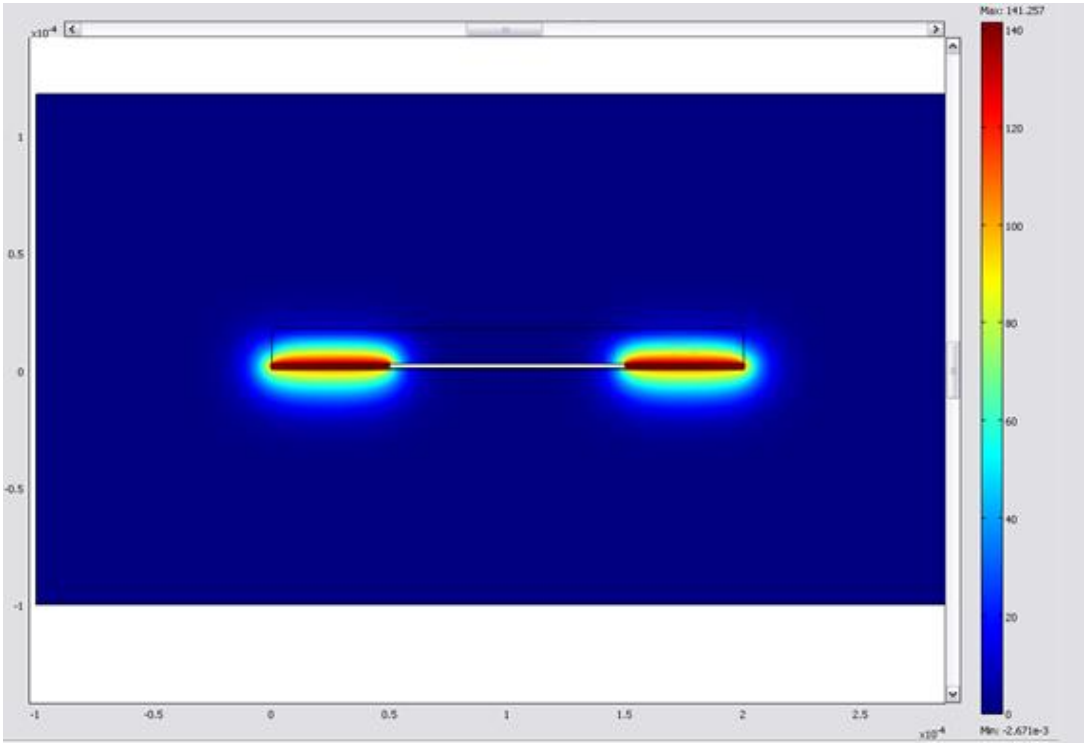

Figure 3.13: Heat distribution

It would be expected that if the heater size is scaled down, the power required to achieve the same temperature would scale down by a similar factor, keeping the length of duration of the heat pulse constant. Else, the time duration of providing the heat at the same power would reduce. Table 3.2 shows a comparison of values, for different combinations of power-pulse durations, for the split heater scenario. It was seen that if the heater width was reduced (keeping the length and thickness same as before, as shown in fig. 3.14) by a factor of 4, then by scaling the power down by 4 (keeping pulse duration constant), a similar temperature could be achieved. The penetration depth increased due to the reduced power. However, if the power was kept constant and the pulse duration was scaled by 4, we achieved a much higher temperature than expected. This value had to be scaled a lot more to get the desired results.

Full Heater				Split Heater			
Power (W)	Pulse duration (ms)	Penetration depth (μm)	Temperature Achieved (°C)	Power (W)	Pulse duration (ms)	Penetration depth (μm)	Temperature Achieved (°C)
1	3.7	8.5	101	1/4	3.7	15	96
1	3.7	8.5	101	1	3.7/4	7	201
1	3.7	8.5	101	1	0.3	6	120
1.5	1.8	7.5	100	1.5/4	1.8	13	105
1.5	1.8	7.5	100	1.5	1.8/4	5.5	178

Table 3.2: Comparison of values after splitting the heaters

Similar results were obtained when different scaling factors were used and different number of heaters placed.

3.3 Conclusions

The HIAD principle seems feasible for being used in the surgical tool. The temperatures required can be achieved with minimal damage to the tissue if the appropriate power and heat pulse duration are chosen. The surrounding tissue can be isolated from the heat by using a thick layer of polyimide between the tissue and the heater. Splitting the heaters does not affect the outcomes as long as the values of the power and heat pulse duration are adjusted accordingly.

Chapter 4: Mask Design

4.1 Incorporation of Wing Designs for the Atalanta Project

Animal flight has always been a field of interest for the scientific community. The development of flapping wing micro air vehicles (MAV's) integrates the human fascination for flight with the ongoing miniaturization of technical designs. At the Department of Precision and Microsystems Engineering at the Faculty of 3mE, TU Delft, there is an ongoing project (Atalanta Project) to make a bug-sized, self-sustaining micro air vehicle that can flap, change direction and attain flight. The goal of the project is to design a mechatronic flying device which can fly in different environments. The whole bug must be completely self-sustaining in terms of energy management and navigation. The design of the MAV exploits resonant properties, as exhibited by flying insects, to reduce the energy expenditure and to provide amplitude amplification. In order to achieve resonance a flexible structure has to be incorporated into the design. The elastic structure used for the body of the MAV is a ring type structure [12,13]. The ring is coupled to the wings by a compliant mechanical amplification mechanism which transforms and amplifies the ring deflection into the large wing root rotation. The MAV is shown in Fig. 4.1. The miniaturization of the wings is however, a point of concern. Currently, the wings are constructed from differently sized carbon beams on which a 0.7 μm thick sheet of Mylar is spanned. The polyimide foils (with beam reinforcements) might provide a solution to this problem. It was decided to include some designs for the wings on the mask for the instruments.

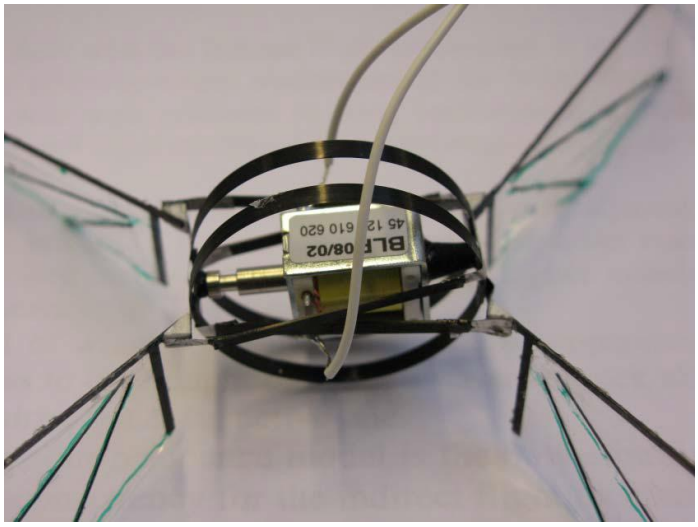

Figure 4.1: The insect inspired Micro Air Vehicle

4.2 Mask Design

The mask design was carried out in Cadence. For the fabrication sequence, 3 contact aligner masks were required. In order to understand the mask designs, a brief introduction of the fabrication sequence is given. Figure 4.2 describes the steps involved in the fabrication of the instrument prototype.

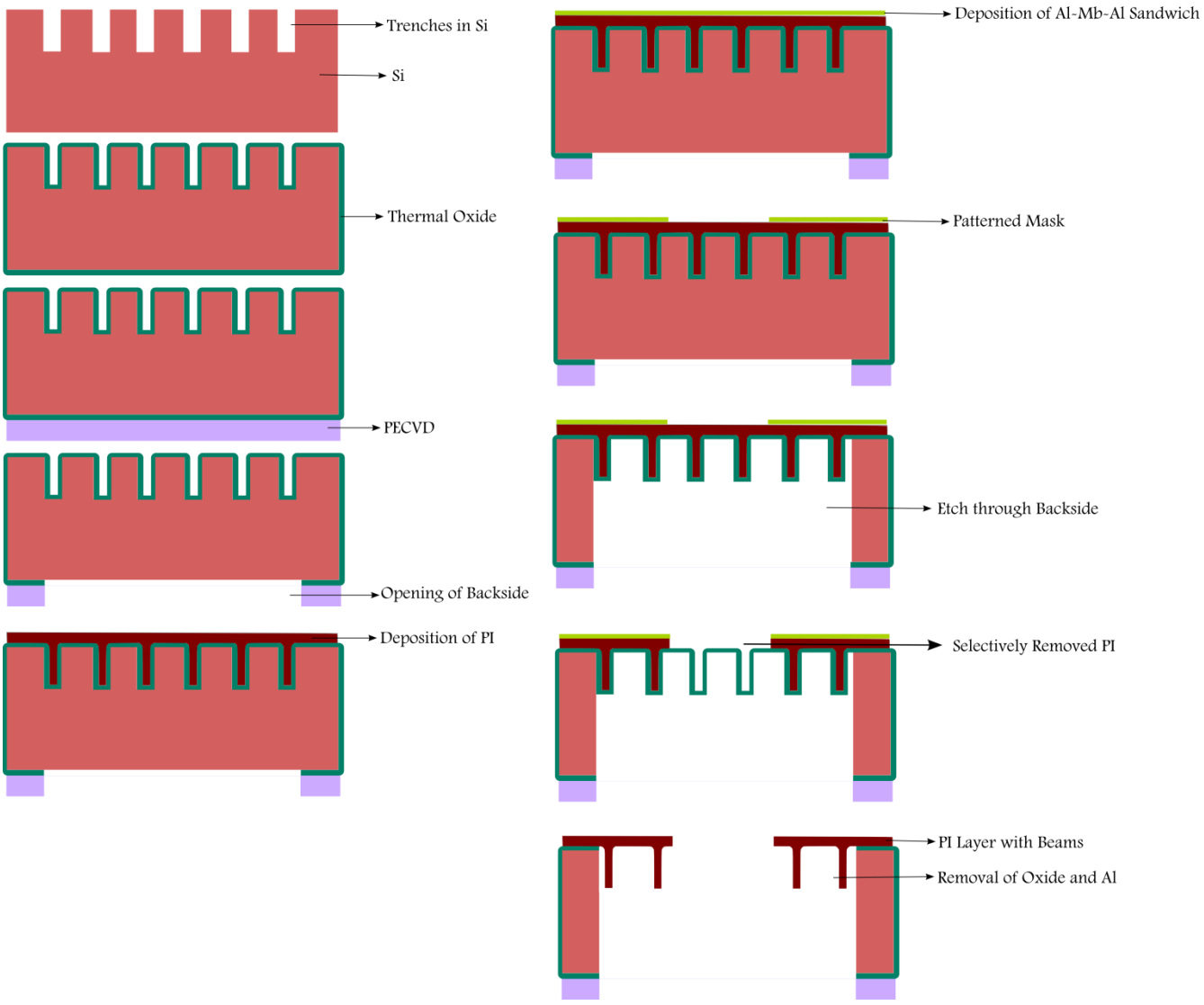

Figure 4.2: Fabrication sequence

The process is initiated by etching trenches of an appropriate depth in the silicon (Fig. 4.2). The wafers are then thermally oxidized at 1000°C to get an oxide thickness of 1µm. Next, 3µm of PECVD oxide is deposited on the backside of the wafers. The oxide is patterned by dry etching to serve as a hard etch mask during DRIE etching later on in the process. Polyimide is spin coated on the topside. An Al-Mb-Al hard etch mask is sputtered onto the

polyimide and patterned in PES etchant. Next the wafer is DRIE etched from the backside using the thick oxide layer as an etch mask and using the oxide layer on the top as an etch stop. The exposed polyimide is dry etched, and subsequently the Al-Mb-Al mask and the remaining oxide are removed by wet etching. We are now left with the instruments made up of a foil of polyimide, with beams running where the trenches were etched. These are attached to the rest of the silicon through polyimide hinges.

For this fabrication sequence, 3 masks were required. The first mask defines the patterns for the trenches that are etched into the silicon wafer. This mask defines the rib patterns on the surface of the instrument. Various patterns were made in order to see which design provided optimum stability and flexibility to the instrument. These patterns were nature inspired and bore resemblance to the rib patterns on leaves and insect wings. The second mask is the back etch mask and the final masks is used to pattern the polyimide. Several pizza plate like shapes were considered and designed for the instruments. This mask also includes the hinges which hold the instrument to the wafer. Some wings were designed as well. Figure 4.3 shows an example of the 3 different masks for 1 instrument design.

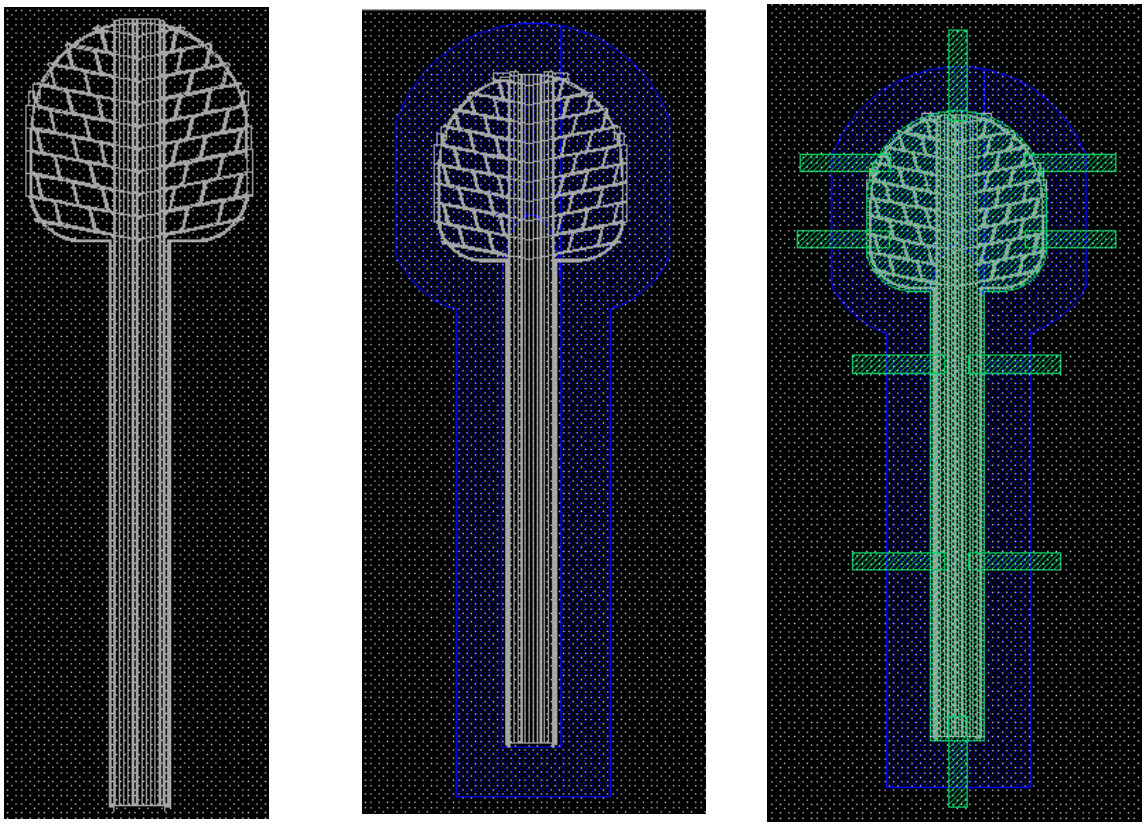

(a) **(b)** **(c)**

Figure 4.3: (a) First mask for the etching of the trenches (grey) (b) Second mask for the backside etching (blue) (c) Third mask for the polyimide (green)

Each instrument was designed to have a length of about 9 mm (Fig. 4.4). The width of the stick was kept at 0.6 mm, while that of the plate was kept to 2mm in order to comply with the standard dimensions of surgical eye instruments. The width of each rib is 20 µm. In the designs where the silicon beams are included, the Si beam is 5 µm wide inside a polyimide rib of 20 µm.

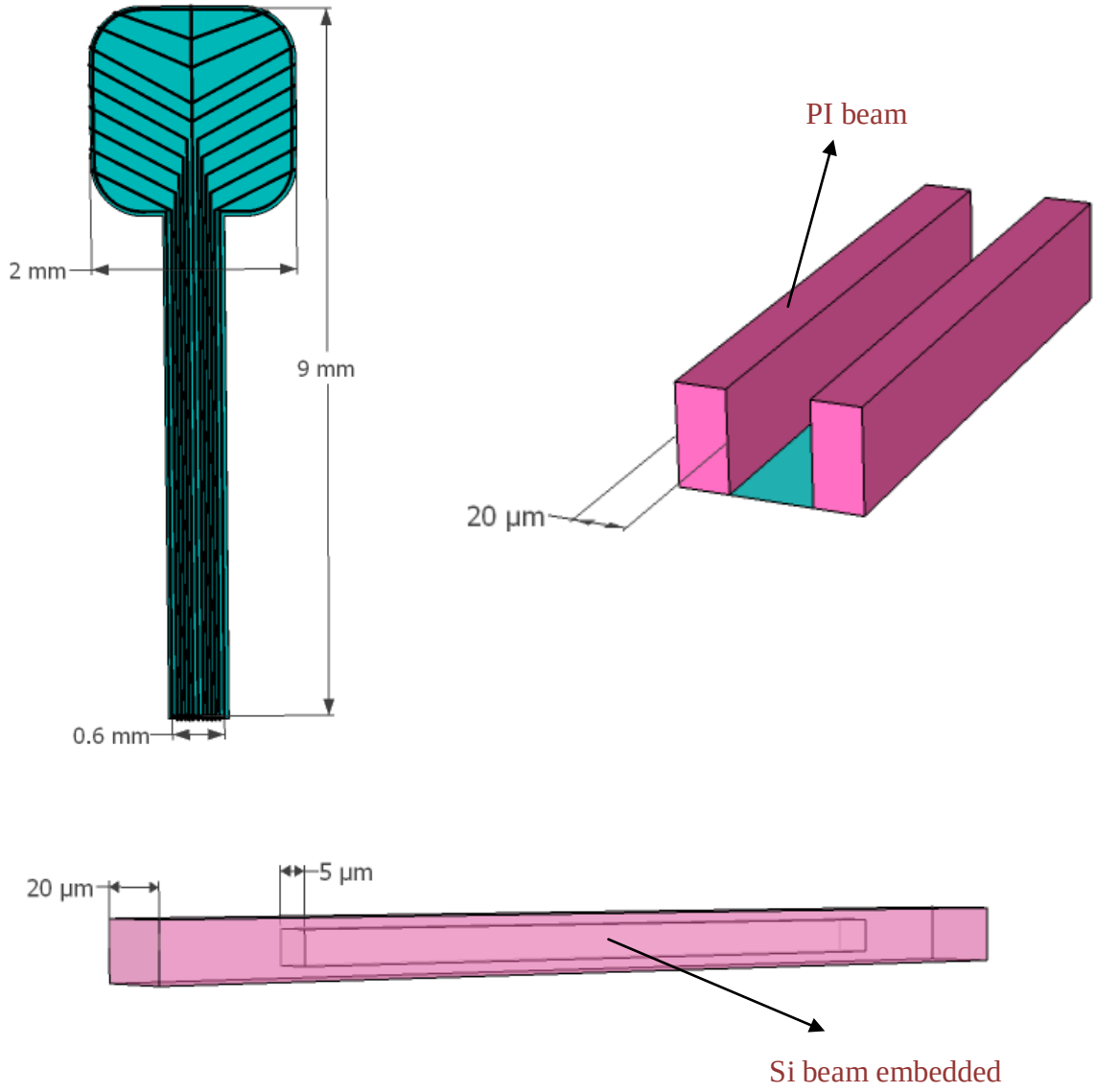

Figure 4.4: Dimensions of the instrument designs

The shapes of the plate part of the instrument were chosen in order to insure a flat surface while the plate is unrolled, ease of folding and structural stability. Due to time constraints, no mechanical simulations were done to determine the optimum design. Figure 4.5 shows the shapes designed (PI mask: green). The shape of the cut umbrella is inspired from commonly

found pop up tents used for camping and the sun shades used for cars that unfold at the slightest change from their folded positions. This shape would presumably fold well but might lack structural balance. The circular and the square (with rounded edges and the ones with curved tops) shapes look even and should fold well. The elongated neck design was added to provide a smooth transition from the plate to the stick of the instrument and thus making it more stable and less prone to faults. It would also allow the instrument to slide back in to the tube with ease. The rib patterns on these shapes play a great role on how stable and flexible the instruments are. Hinges were provided on each instrument to keep it connected to the wafer. Figure 4.6 shows the complete PI mask for 1 design.

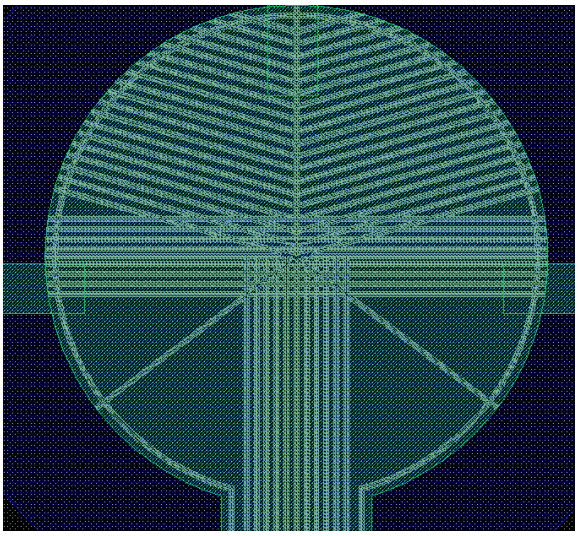

(a)

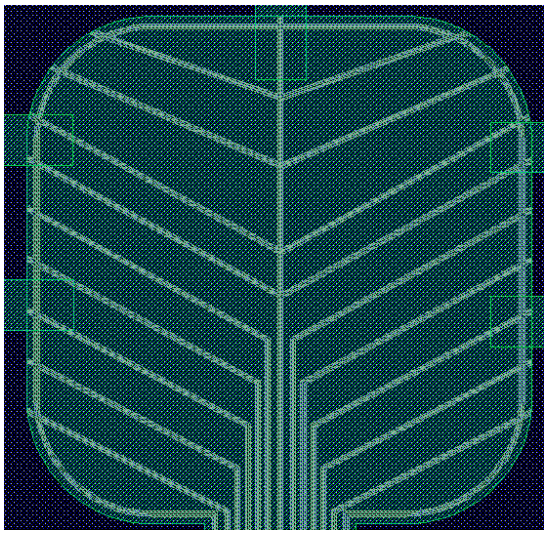

(b)

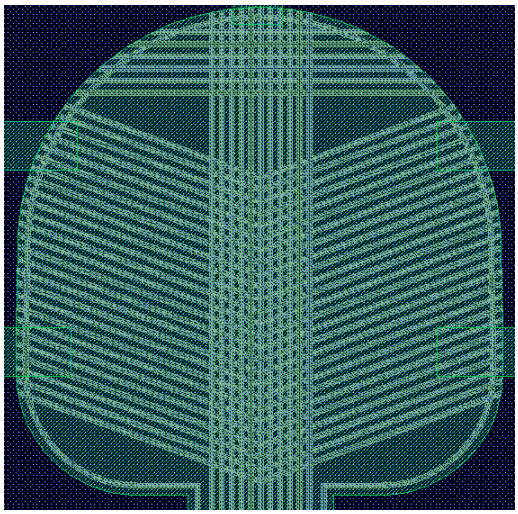

(c)

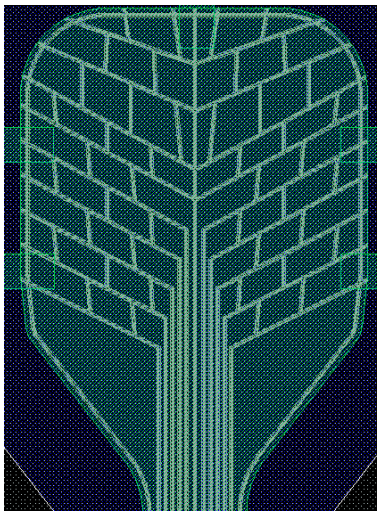

(d)

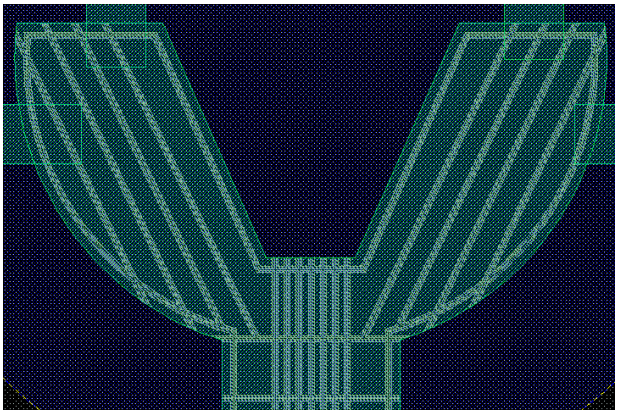

(e)

Figure 4.5: Pizza plate shapes for the mask (a) Circle (b) Square with rounded edges (c) Square with rounded edges and a curved top (d) Elongated neck (e) Cut umbrella

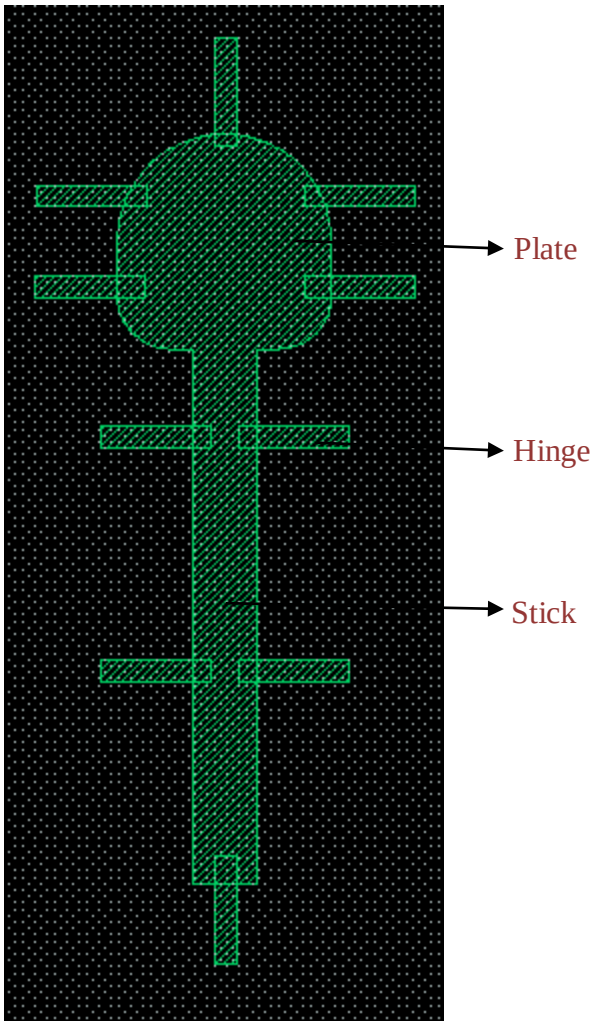

Figure 4.6: PI mask

There were two main variations for the rib patterns (Trench mask: grey). Some designs were meant only for polyimide ribs while some incorporated free standing silicon beams within the polyimide beams. The designs were inspired from leaf and insect wing patterns. The stick, along with the centre of the plate, was given extra stability like the backbone in a human body. The branching ribs spread out into the plate in various forms. The different rib patterns are shown in Fig. 4.7.

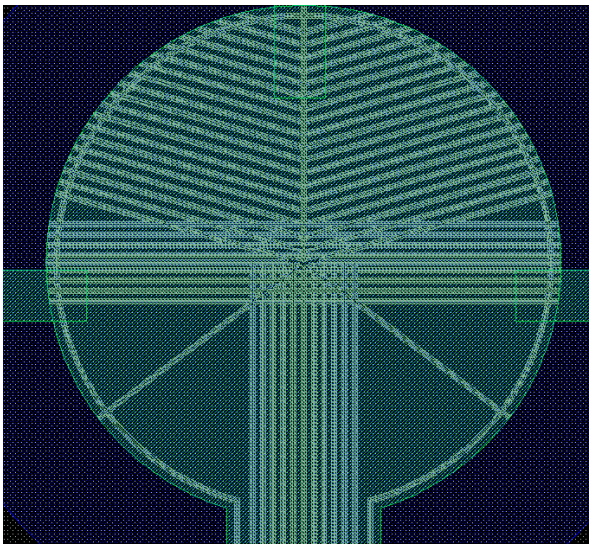

(a)

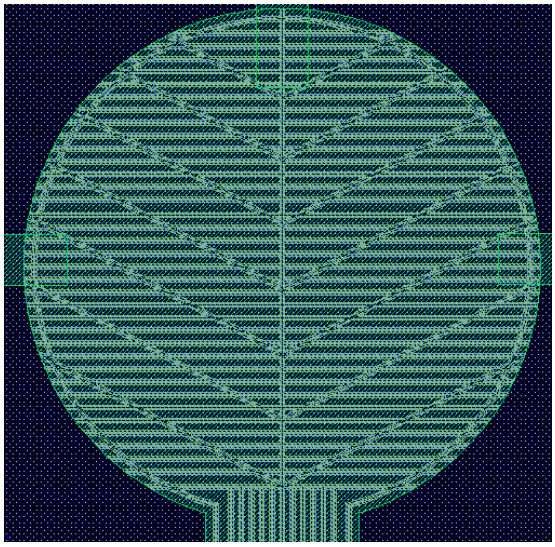

(b)

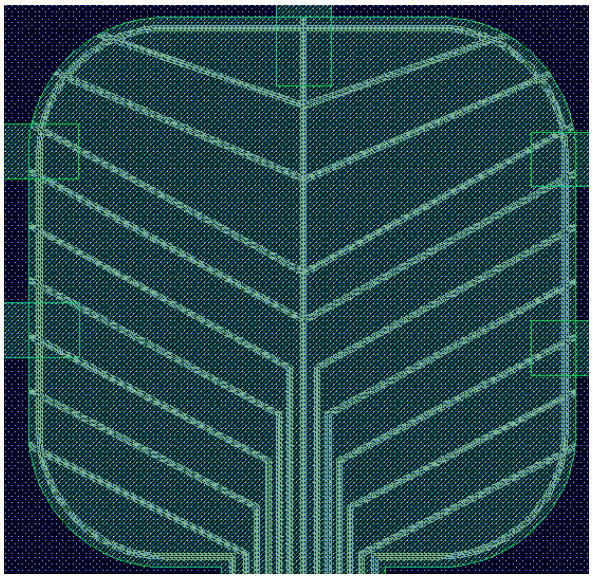

(c)

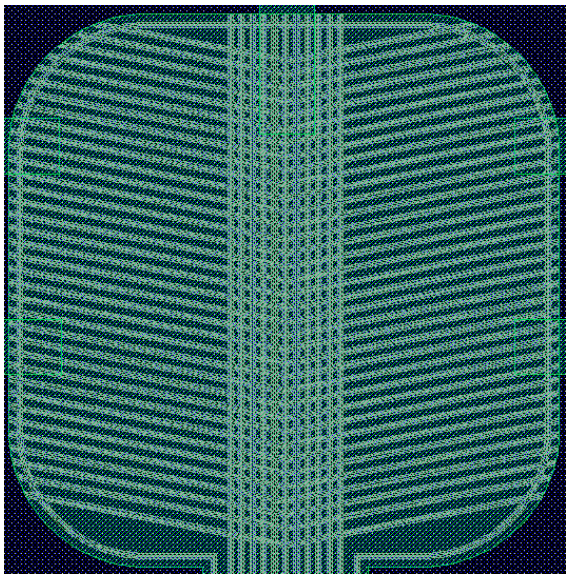

(d)

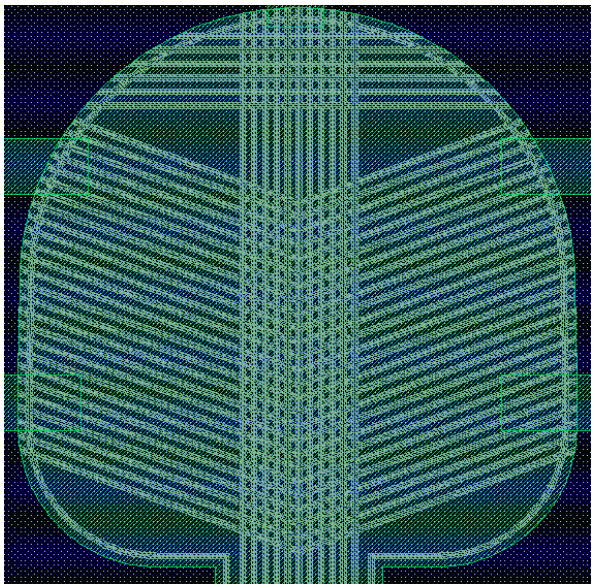

(e)

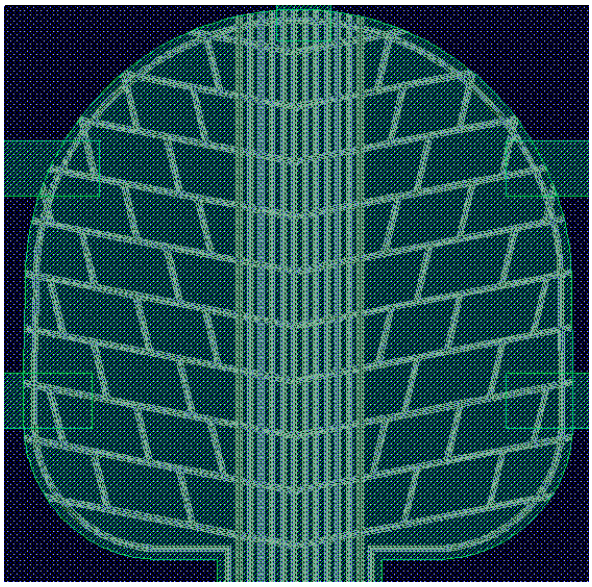

(f)

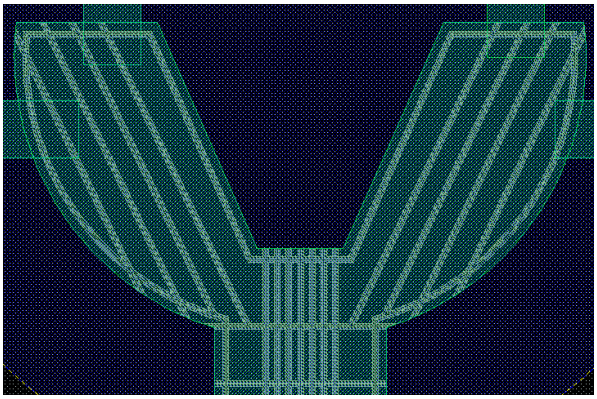

(g)

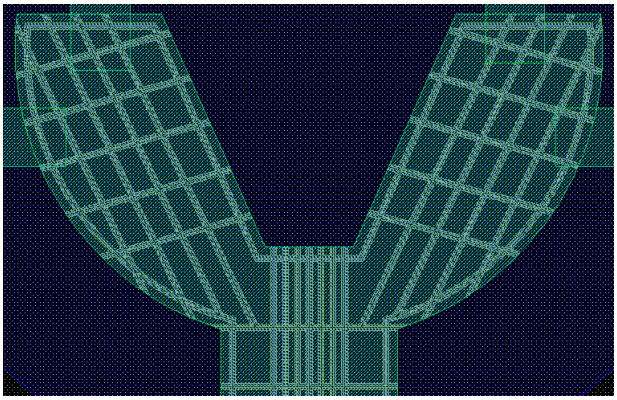

(h)

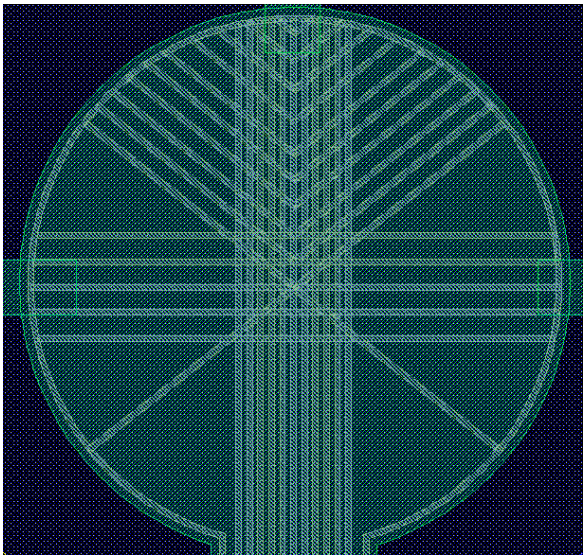

(i)

Figure 4.7: Different rib patterns

These patterns, in combination with different shapes were included on the mask. Each pattern had a version with only polyimide beams and one with Si beams inserted. Figure 4.8 shows these differences using 1 design.

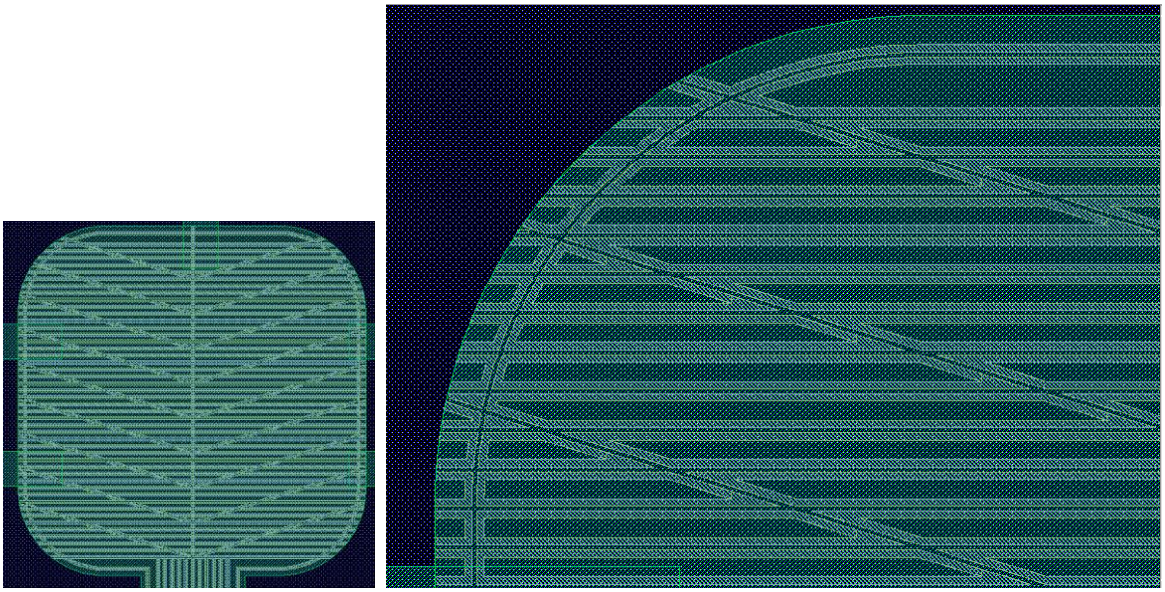

(a)

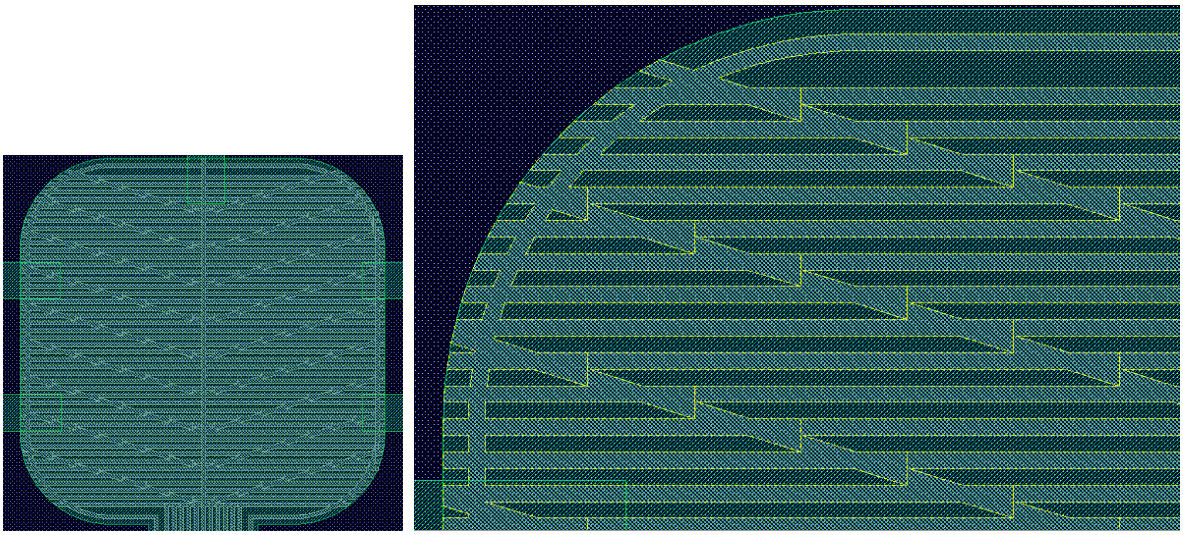

(b)

Figure 4.8: (a) pattern with Si beam within the PI beam (b) pattern with PI beam

Some designs have an additional support in the form of a Si beam on the stick. This was done by appropriate changes in the back etch mask. Figure 4.9 shows the back etch mask for such a variation.

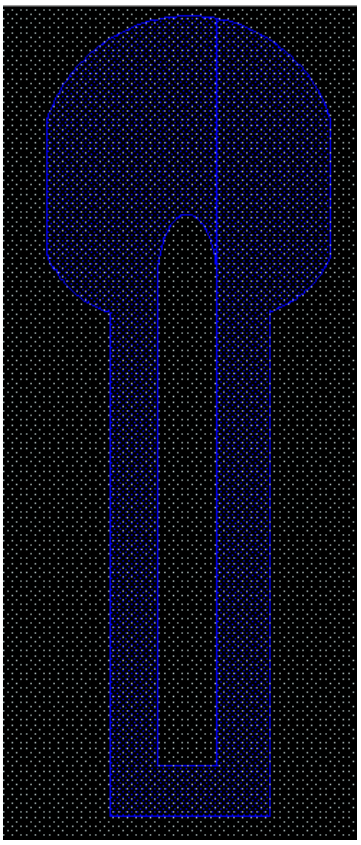

Figure 4.9: Back etch mask to provide a Si beam on the stick

The wing design was done on the same principle and the included designs are shown in Fig. 4.10.

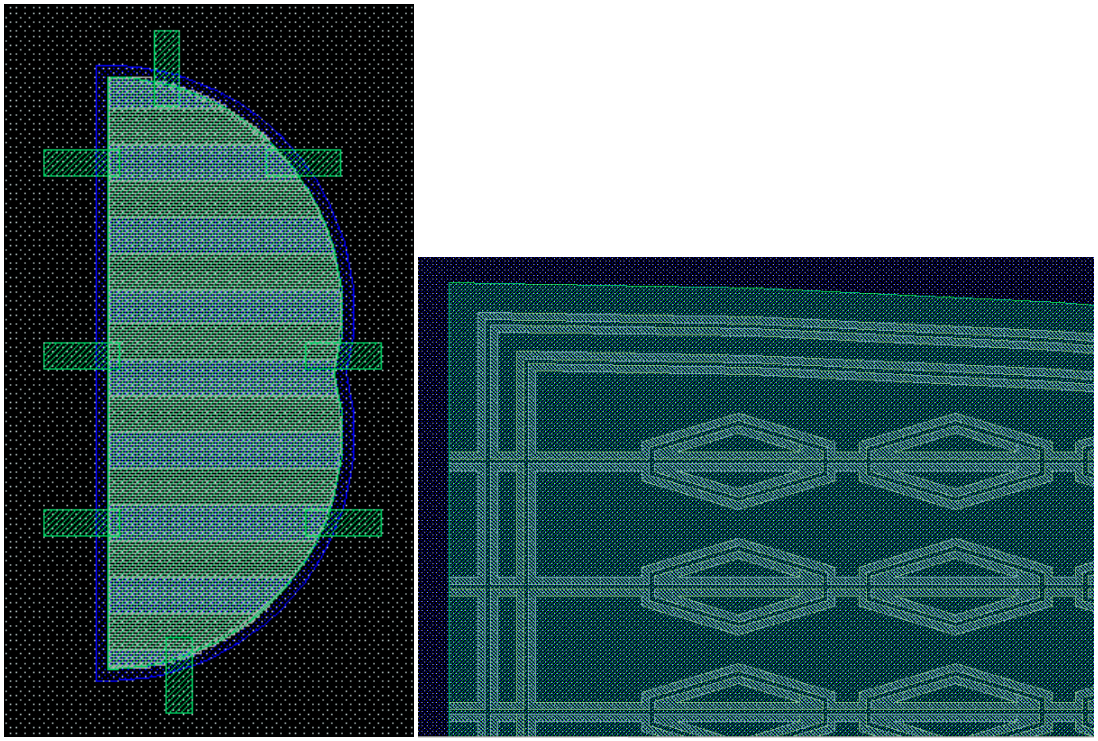

(a)

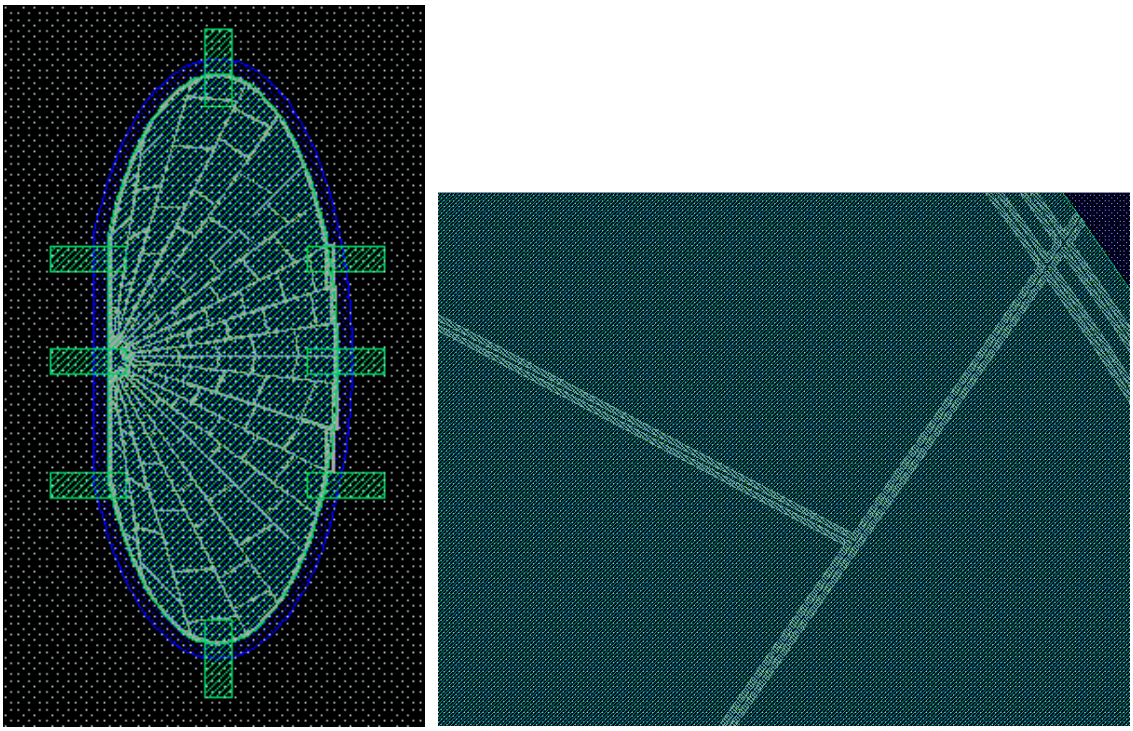

(b)

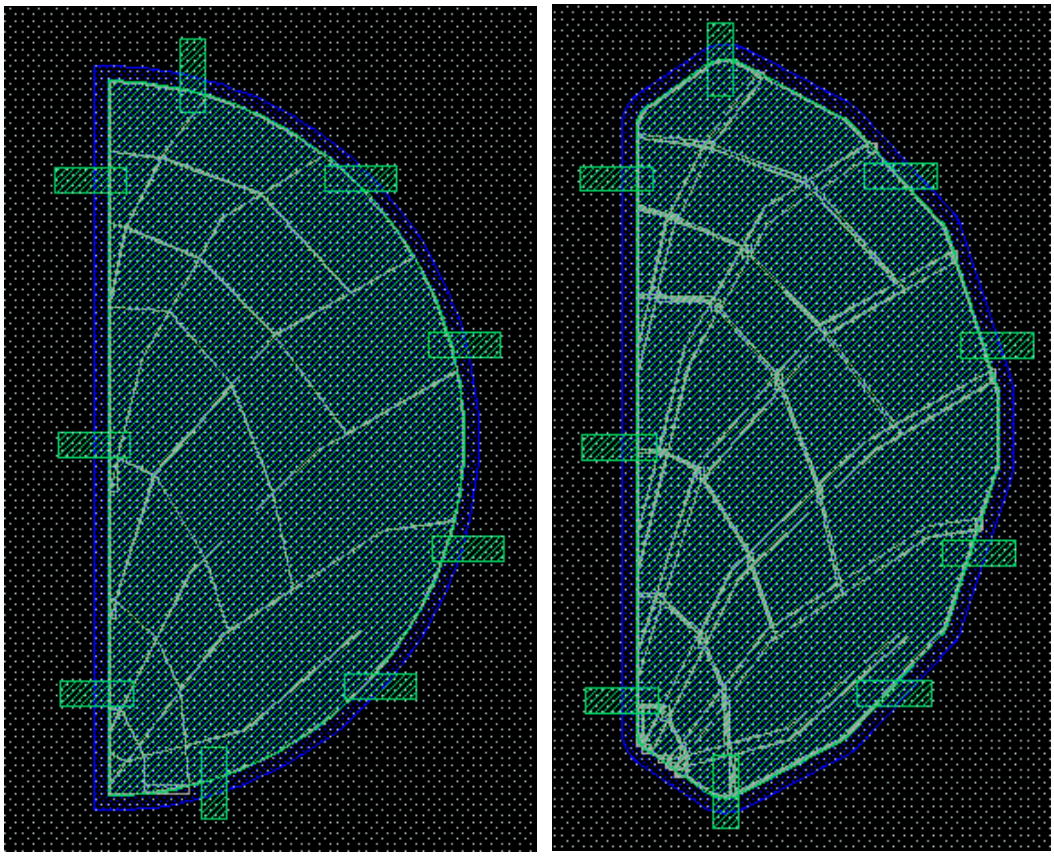

(c)

Figure 4.10: Wing designs (a) B shaped with honeycomb pattern (b) Fly inspired (c) Other variations

The completed mask is shown in Fig. 4.11.

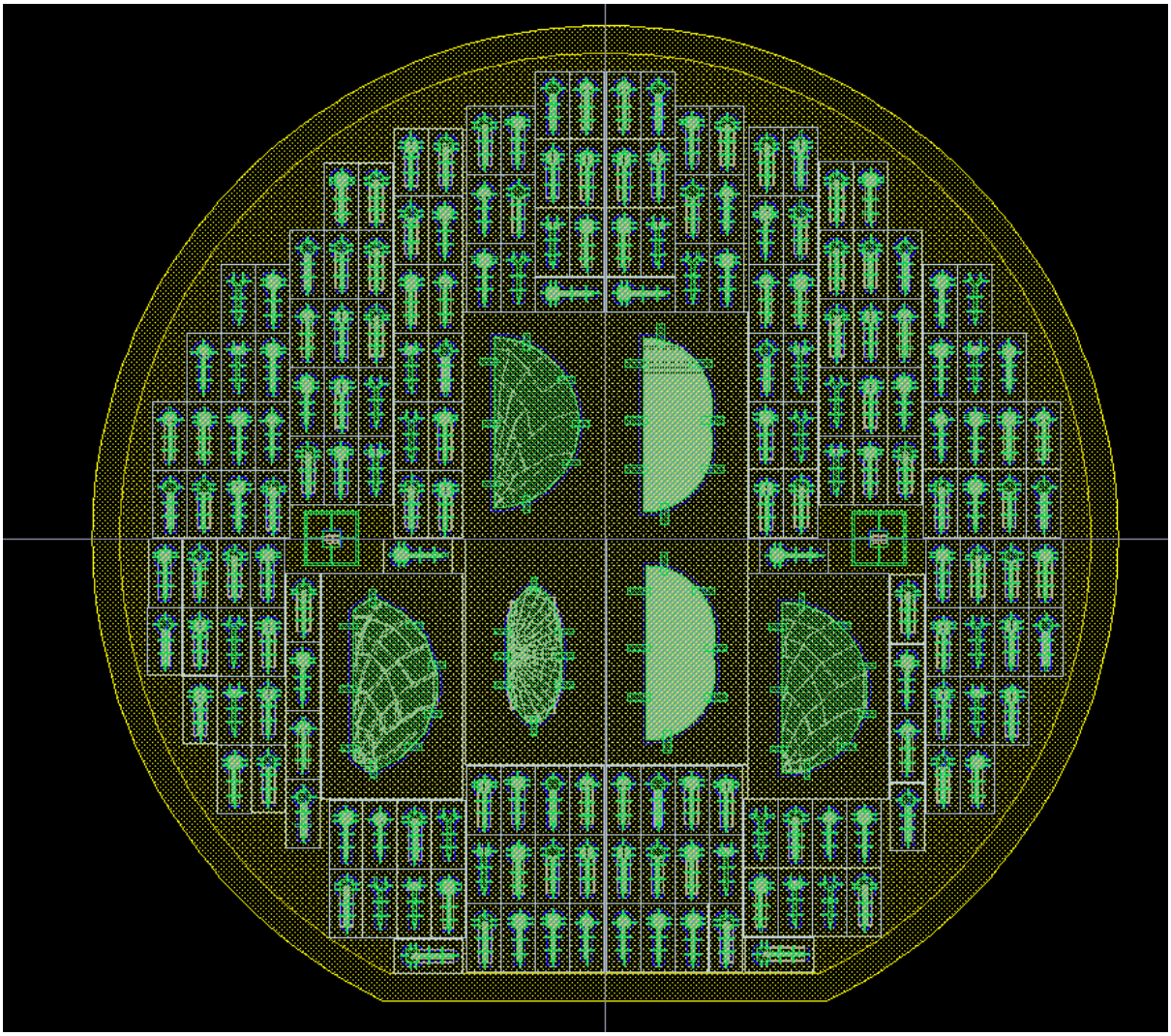

Figure 4.11: Completed mask

Chapter 5: Fabrication

5.1 Short-Loop Experiment:

Before the design of a dedicated mask-set an initial experiment was conducted using a test mask containing straight lines of varying width and pitch (Berend Street Mask) to test if the idea of polyimide foils with polyimide beam reinforcement was feasible and suitable for the requirements of the project. The process flow for this short loop experiment is described in the following sub section.

5.1.1 Process Flow of the Short-Loop Experiment:

The process was initiated by etching trenches to a depth of 5, 10 and 20 μm in the silicon using the Bosch process (Fig. 5.1). The wafers were then thermally oxidized at 1000°C to obtain an oxide thickness of 1 μm. Next, 2 μm of PECVD oxide was deposited on the backside of the wafers. The oxide was patterned by dry etching on the backside of the wafer to define the areas where the silicon will be removed by deep RIE etching. Polyimide was spin coated on the topside of the wafer. After curing of the polyimide at 400°C, the wafer was etched from the backside with the Bosch DRIE process using the 3 μm thick oxide layer as an hard etch mask and the oxide layer on the front side of the wafer as an etch stop. Once the oxide was removed by wet etching, a foil of polyimide, with reinforcement beams where the trenches were etched, was obtained. A detailed flowchart of the process is provided in Appendix A.

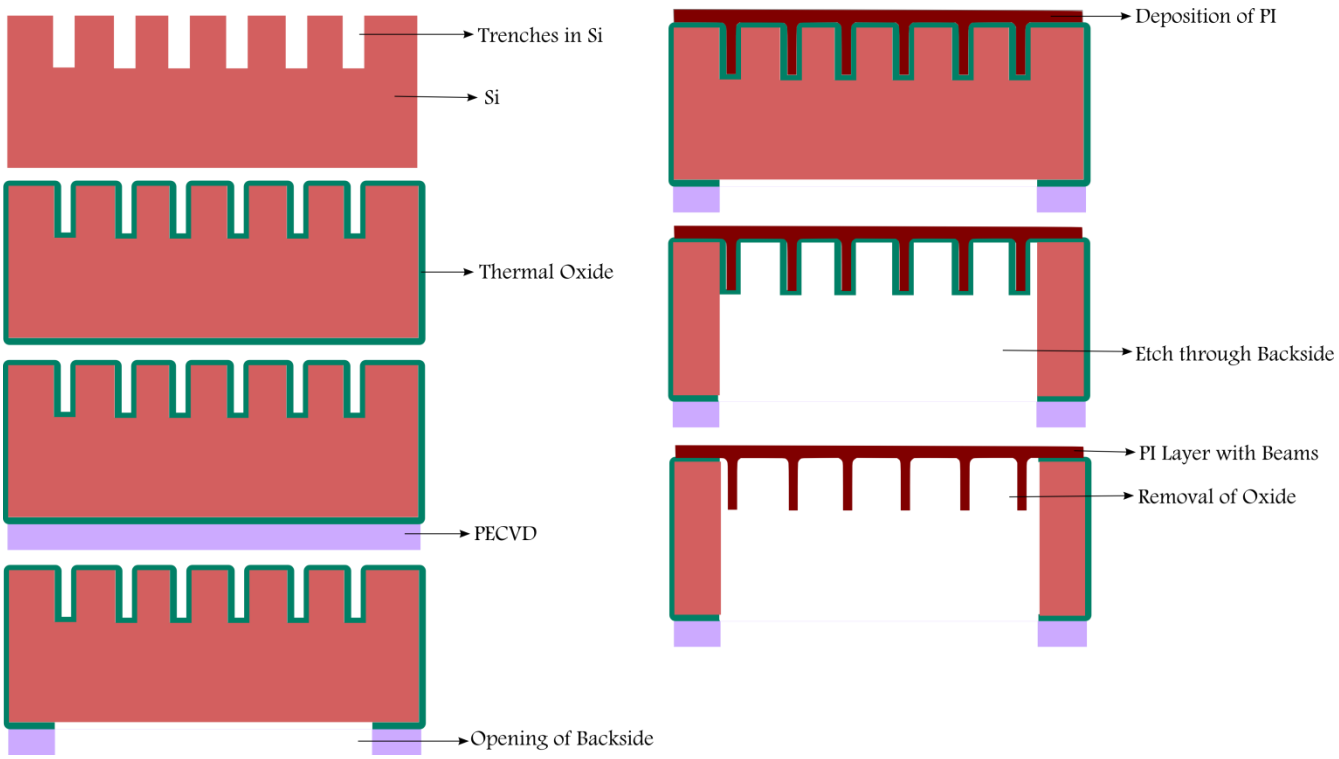

Figure 5.1: Process Flow for the Short Loop Experiment

The wafer with a trench depth of 5 µm was successfully completed. When the final wafer was inspected with a SEM (Scanning Electron Microscope), it was observed that the polyimide structures were very well defined (Fig. 5.2). A foil of polyimide supported by polyimide beams was obtained. The step height of the beams is 5 µm. The profile of the polyimide on the top side was also very smooth (Fig. 5.3).

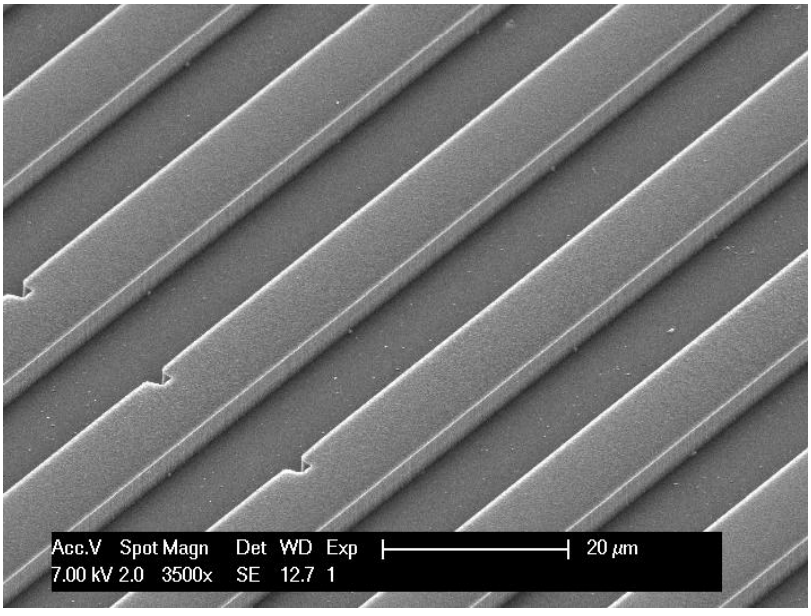

Figure 5.2: Polyimide foils with polyimide beam reinforcement

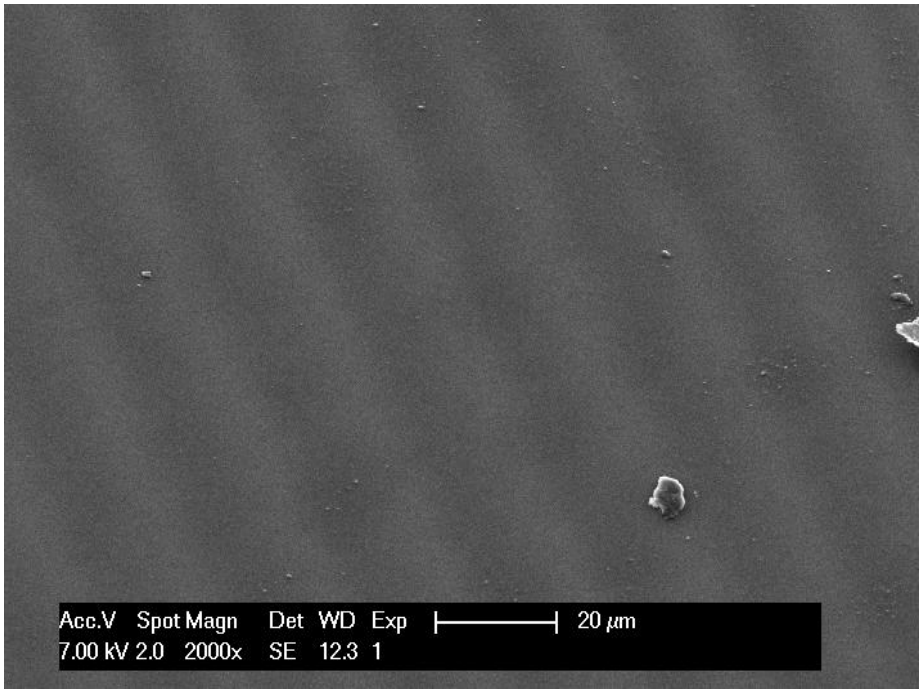

Figure 5.3: Flat polyimide layer as seen from the top

There was a problem with coating polyimide on the wafers with the deeper trenches (10 and 20 µm). Even though the layer of PI looked very uniform and smooth after spin coating, after curing (in the Koyo oven at 400 °C) it was observed that it was not properly distributed over the trenches and was completely absent in parts. After spin coating of the PI, the wafer is normally soft baked for 6 minutes on a hot plate at 120°C to remove the solvents from the polyimide. This is followed by a curing step at 400°C to crosslink the polyimide. It was hypothesized that the air trapped in the trenches might have escaped through the PI during the curing process or at the time of spin coating. Possibly the acceleration rate chosen for the spin coating process, might not be slow enough for the PI to settle into the trenches well. As a solution to this, a much slower acceleration was used during the spinning of polyimide to allow it to go into every trench. After the spin coating, the wafer was kept in a heated vacuum oven at 40°C for about 15 minutes (or till the structures were visibly well defined). This caused any trapped air to be sucked out of the trenches while the PI layer was still not set. Then the wafer was soft baked and subsequently cured. After this process modification a uniform coverage of polyimide was obtained and the trenches were completely filled.

5.2 Main Fabrication Sequence:

Since the masks that were designed contained two designs for the two different rib constructions; the first being the polyimide foil with beams of polyimide and the second with added silicon beams inside the polyimide beams, the wafers were divided in to two lots, and the processing of both variations was carried out in parallel.

5.2.1 Fabrication Sequence for the Polyimide-Only Beam Reinforcement

This process was essentially similar to the one done earlier, except for the additional patterning of the polyimide. Trenches of depth 10 – 25 μm were etched in silicon (Fig. 5.4). The wafers were then thermally oxidized at 1000°C to obtain an oxide thickness of 1 μm. Next, 2 μm of PECVD oxide was deposited on the backside of the wafers. The oxide was patterned by dry etching to serve as a hard etch mask during the DRIE etching later on in the process. Polyimide was spin coated on the topside. After the air in the trenches was removed by placing the wafers in a vacuum oven, the PI was soft baked on a hot plate and subsequently cured at 400°C to allow the polymer to crosslink. An Al-Mb-Al hard etch mask was sputtered onto the polyimide and patterned in PES etchant. Next the wafer was DRIE etched from the backside using the thick oxide layer at the bottom as a hard etch mask and the oxide layer on the top side as an etch stop. The exposed polyimide was dry etched, and subsequently the Al-Mb-Al mask and the remaining oxide were removed by wet etching. A detailed flowchart of the process is provided in Appendix B.

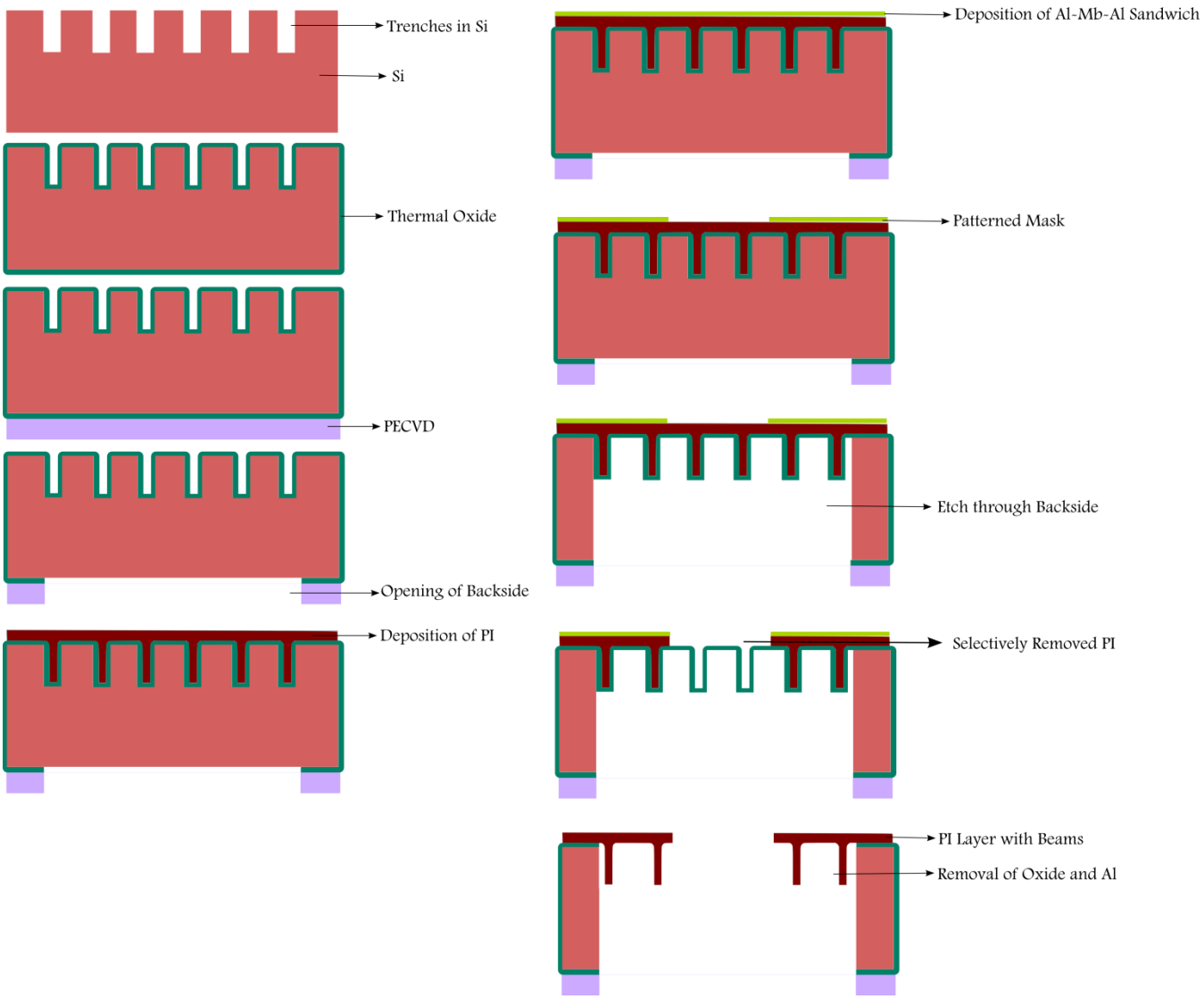

Figure 5.4: Fabrication sequence

Certain stages of the fabrication sequence are discussed next. Once the PI was cured, the wafer was DRIE etched from the backside using the 3 µm layer of oxide as the hard etch mask and the 1 µm layer of oxide on the top as the etch stop. The oxide hard etch mask layer thickness used was the same thickness as used in another project where a complete 6-inch wafer was etched through. In that project large only areas with dimensions in the millimeter range were etched. However, in this case once the DRIE etch reaches the high aspect ratio polyimide ribs the etch rate of the silicon in between the polyimide ribs reduces significantly resulting in a much longer etch time required to completely remove all the silicon. As a result the 3 µm thick oxide layer was too thin. Therefore, for the next fabrication sequence, thinner (400 µm instead of the standard 675 µm), double side polished wafers (to allow for lesser thickness variation) were used and 3 µm of PECVD oxide was deposited on the backside as

opposed to the 2 μm used before. This gave an additional micron of thickness to the hard etch mask and lesser Si to be etched through. The process was repeated, and DRIE etching was successful with these changes. The wafer at this stage is shown in Fig. 5.5.

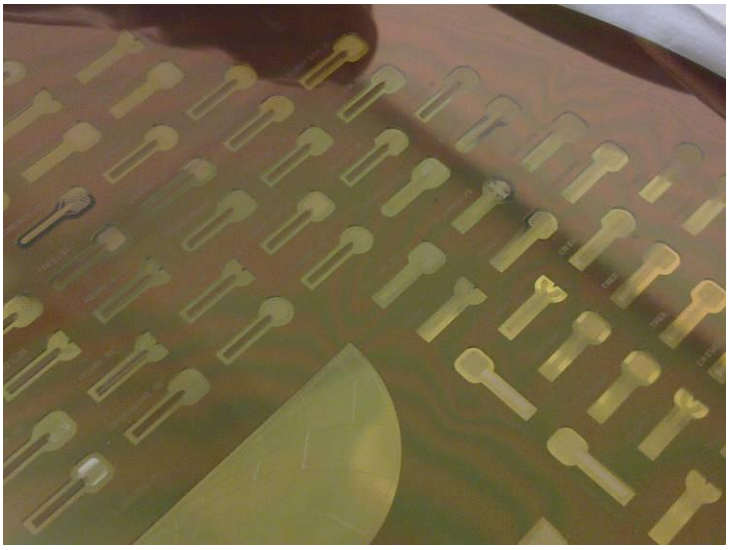

Figure 5.5: Wafer with cured PI

The instruments were inspected with a microscope and Fig. 5.6 shows a few images acquired.

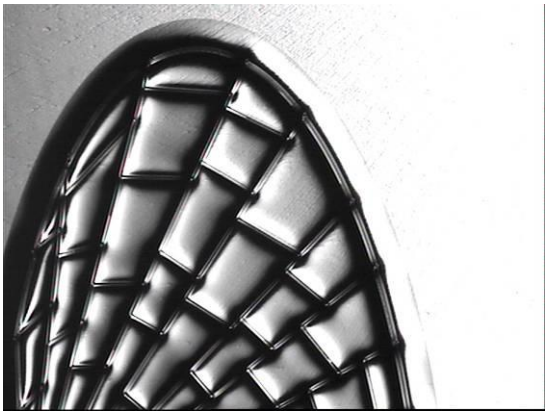

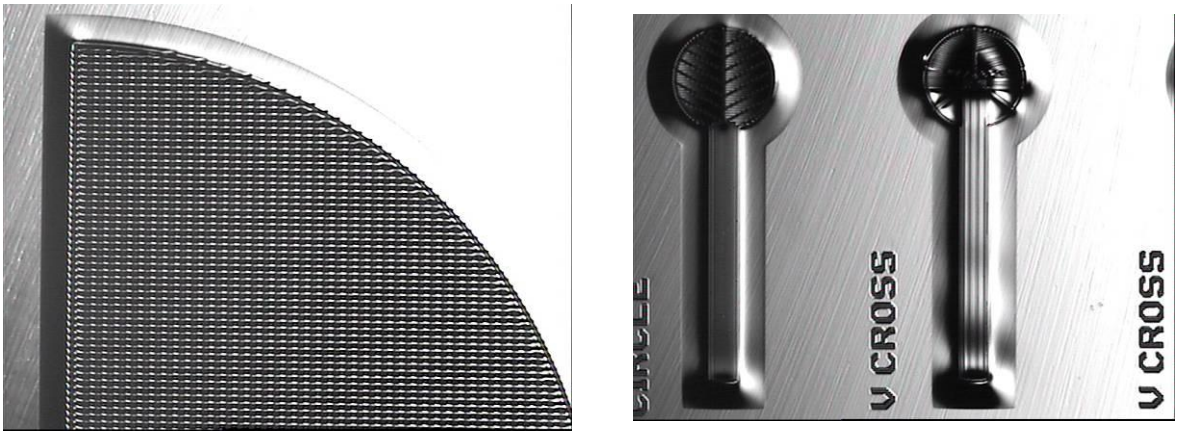

Figure 5.6: Microscopic inspection of the wafer after successful DRIE etching using the thinner wafers and thicker hard etch mask

Individual instruments were inspected with the SEM and the results are shown in Fig. 5.7. It is to be noted that at this stage the fabrication sequence is the same as the short loop since the 3rd mask has not been used yet. The oxide layer has also not been wet etched. Figure 5.7(a) shows one instrument with a Si beam support on its stick. Figures 5.7 (a, b, c) show the extremely well defined polyimide structures. The last two pictures in the figure show the Si beam supporting the instrument. The polyimide structures have very sharp, clearly defined walls even at the point where they meet the Silicon beam.

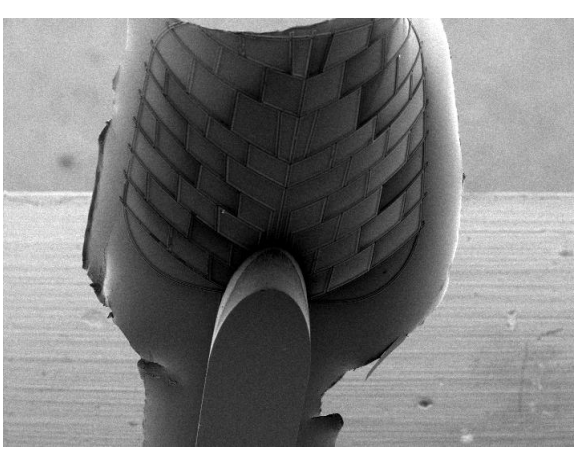

(a)

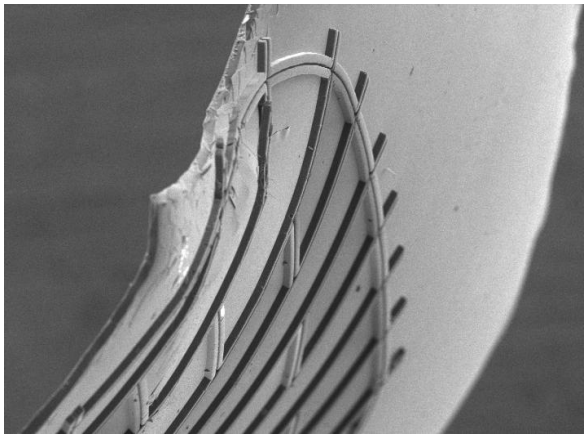

(b)

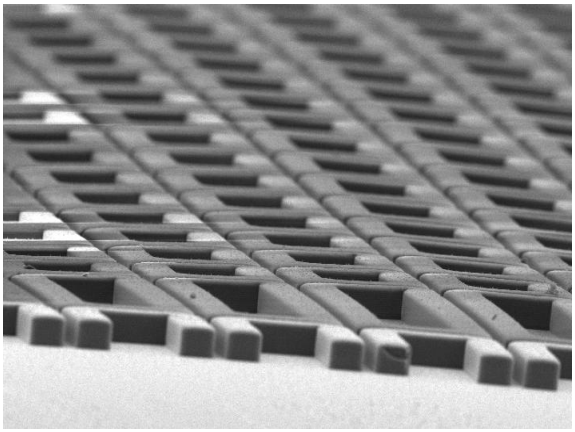

(c)

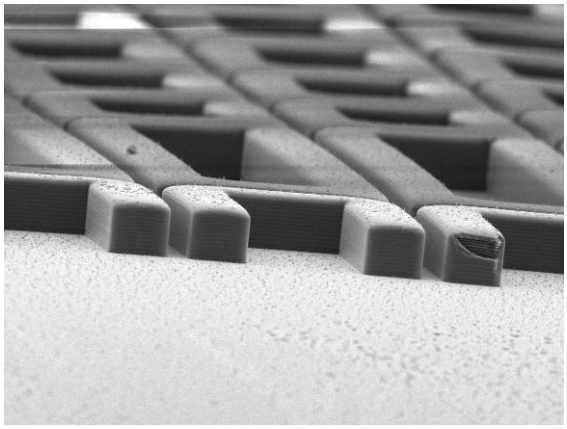

(d)

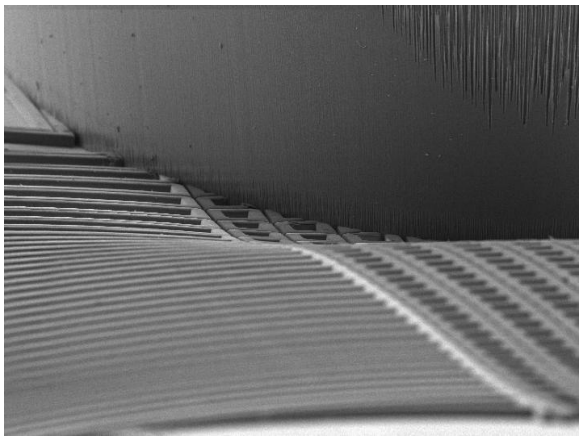

(e)

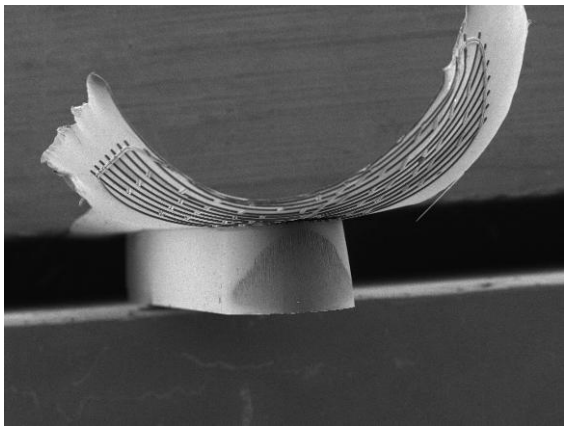

(f)

Figure 5.7: SEM inspection of the instruments after DRIE etch

The fabrication was continued and the Al-Mb-Al hard etch mask was sputtered on the top side of the wafer. The purpose of using the sandwich of Al and Mb instead of just a layer of Al is to ensure that pinholes occurring in the layer during sputtering do not propagate through the whole layer stack, thereby preventing defects to occur during the etching steps which follow.

Once this mask was patterned in PES etchant, the wafer was DRIE etched from the backside as before, using the 4 μm of oxide as the hard etch mask and the 1 μm of oxide layer on the top as the etch stop. The wafer was placed in the barrel with a standard PI etching recipe to selectively etch the PI. However, the samples were separated from the wafer during this process. There could be a few explanations for this to occur. One would be that the etching was done for too long and there was an extreme undercut of the polyimide even below the protective Al-Mb-Al mask. The hinges were etched away and the instruments separated. The

second explanation may be that the mask lifted off during the etching, leaving the required parts of the polyimide unprotected. A microscopic inspection of the samples was done. Figure 5.8 shows some pictures. It is obvious that the polyimide (yellow) was etched even below the hard etch mask of Al-Mb-Al (metallic silver). The green parts are the oxide layer. The undercut is very severe and not likely to have been caused due to over etching. It is therefore probable that the mask lifted during the process. In order to avoid this, it is suggested to sputter etch the wafer for 20 nm before the sputtering of the mask. It is expected that this will provide a better adhesion between the mask and the polyimide layer.

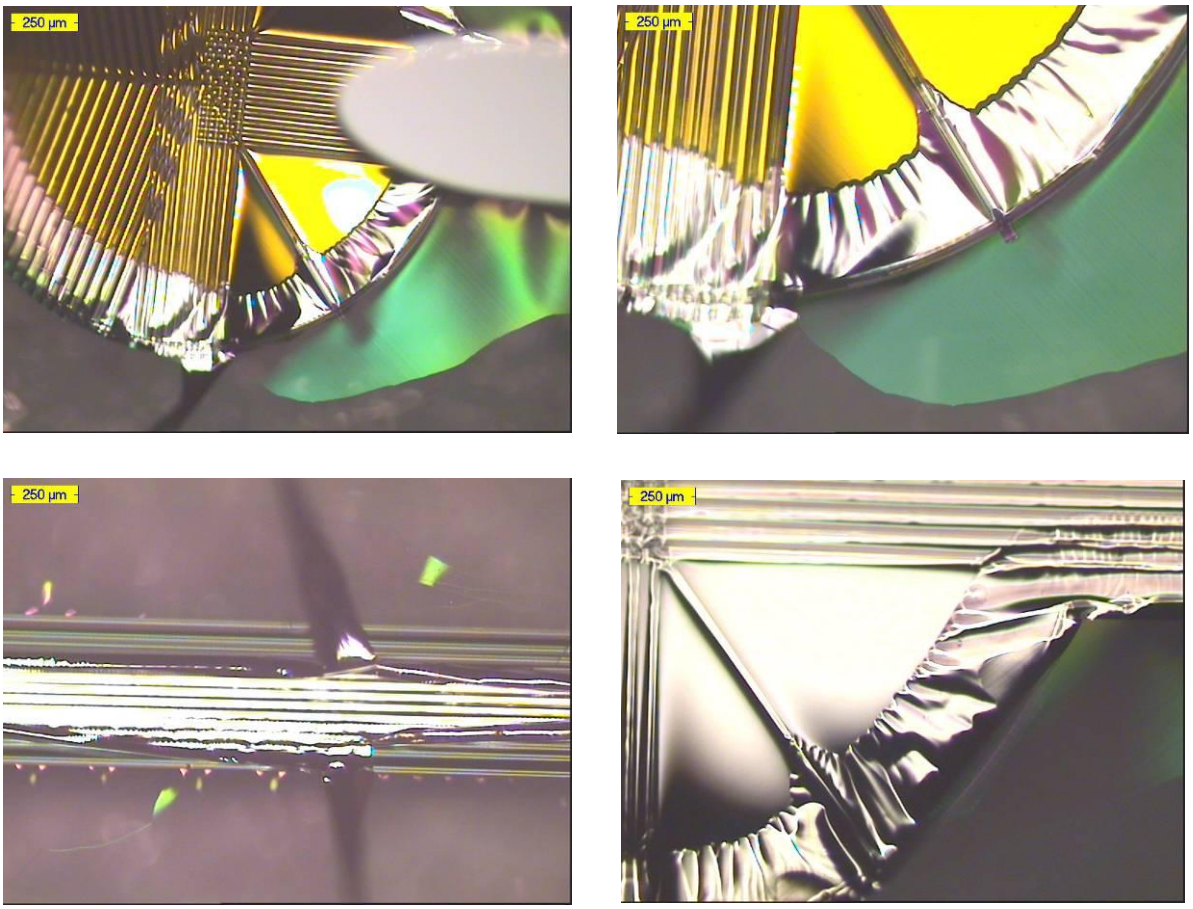

Figure 5.8: Samples after dry etching of polyimide

SEM images of these samples are shown in Fig. 5.9. The polyimide is visibly etched away from underneath the mask.

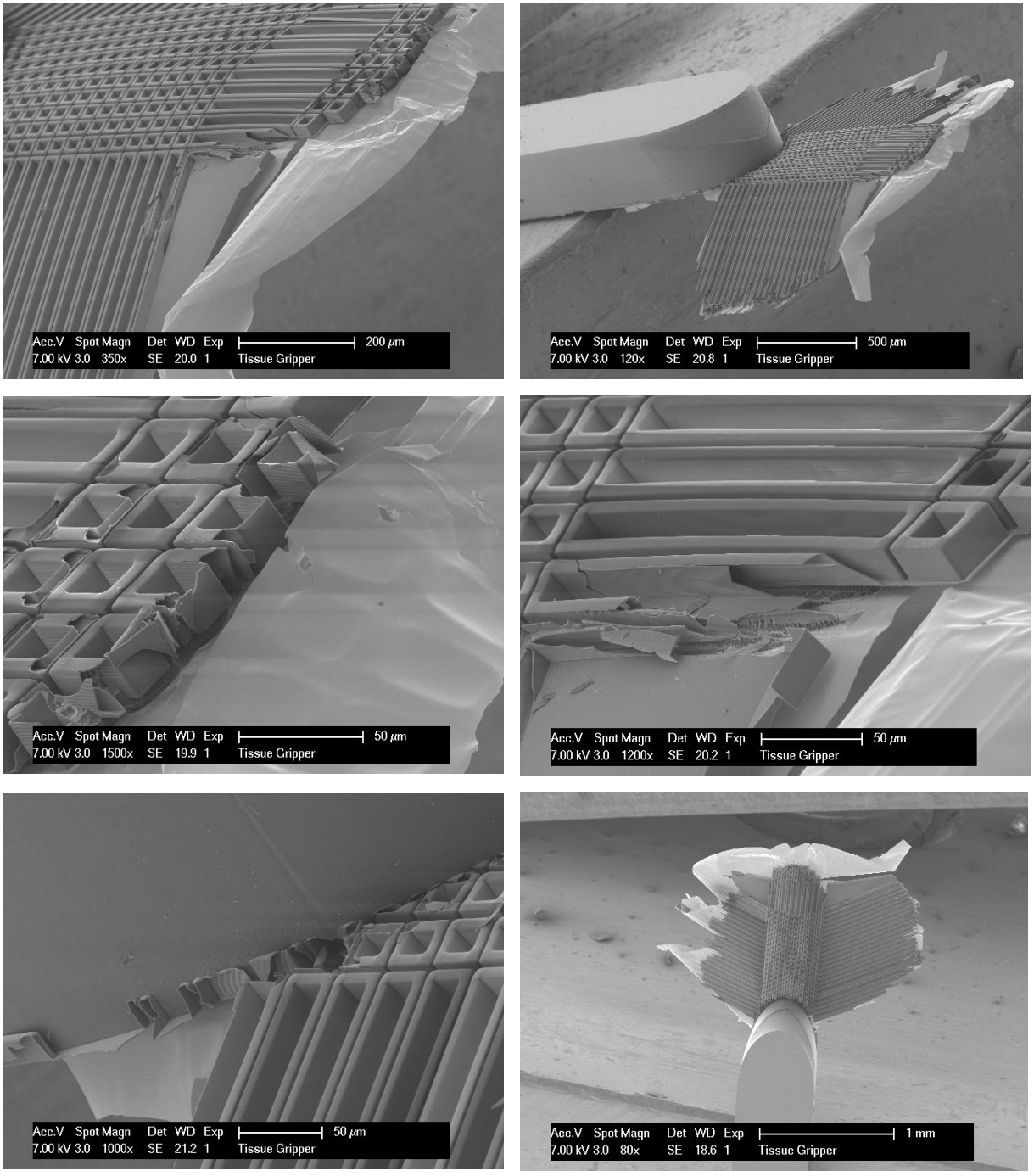

Figure 5.9 SEM images of the samples after polyimide etching

Since the samples got separated from the wafer, individual instruments (and wings) had to be wet etched (cold KOH for the Al and BOE for the oxide) to obtain the final samples. The details of the process are provided in Appendix B. Figure 5.10 shows one sample compared

to a normal staple pin for reference in order to appreciate the small feature size of the instrument.

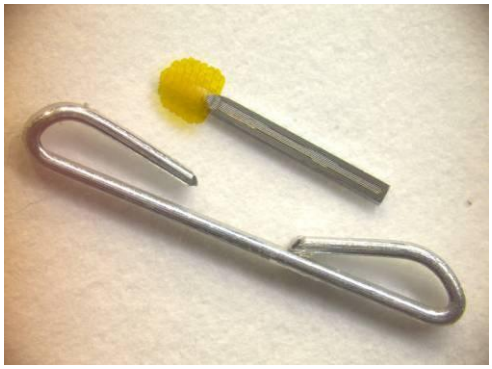

Figure 5.10: Instrument sample compared to a staple pin for reference.

Figure 5.11 micro-photographs of some prepared samples. It is seen that the very heavy patterns, having a dense rib pattern like in Fig. 5.11 (c, d) are not flat. The picture in Fig. 5.11 (e) shows the polyimide stick of the instrument supported on the Si beam (the undercut is evident). Figure 5.11 (f) shows a close up of the foil with the beam patterns.

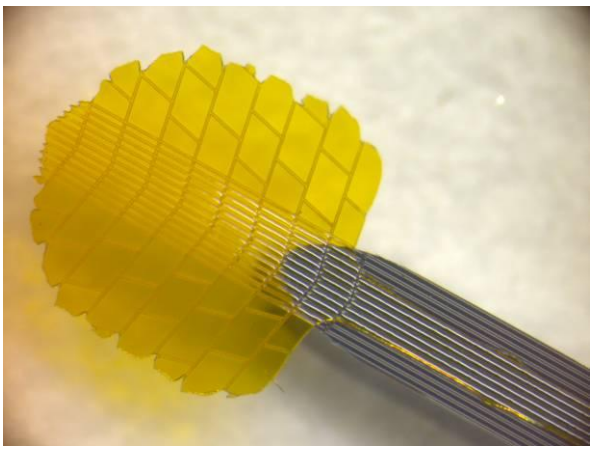

(a)

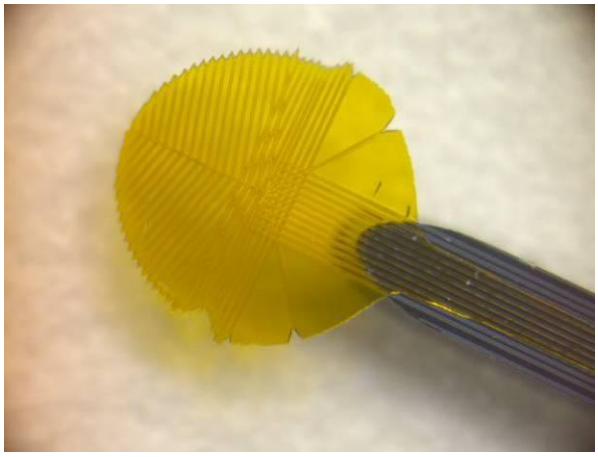

(b)

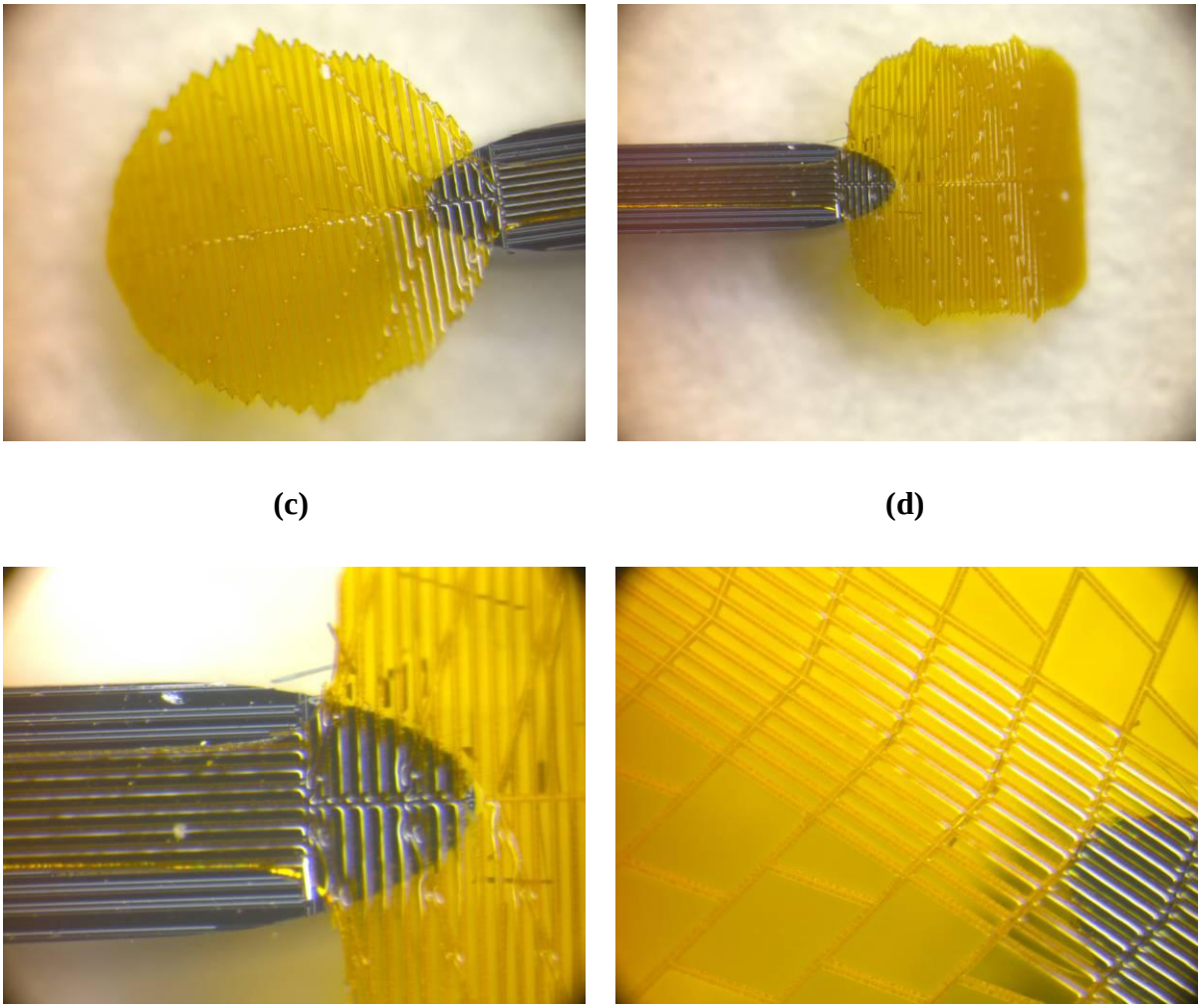

(c) **(d)**

(e) **(f)**

Figure 5.11: Prepared Samples as viewed under a microscope

Some samples were inspected with the SEM and Fig. 5.12 shows the images captured.

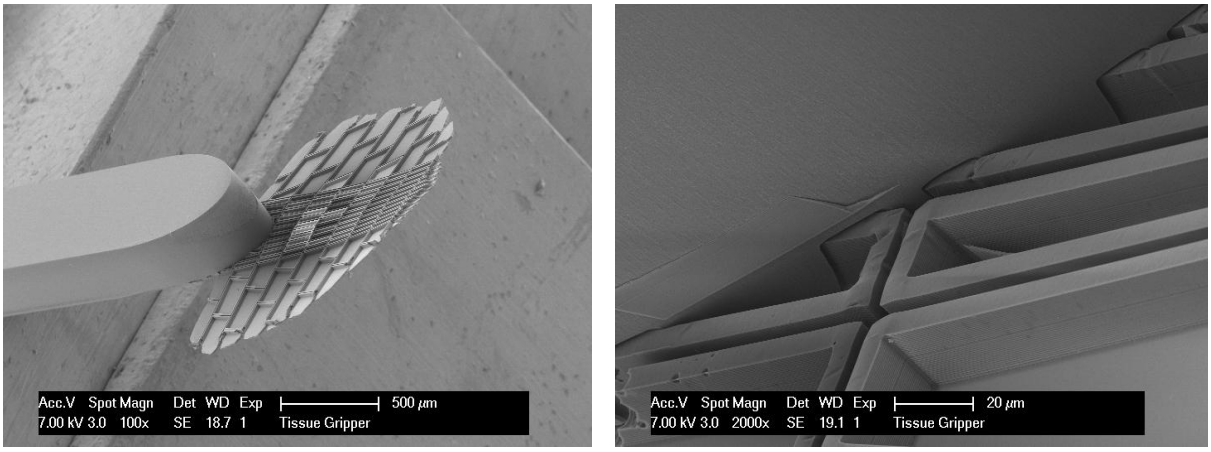

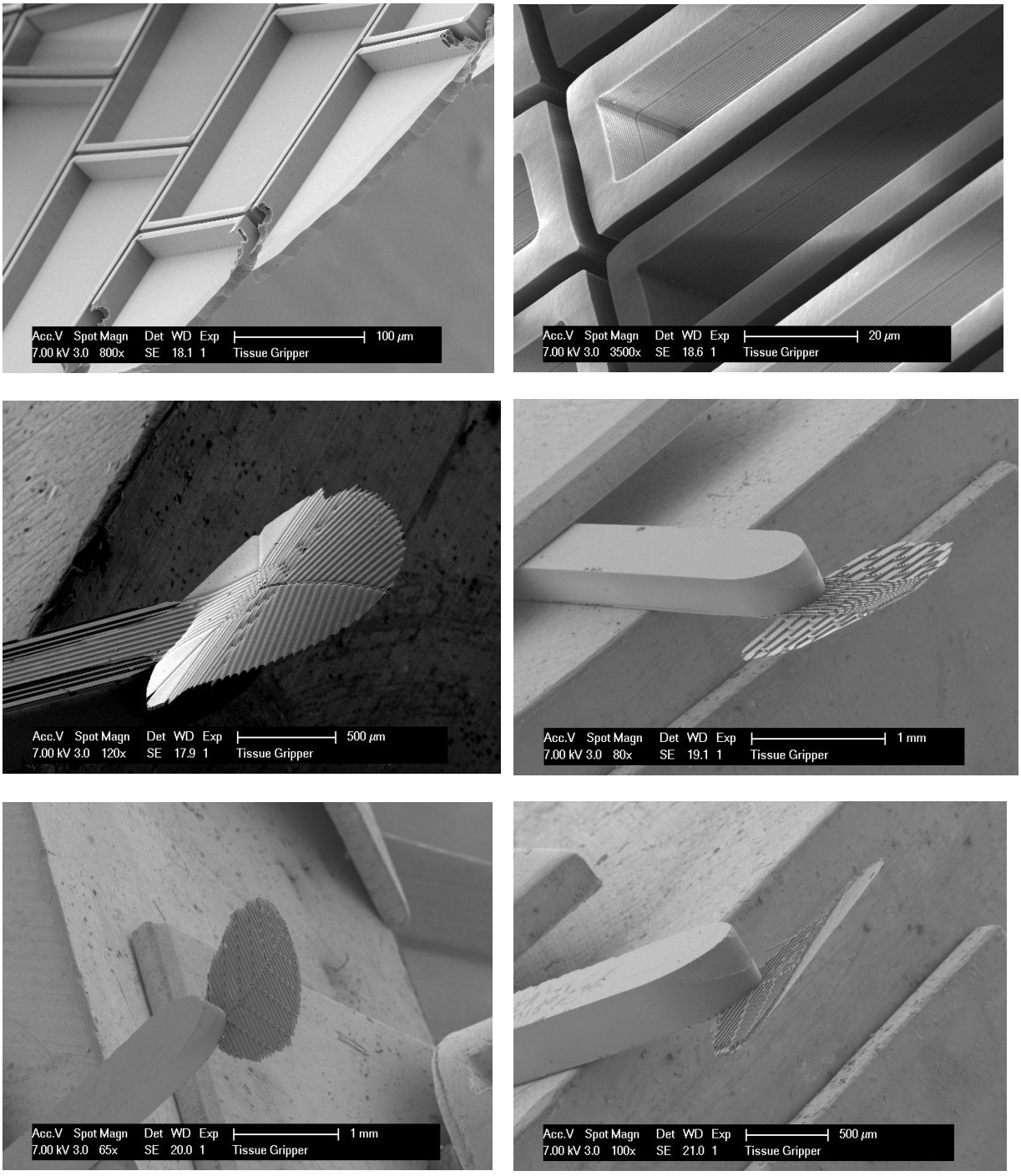

Figure 5.12: SEM images of the final samples

The edges of the samples are ragged due to the undercut during the PI etch. Apart from that, the instruments look promising. The PI beams (25 µm deep from the surface of the foil for these samples) have a well defined structure and the patterns in which they are made affect the flatness and stiffness of the instruments. It is seen that the instruments with very heavy patterns curve to the side of the foil which contain the beams. The beam patterns must be refined before the next fabrication sequence starts. Samples were also viewed from the side

of the instrument where the polyimide layer is supposed to be flat in order to see the conformity of the polyimide during spin coating. It is not desirable to have bumps during deposition (Fig. 5.13).

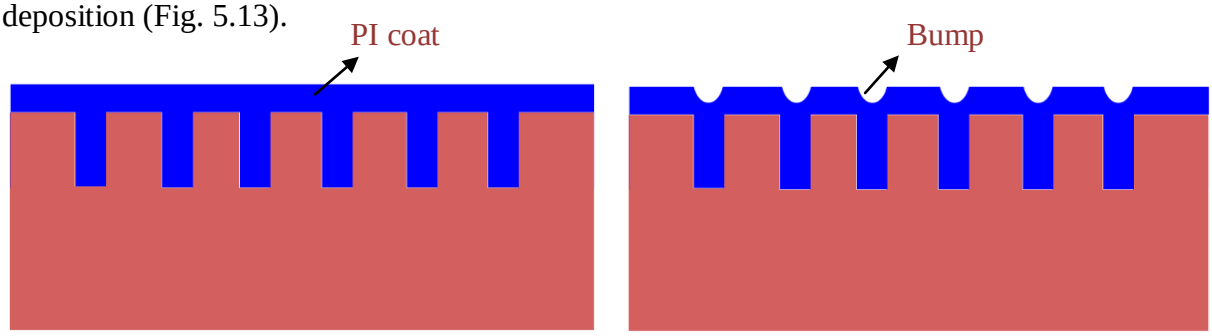

(a) **(b)**

Figure 5.13: (a) Conformal deposition of PI (b) Bumps in the coating where trenches exist

The SEM pictures are shown in Fig. 5.14. The polyimide is reasonably flat and uniformly deposited. The depth of the trenches for these wafers is 25 μm. Pictures e and f are taken from the samples which were made without the use of the third mask. They too show a flat and well deposited polymer.

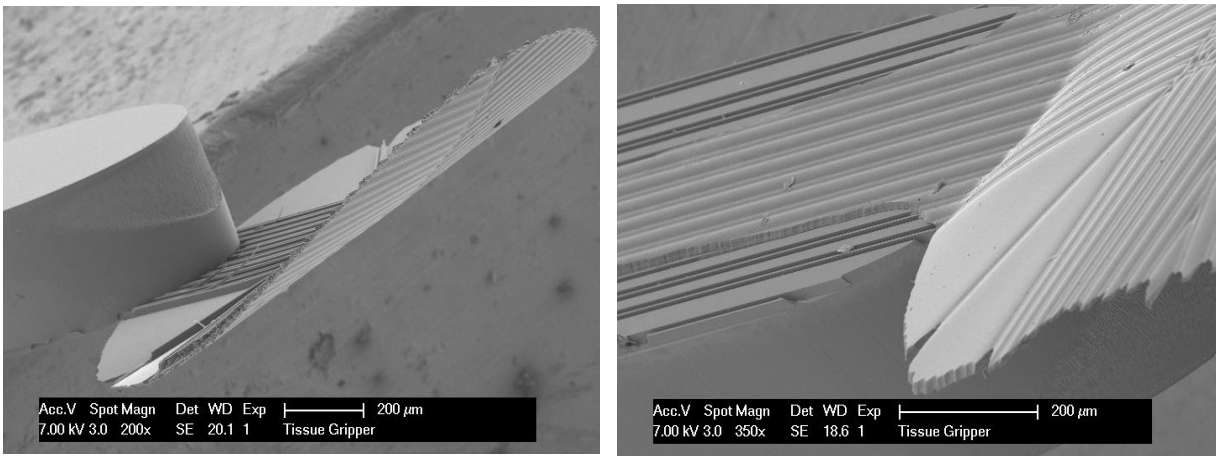

(a) **(b)**

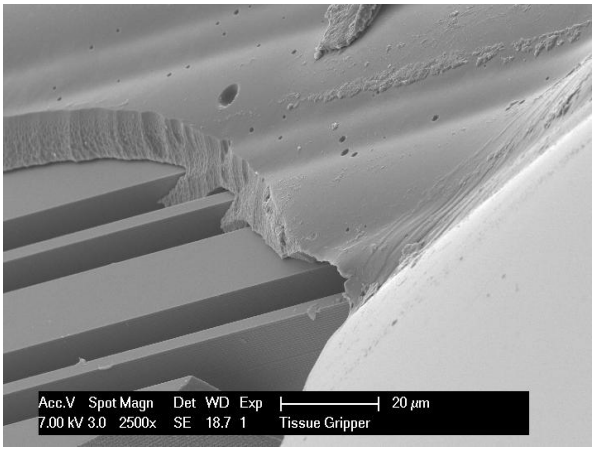

(c)

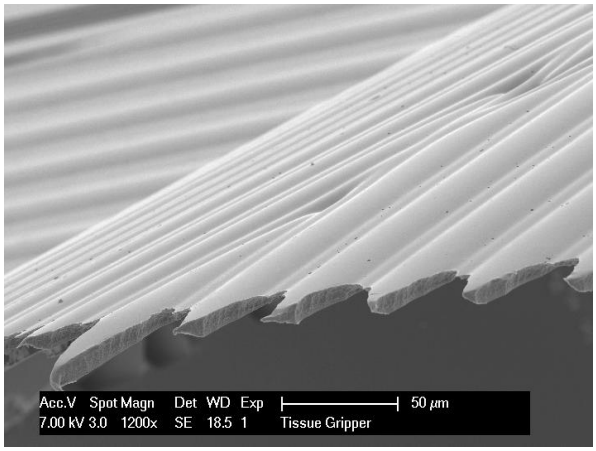

(d)

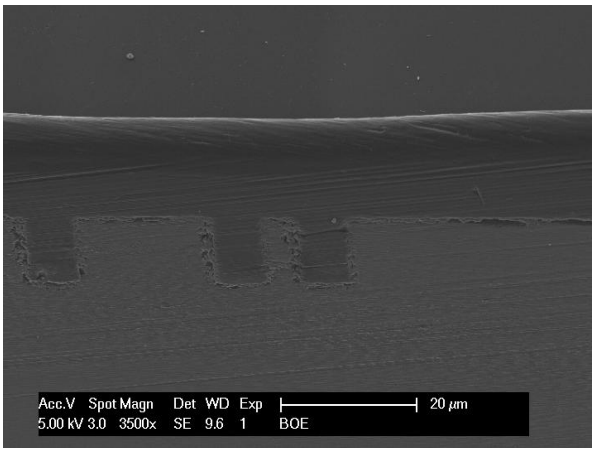

(e)

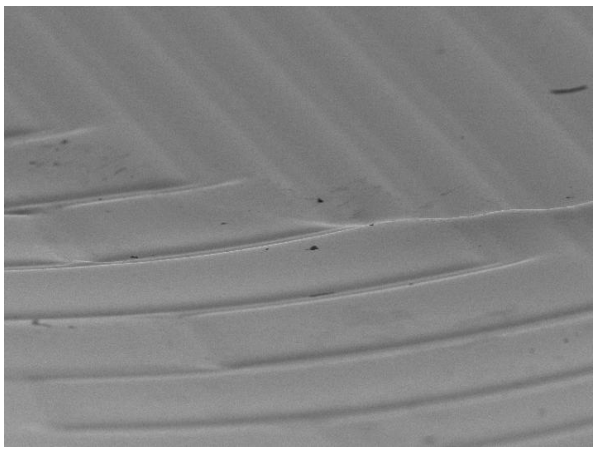

(f)

Figure 5.14: SEM pictures to inspect the flatness of the PI layer

The stiffness of these samples was measured and the findings are presented in the next Chapter.

5.2.2 Fabricating Instruments with Free Standing Silicon Beams Inserted into the Polyimide Beams

The addition of Si beams would provide more strength to the beams and thus give better support to the instruments. The idea behind the fabrication of the silicon reinforced beams is to etch anisotropically to a certain depth and then isotropically until the beams are released. This is depicted in Fig. 5.15.

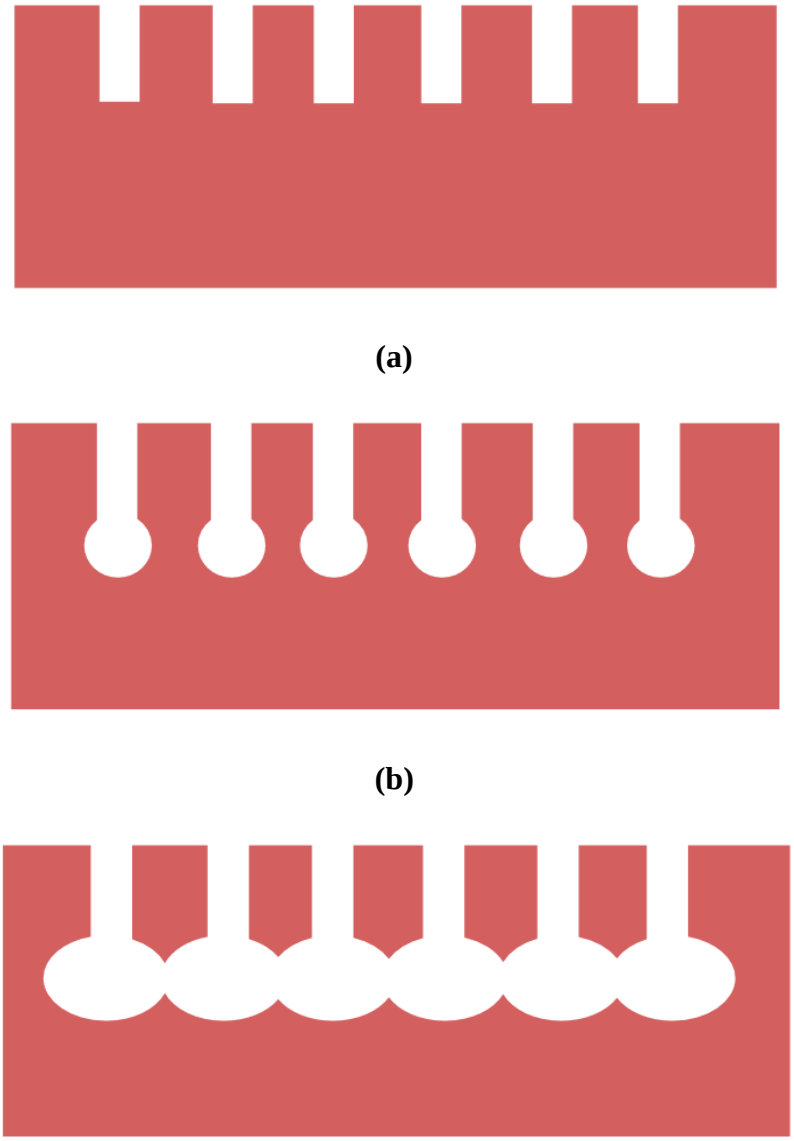

Figure 5.15: Fabricating free standing Si beams

Apart from this step, the rest of the fabrication sequence continues like in Fig. 5.4. Various recipes for the etching procedure were tried. However, the free standing beams could not be obtained. Fig. 5.16 shows the various tries to obtain the free standing structures. In the first experiment, the trenches were anisotropically etched for 20 minutes and 30 seconds and then a passivation layer was deposited for 1 minute. A 30 second clear bottom cycle followed to remove the passivation and isotropic etching was then done for 3 minutes. This did not work and the structures were completely destroyed. There was a huge undercut and the beams were eaten away (Fig. 5.16 (a)). In order to understand what was happening, the experiment was repeated but without the isotropic etching at the end. It was seen that just with the clear

bottom step, the beams were isotropically etched 2 μm deep and there was an undercut of about 400 nm to the sides (Fig. 5.16 (b)). As a result, the clear bottom step was extended to 90 seconds. Even though the beams were close to separation, severe damage was done to the tops of the beams (Fig. 5.16 (c)). The clear bottom cycle was extended and made 100 seconds but the undercut was huge and the beams were eaten away.

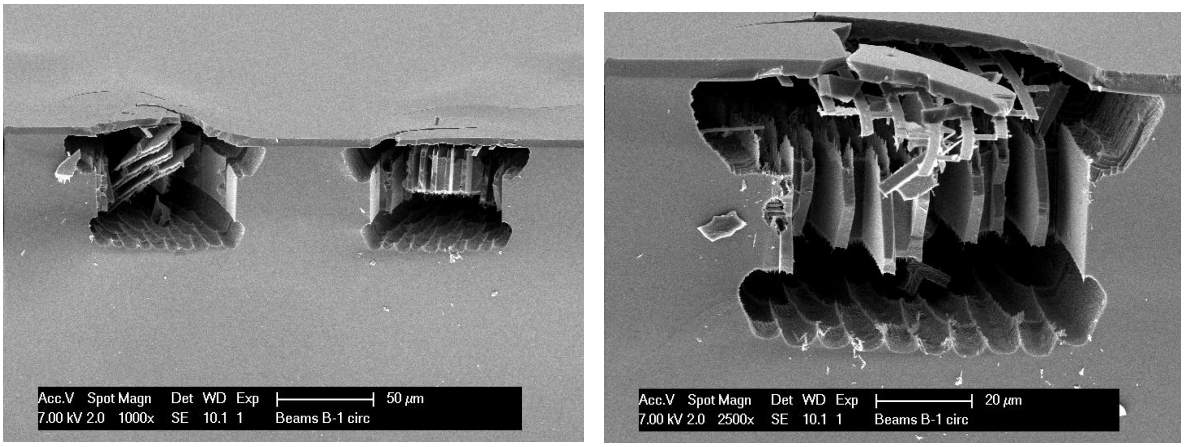

(a)

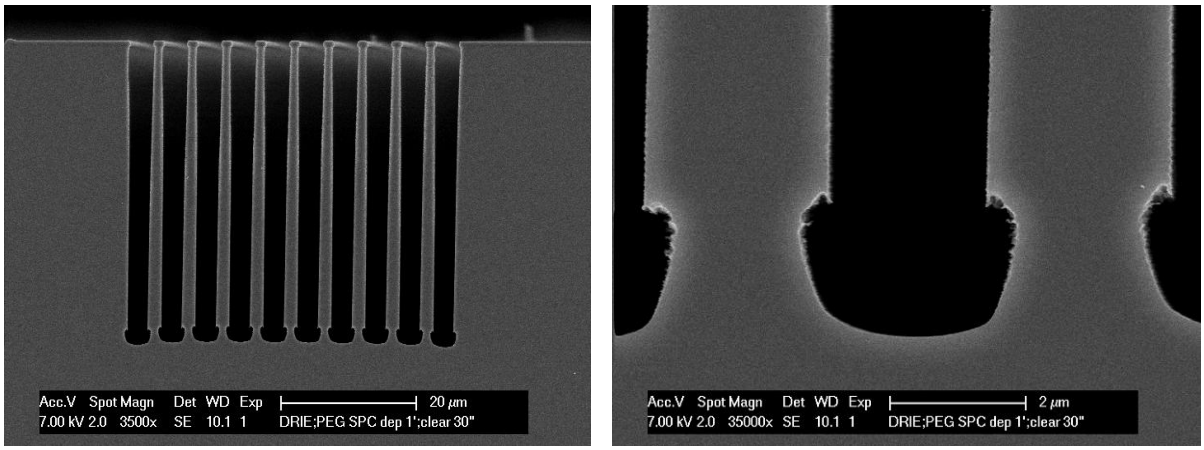

(b)

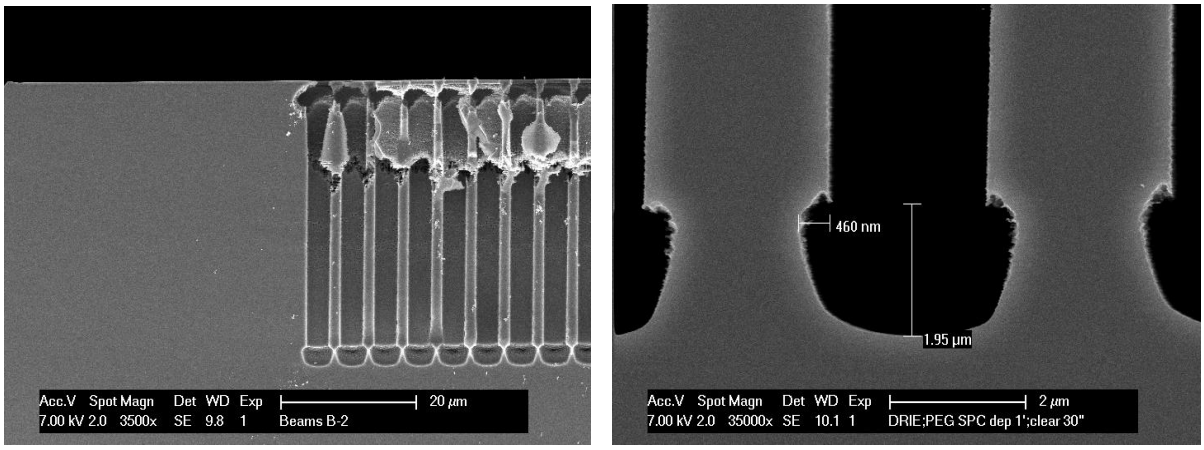

(c)

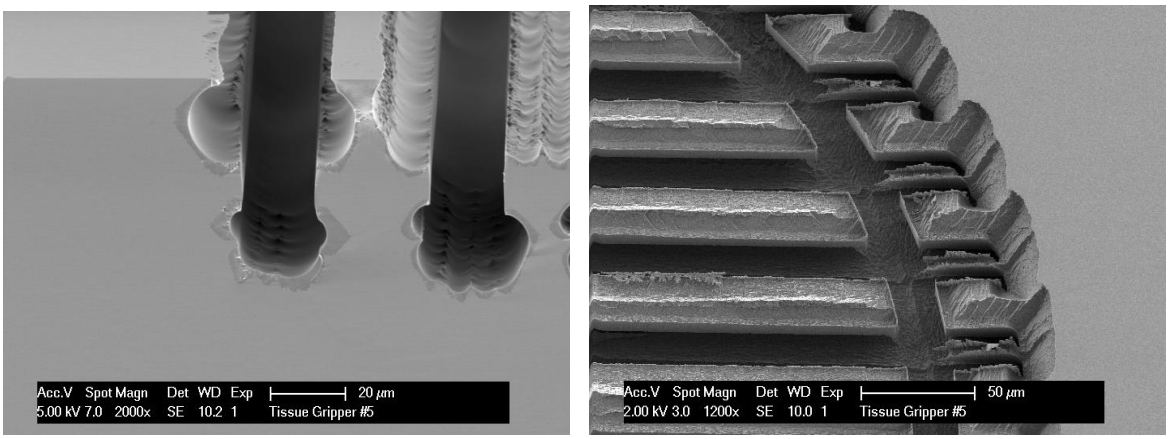

(d)

Figure 5.16: Various tries to obtain free standing beams

This aspect of the fabrication needs to be improved upon and the correct recipe found to obtain free standing beams.

Chapter 6: Stiffness Measurements

6.1 Measurement Setup and Results

In order to understand the effect of the different rib patterns on the strength and flexibility of the instruments, their stiffness was measured. The measurement set up consisted of a silicon based force and torque sensor which was designed and fabricated at the Faculty of 3mE, Department of Precision and Microsystems Engineering, TU Delft (Fig. 6.1). The setup had independent force/torque detection with six degrees of freedom (DOF) (using 16 silicon integrated piezoresistors), a wide force range (30 - 37 mN) and a high resolution (at µN and µNmm level) [14]. A micro needle was used to deflect the instrument and the force in the direction of the needle was measured. The stiffness was calculated from the force and the resulting displacement.

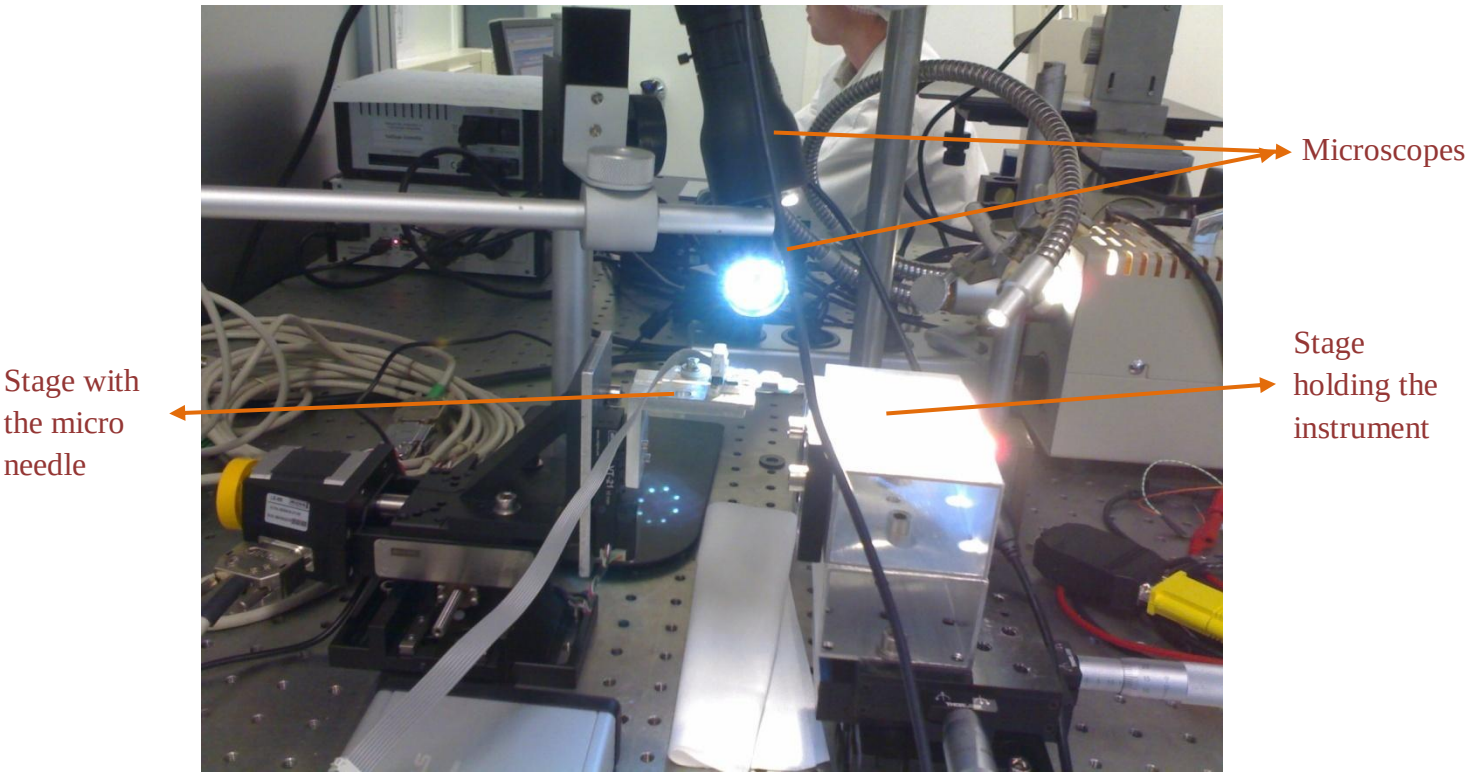

Figure 6.1: Measurement setup

The DMC Smart Terminal was used to manipulate the positioning of the needle by moving the stages supporting the setup, and the Femtotools Controller was used in order to register the force. Two microscopes were strategically positioned to accurately observe the position

of the needle. The needle could be moved in steps of 78.125 nm. Figure 6.2 shows a snapshot of the softwares used.

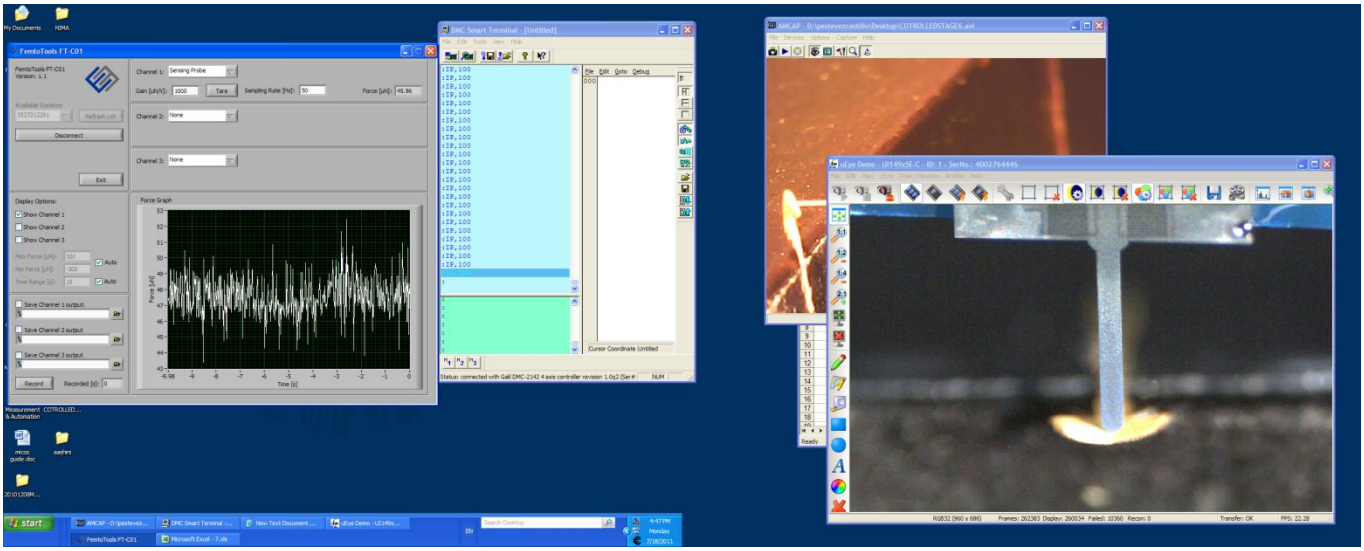

Figure 6.2 Softwares used for measuring the stiffness

The main commands used in the DMC Smart Terminal are listed in Table 6.1.

Command	Action
SH	Turn on, to control the setup via the software
IP (IPval,val,val,val)	Increment position (move table sideways, move table forward or backwards, not connected, move table up or down)
MO	Motor off, allowing for manual positioning of the setup table

Table 6.1: Commands used in the DMC Smart Terminal

To calculate the stiffness, the needle was made to push against the instrument. As the instrument was bent, the force was measured and noted for different displacements. The number of steps (between 2 force measurements) given to the needle were noted. The displacement was calculated by multiplying the number of steps with the step size of 78.125 nm. The stiffness was then calculated by dividing the difference in force values by the displacement. The results are presented in Fig. 6.3.

a)

Instrument:	Camera 1:
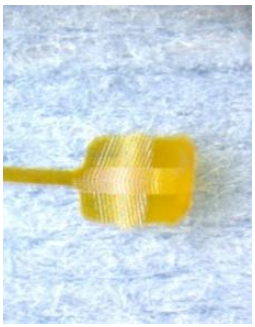	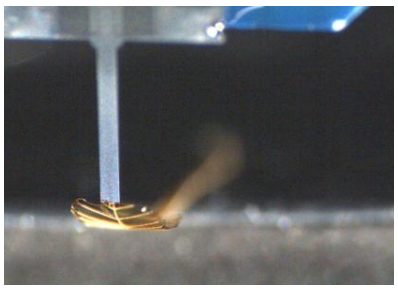
Camera 2:	**Stiffness:**
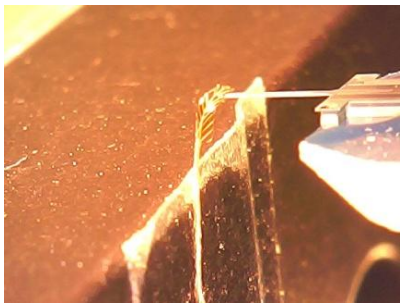	Number Steps 1300 Distance 0.000102 Force1 26 Force 2 44 Stiffness 0.177231 The force is in µN and the stiffness in µN/m

b)

Instrument:	Camera 1:
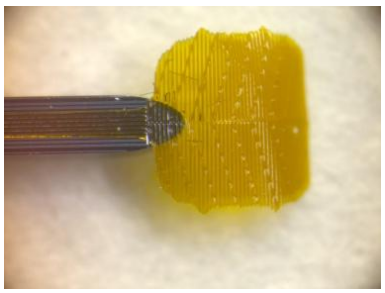	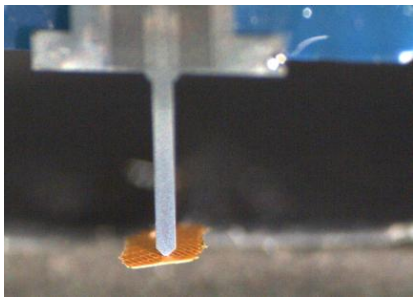
Camera 2:	**Stiffness:**
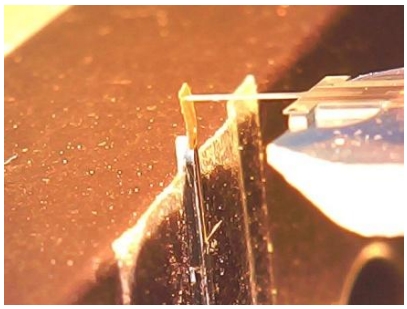	Number Steps 800 Distance 6.25E-05 Force1 49 Force 2 92 Stiffness 0.688 The force is in µN and the stiffness in µN/m

c)

Instrument: 	Camera 1: 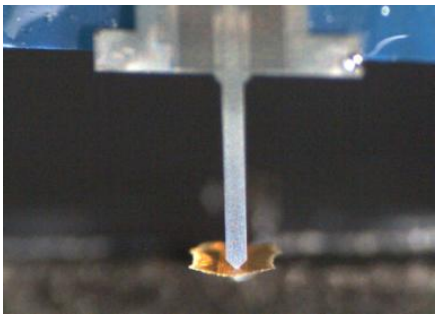
Camera 2: 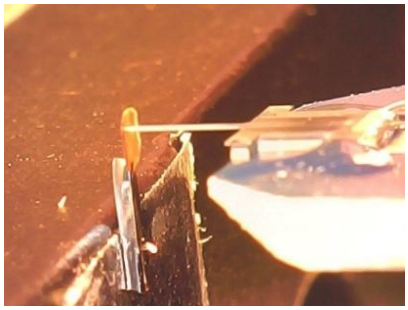	Stiffness: Number Steps 500 Distance 3.91E-05 Force1 178 Force 2 420 Stiffness 6.1952 The force is in µN and the stiffness in µN/m

d)

Instrument: 	Camera 1: 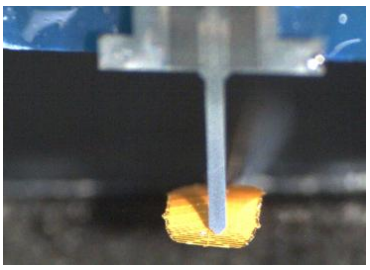
Camera 2: 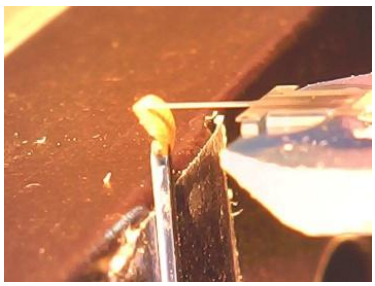	Stiffness: Number Steps 400 Distance 3.13E-05 Force1 20 Force 2 30 Stiffness 0.32 The force is in µN and the stiffness in µN/m

e)

<table>
<tr>
<td>Instrument:
 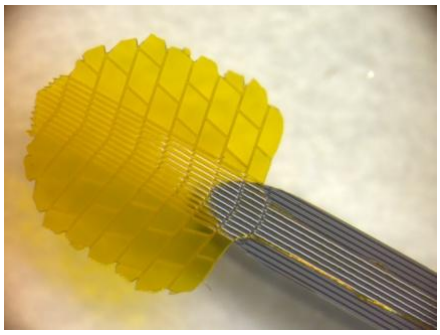 </td>
<td>Camera 1:
 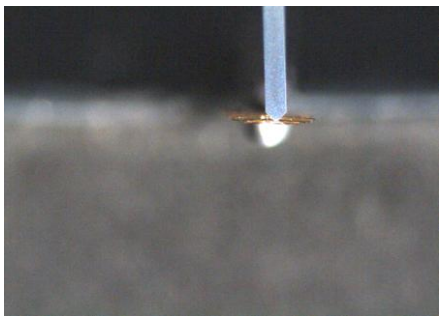 </td>
</tr>
<tr>
<td>Camera 2:
 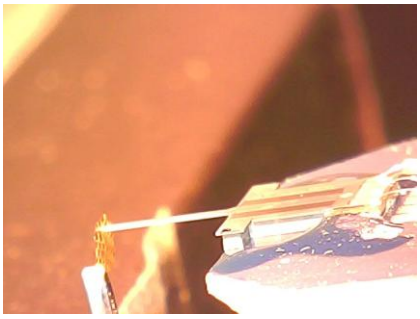 </td>
<td>Stiffness:
<table><tr><td>Number Steps</td><td>800</td></tr><tr><td>Distance</td><td>6.25E-05</td></tr><tr><td>Force1</td><td>94</td></tr><tr><td>Force 2</td><td>147</td></tr><tr><td>Stiffness</td><td>0.848</td></tr></table>
The force is in μN and the stiffness in μN/m</td>
</tr>
<tr>
<td>Same pattern without the support of the Si beam in the stick of the instrument</td>
<td>Camera 1:
 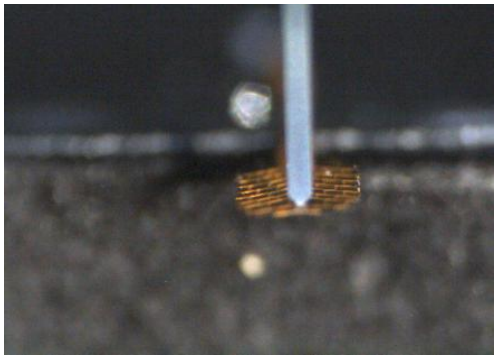 </td>
</tr>
<tr>
<td>Camera 2:
 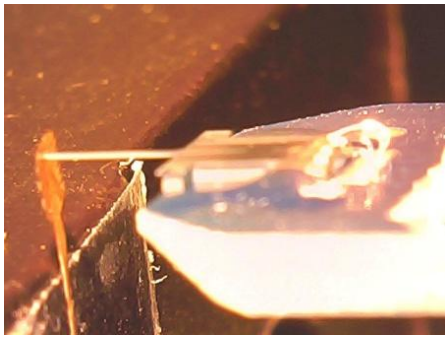 </td>
<td>Stiffness:
<table><tr><td>Number Steps</td><td>1400</td></tr><tr><td>Distance</td><td>0.000109</td></tr><tr><td>Force1</td><td>21</td></tr><tr><td>Force 2</td><td>32</td></tr><tr><td>Stiffness</td><td>0.100571</td></tr></table>
The force is in μN and the stiffness in μN/m</td>
</tr>
</table>

f)

<table>
<tr>
<td>Instrument:
 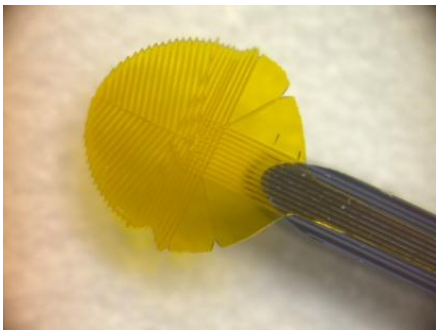 </td>
<td>Camera 1:
 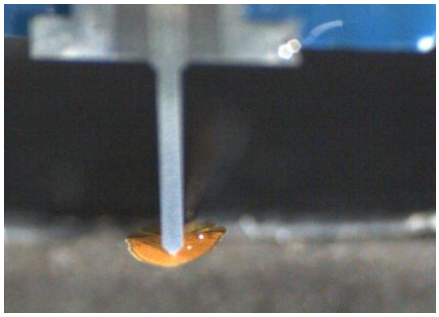 </td>
</tr>
<tr>
<td>Camera 2:
 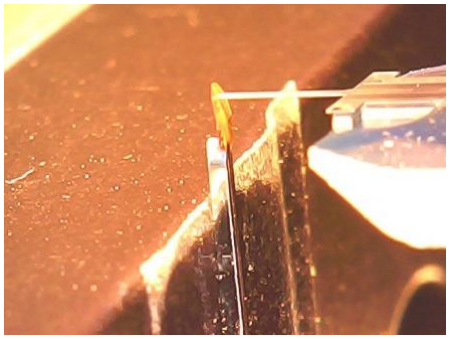 </td>
<td>Stiffness:
<table><tr><td>Number Steps</td><td>700</td></tr><tr><td>Distance</td><td>5.47E-05</td></tr><tr><td>Force1</td><td>80</td></tr><tr><td>Force 2</td><td>160</td></tr><tr><td>Stiffness</td><td>1.462857</td></tr></table>
The force is in μN and the stiffness in μN/m</td>
</tr>
<tr>
<td>Same pattern without the support of the Si beam in the stick of the instrument</td>
<td>Camera 1:
 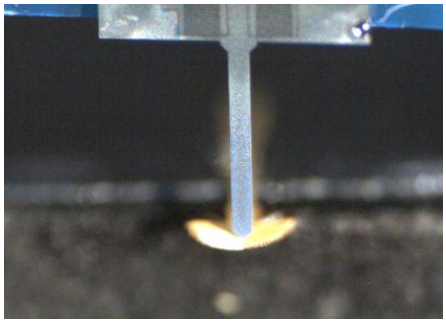 </td>
</tr>
<tr>
<td>Camera 2:
 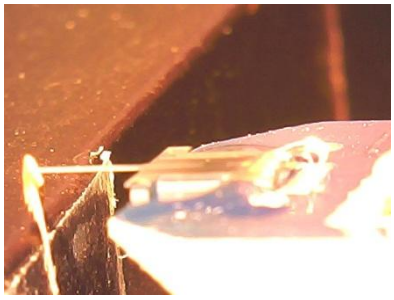 </td>
<td>Stiffness:
<table><tr><td>Number Steps</td><td>1400</td></tr><tr><td>Distance</td><td>0.000109</td></tr><tr><td>Force1</td><td>32</td></tr><tr><td>Force 2</td><td>51</td></tr><tr><td>Stiffness</td><td>0.173714</td></tr></table>
The force is in μN and the stiffness in μN/m</td>
</tr>
</table>

g)

Wing:

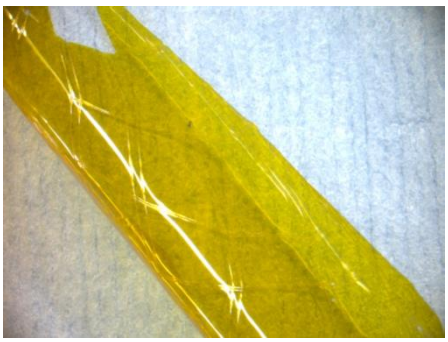

Camera 1:

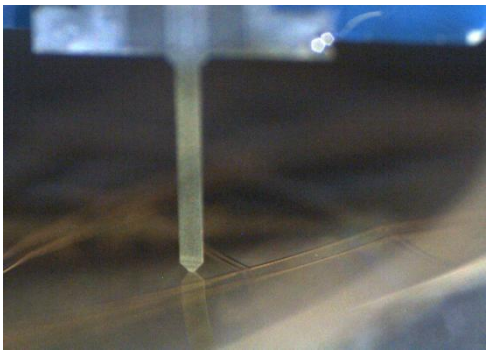

Camera 2:

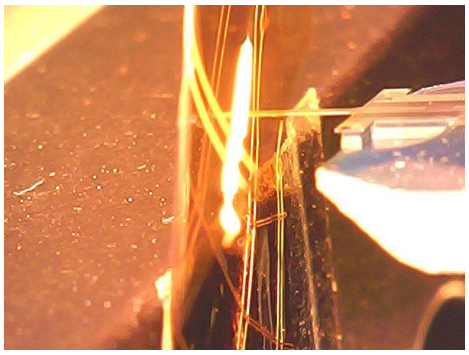

Stiffness:

Number Steps	400
Distance	3.13E-05
Force1	135
Force 2	268
Stiffness	4.256

The force is in μN and the stiffness in μN/m

Figure 6.3: Measurement Results

The stiffness depended greatly on the positioning of the instrument on the set up. The aim was to have a standard length off the instrument available to be pushed but this is one area which might have caused errors in the measurements. It is seen in Fig. 6.3 (e) and (f) that the same design has a different stiffness because of the presence of the silicon beam support in the stick. However, this is more likely due to the positioning of the instrument on the setup and not the presence of the beam itself. Also, the position at which the needle touches the instrument could have an effect on the reading. For the cases (d) and (e) in fig. 6.3, measurements were also taken by placing the needle lower. Table 6.2 shows the results obtained.

	Stiffness Before (μN/m)	Stiffness After (μN/m)
d)	0.32	0.45
e)	0.100	0.128

Table 6.2: Stiffness variation with change in needle position

As expected, the stiffness increases if the needle is placed lower (since it has to push down a much larger surface area).

6.2 Conclusions:

Designs with a very dense rib pattern in the centre (like in (c)) have a very high stiffness. However, they are not very flat and tend to bend towards the side with the beams. The most flat looking instruments (e) have a well spaced, not too closely packed rib pattern. The stiffness however, is lower in this case. Thus, for the next stages of design, a rib pattern similar to (e) but with a more dense centre pattern should be chosen. The presence of the Si beam in the stick helps in the handling of the instrument (cannot be said without a possibility of error if it causes a difference in the stiffness) and must be included in the design.

Chapter 7: Conclusions and Future Work

7.1 Conclusions

It has been demonstrated through numerical simulations that it is possible to achieve the required temperatures (for attachment and detachment of the tissue graft) by providing heat pulses using reasonable amounts of energy. The heat penetration into the surrounding tissue (and thus the damage to heat) is minimal due to the very small heat capacity of the chosen material (polyimide).

The idea of making the instrument from a polyimide foil using the F2R platform (with polyimide beam reinforcement) has been proven feasible. The procedure to make such foils by filling trenches with polyimide (without any voids) has been successfully developed.

The design and the spacing between the ribs affect the stiffness of the instruments (as seen in Chapter 6). The instruments with a very densely packed rib pattern were stiffer than those with a widely spaced pattern. Thus, the patterns for the beams must be carefully selected. From the observations on the instruments made and the measurements done, it can be concluded that the ideal rib pattern would not be too dense (closely packed) and would spread out through the plate (like the pattern shown in the instrument in Fig. 7.1). The centre part of the plate can have more closely packed ribs (like in Fig. 7.2) to get more stiffness.

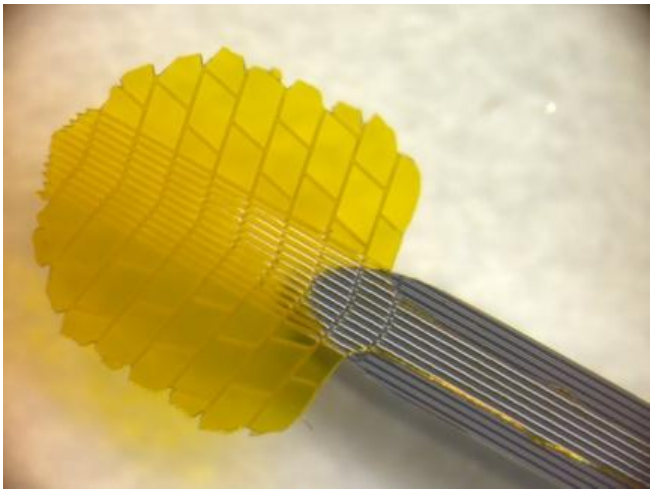

Figure 7.1: Well spread out pattern on the plate

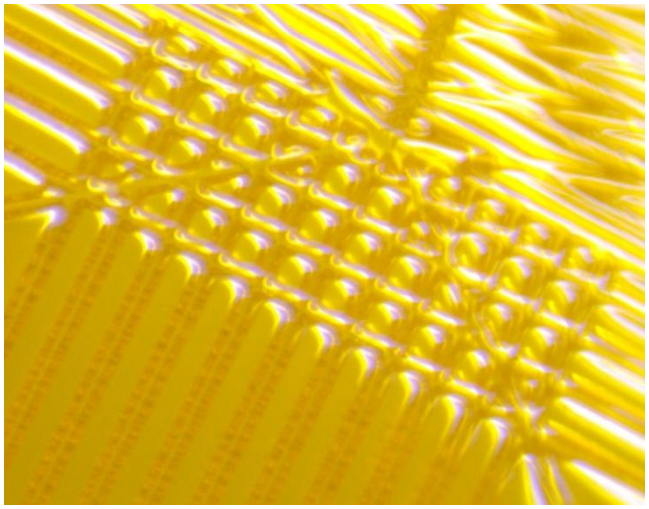

Figure 7.2: Closely packed rib pattern for the centre

The stick of the instrument must have the Si beam support for ease of handling. The fly wings (for the Atalanta project) must also be designed with a denser pattern (like in Fig. 7.3) in order to avoid curling up. The pattern itself can be similar to the one in the wing used for measurements (Fig. 7.4), by reducing the spacing between the ribs.

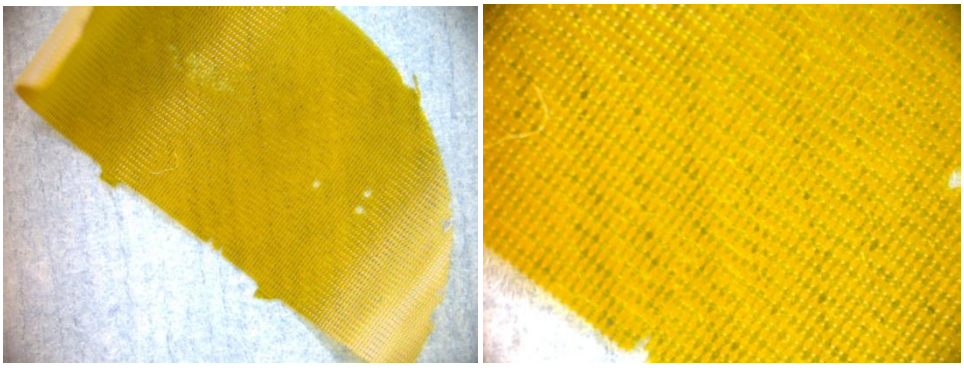

Figure 7.3: Denser pattern for the wings

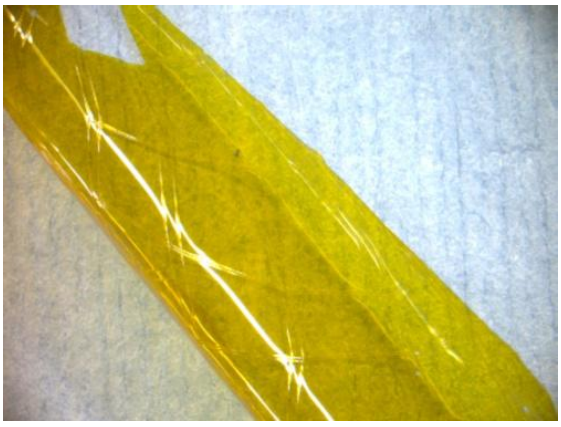

Figure 7.4: Wing used for measurements

7.2 Future Work

The fabrication recipe for the free standing Si beams requires further process development. It is possible to deposit a layer of PECVD oxide after the anisotropic etch step in order to protect the structures during the isotropic etch, however this would lead to an additional fabrication step. The etch times and the passivation deposition must be manipulated in order to achieve the results needed.

It could be possible to design the instrument using a layer of polyimide on one side of the heater and parylene on the other (Fig. 7.5). In the design presented in this thesis, the same material is used on either side of the heater. As a result, parylene (with a heat capacity similar to Si) could not be used since it conducted the heat quickly to the surrounding tissue. It would be beneficial to use parylene to transfer the heat to the target tissue while using polyimide to slow the heat transfer to the untargeted tissue.

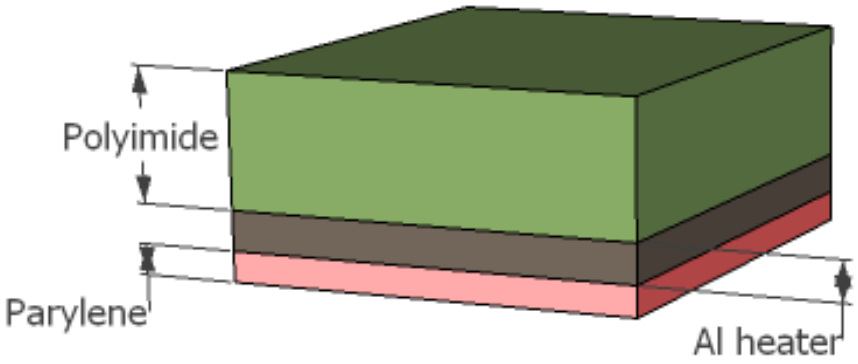

Figure 7.5: Inclusion of parylene as the bottom layer

It would be helpful to do some numerical simulations to be able to predict the mechanical behaviour of the device without starting with its fabrication. Apart from choosing the most suitable rib pattern, the simulations would help in determining the depth to which the trenches must be etched in order to get the most effective reinforcement from the beams.

The next step in this work would be to redesign the masks based on the observations in Section 7.1 (and the findings of simulations mentioned above). Subsequently, a fourth mask has to be implemented for the heaters which will be incorporated into the instrument. The final instrument will have 4 (or more) Al heaters sandwiched between two polyimide layers (Fig. 7.6).

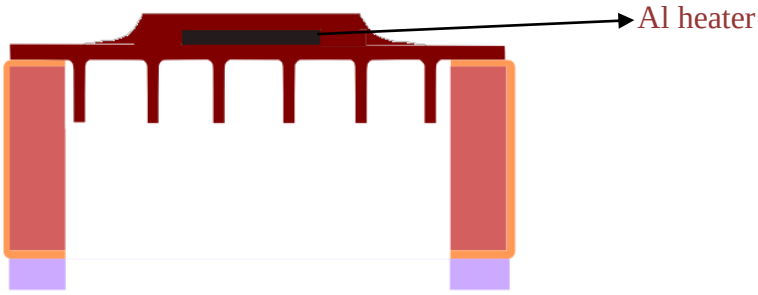

Figure 7.6: Instrument after the addition of heaters

The specific resistivity ρ for aluminium is 2.65 μΩcm. The resistance R is related with the length of the heater L_h and its area A by the formula: $R= \rho L_h /A$. Since the resistance R is related to power P and voltage V by the relation: $R=V^2/P$, the heaters can be designed for a particular power and voltage. Considering the dimensions of the pizza plate, it can be said that 4 heaters, each covering a square of 1x0.5 mm (placed at 4 different locations on the plate as explained in Chapter 2) would be appropriate. If a meander shape like in Fig. 7.7 is chosen, then the length of the heater L_h is given by:

L_h = L*(number of vertical paths) + (2n + x)*(number of horizontal paths)

The area A would be given by:

A= L*n*(number of vertical paths) + (2n + x)*n*(number of horizontal paths)

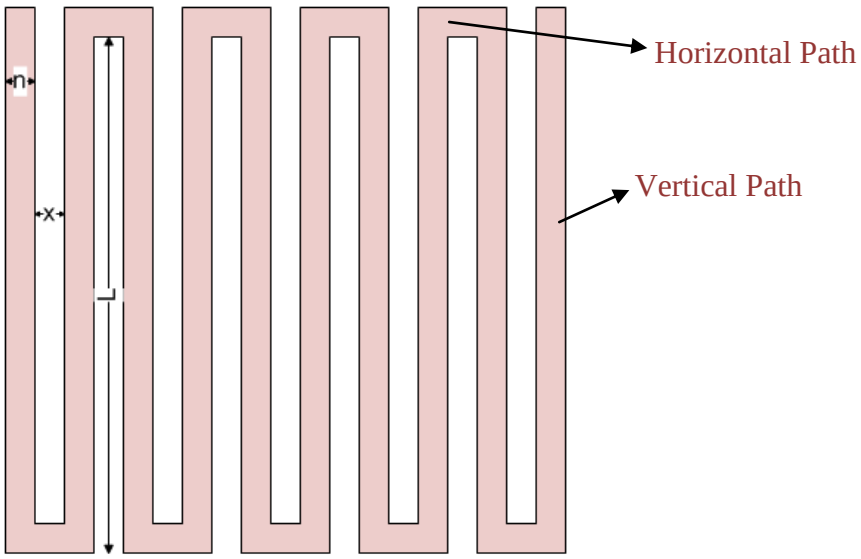

Figure 7.7: Heater Design

By careful selection of values for n and x, the optimum heater design for a given power and voltage can be obtained.

Apart from the incorporation of the polyimide rib reinforcement the fabrication of the instrument would closely follow the F2R processing sequence. The instruments made would again be checked for stiffness, flexibility and flatness. Hereafter, tests would be done to check if a piece of tissue could be attached/detached by applying heat through the heaters present on the instrument plate.

References

1. A.A. Tukker, “Heat Induced Attachment and Detachment of Delicate Tissues: Towards a New Micro Tissue Gripper”, Master Thesis, Delft University of Technology.

2. Kristel Maaijwee, Jan Van Meurs, et.al, “Retinal Pigment Epithelium and Choroid Translocation in Patients with Exudative Age Related Macular Degeneration: Long Term Results”, Graefe’s Arch Clin Exp Ophthalmol (2007) 245:1681–1689

3. Surgery video courtesy Dr. Jan Van Meurs.

4. Benjamin Mimoun, et.al, “Flex-to-Rigid (F2R): A Novel Ultra-Flexible Technology for Smart Invasive Medical Instruments”

5. Panda-Jonas S, et.al, “Retinal photoreceptor count, retinal surface area, and optic disc size in normal human eyes”, Ophthalmology 1994 Mar;101(3):519-23

6. Murashima Y.L, et.al, “Gamma-Aminobutyric acid system in developing and degenerating mouse retina”, J Neurochem 1990 Mar;54(3):893-8

7. Y. Haga and M. Esashi, Proceeding of the IEEE 92, 98 – 114 (2004).

8. K-T. Park and M. Esashi, Journal of Microelectromechanical Systems 8, 349 – 357 (1999).

9. X. Zhuang, D-S Lin, O. Oralkan and B. T. Khuri-Yakub, MEMS. IEEE 20th International Conference, 73 – 76 (2007).

10. Rogers, J.A., T. Someya, and Y. Huang, Science, 1603 – 1607 (2010).

11. SCS Parylene Properties, © Copyright 2010 Specialty Coating Systems, Inc.

12. Caspar T. Bolsman, et.al, “The Use of Resonant Structures for Miniaturizing FMAVs”, 3rd US-European Competition and Workshop on Micro Air Vehicle Systems (MAV07) & European Micro Air Vehicle Conference and Flight Competition (EMAV2007), 17-21 September 2007, Toulouse, France.

13. Caspar T. Bolsman et.al, “Design and Realization of Resonant Mechanisms for Wing Actuation in Flapping Wing Micro Air Vehicles”, Paper Ref: S1207_P0290 3rd International Conference on Integrity, Reliability and Failure, Porto/Portugal, 20-24 July 2009.

14. J.M. Bank, et.al, “Development of a novel 6 DOF interaction force sensor for micro-gripper applications”, Master thesis, Department of Precision and Microsystems Engineering, Faculty of 3mE, TU Delft, June 18, 2010.

Appendix A

A.1 Flowchart of the Short Loop Experiment:

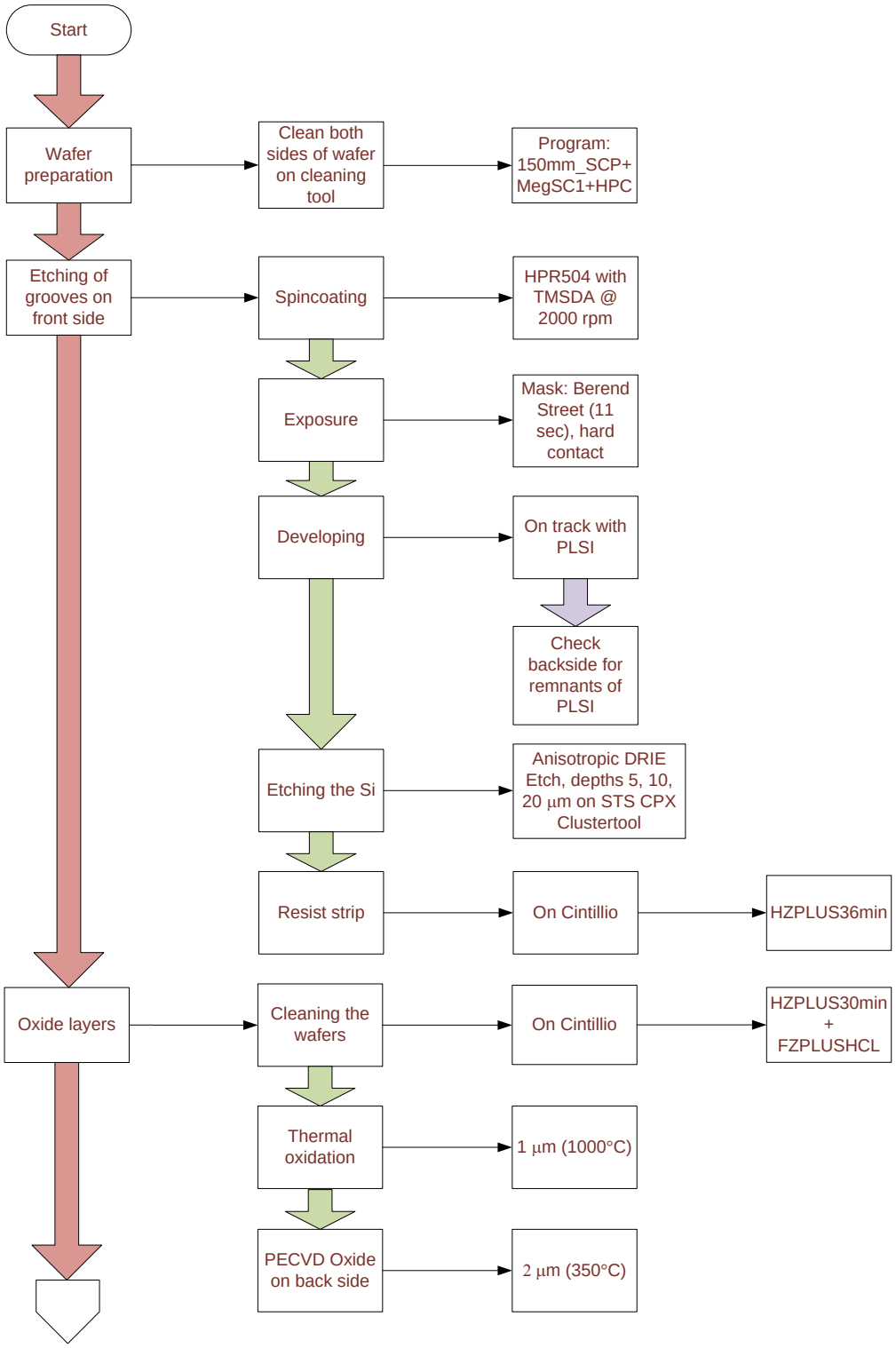

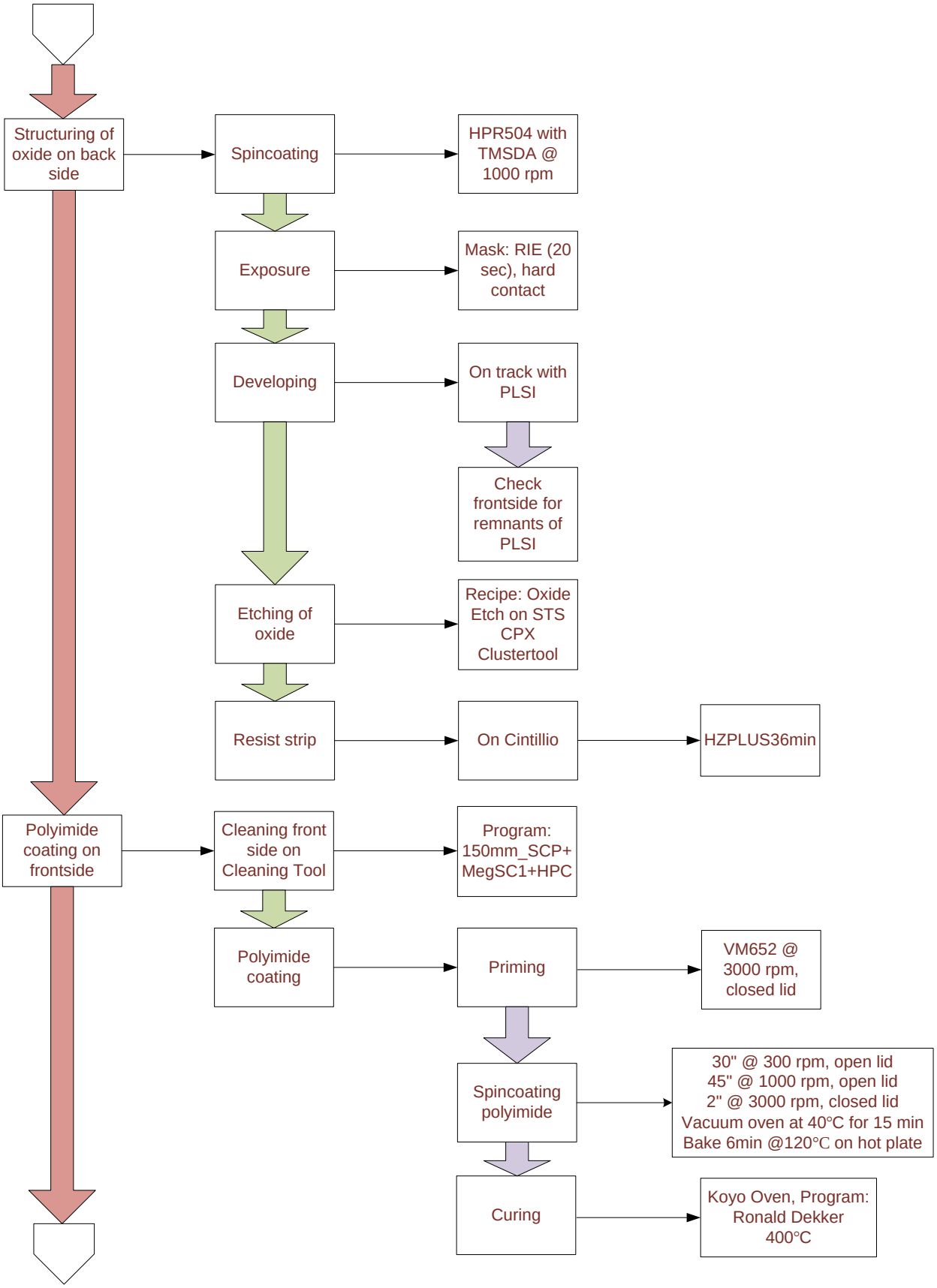
Structuring of oxide on back side
Spincoating
HPR504 with TMSDA @ 1000 rpm
Exposure
Mask: RIE (20 sec), hard contact
Developing
On track with PLSI
Check frontside for remnants of PLSI
Etching of oxide
Recipe: Oxide Etch on STS CPX Clustertool
Resist strip
On Cintillio
HZPLUS36min
Polyimide coating on frontside
Cleaning front side on Cleaning Tool
Program: 150mm_SCP+ MegSC1+HPC
Polyimide coating
Priming
VM652 @ 3000 rpm, closed lid
Spincoating polyimide
30" @ 300 rpm, open lid
45" @ 1000 rpm, open lid
2" @ 3000 rpm, closed lid
Vacuum oven at 40°C for 15 min
Bake 6min @120°C on hot plate
Curing
Koyo Oven, Program: Ronald Dekker 400°C

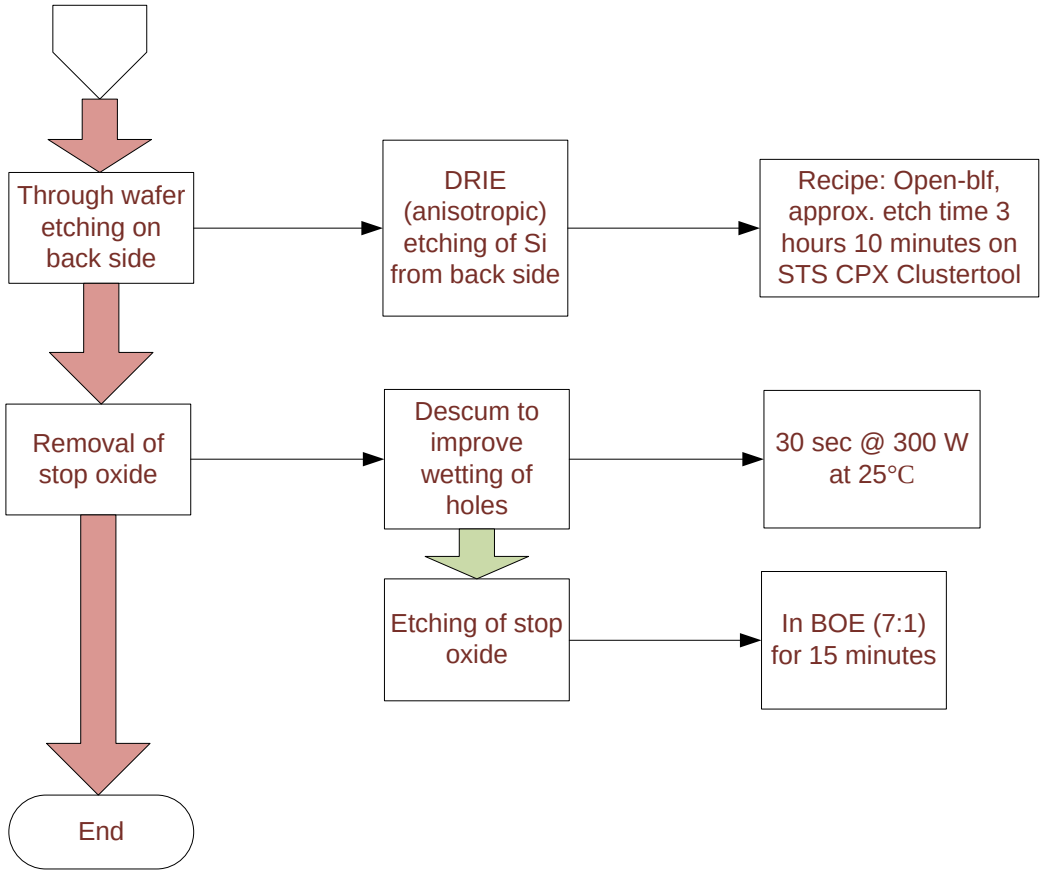
Through wafer etching on back side
DRIE (anisotropic) etching of Si from back side
Recipe: Open-blf, approx. etch time 3 hours 10 minutes on STS CPX Clustertool
Removal of stop oxide
Descum to improve wetting of holes
30 sec @ 300 W at 25°C
Etching of stop oxide
In BOE (7:1) for 15 minutes
End

Appendix B

B.1 Flowchart for the Final Fabrication Sequence

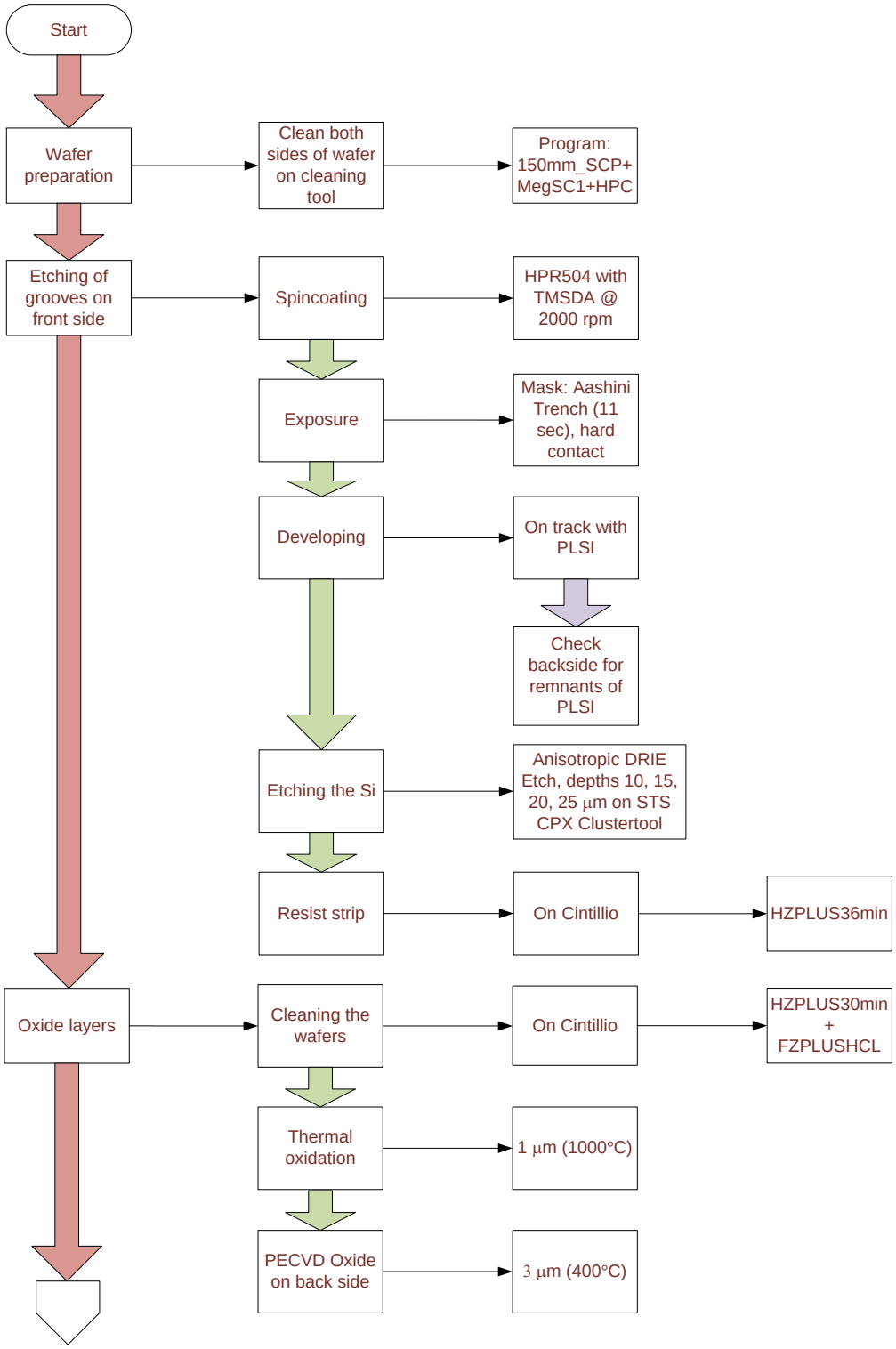

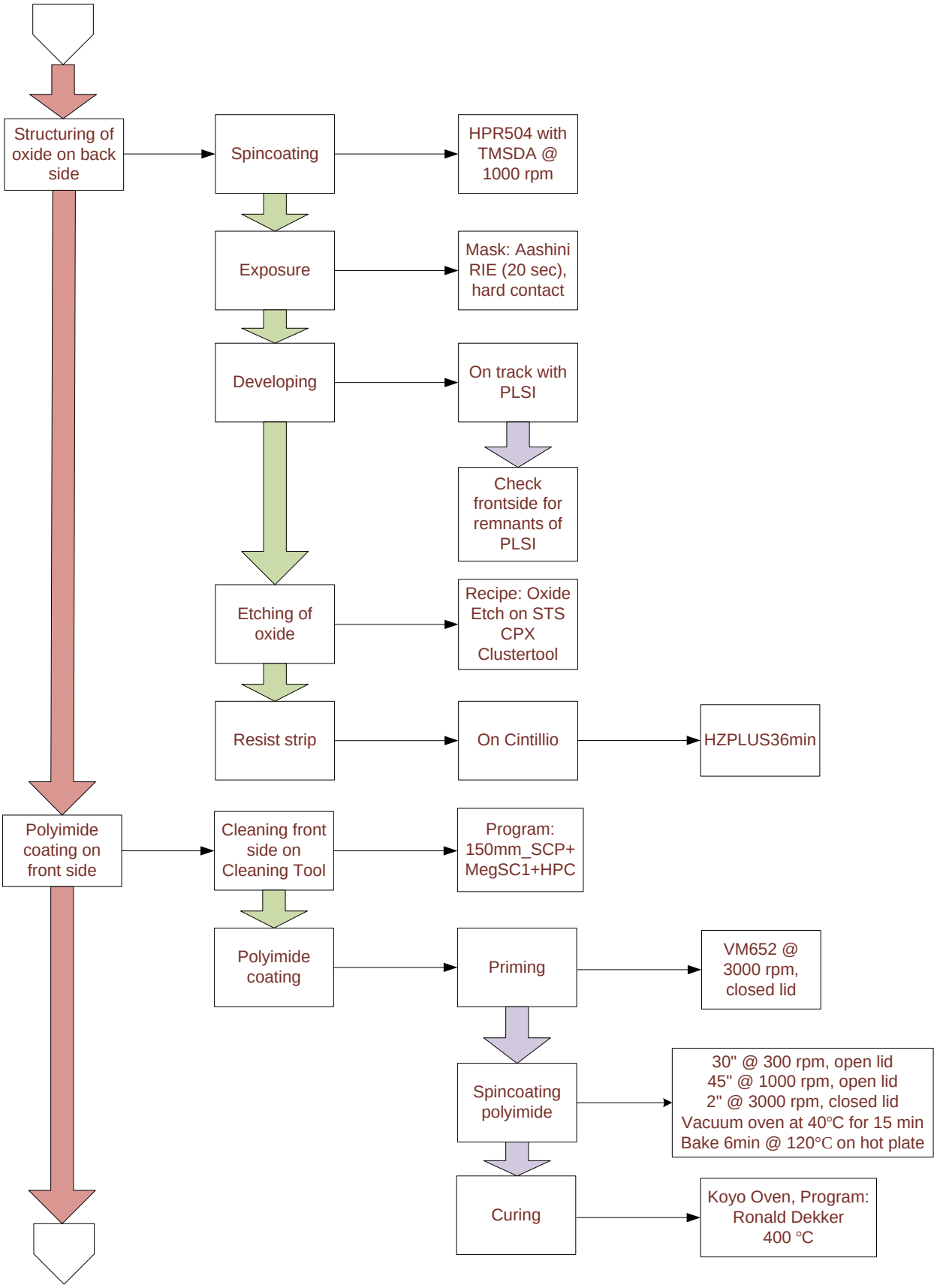
Structuring of oxide on back side
Spincoating
HPR504 with TMSDA @ 1000 rpm
Exposure
Mask: Aashini RIE (20 sec), hard contact
Developing
On track with PLSI
Check frontside for remnants of PLSI
Etching of oxide
Recipe: Oxide Etch on STS CPX Clustertool
Resist strip
On Cintillio
HZPLUS36min
Polyimide coating on front side
Cleaning front side on Cleaning Tool
Program: 150mm_SCP+ MegSC1+HPC
Polyimide coating
Priming
VM652 @ 3000 rpm, closed lid
Spincoating polyimide
30" @ 300 rpm, open lid
45" @ 1000 rpm, open lid
2" @ 3000 rpm, closed lid
Vacuum oven at 40°C for 15 min
Bake 6min @ 120°C on hot plate
Curing
Koyo Oven, Program: Ronald Dekker
400 °C

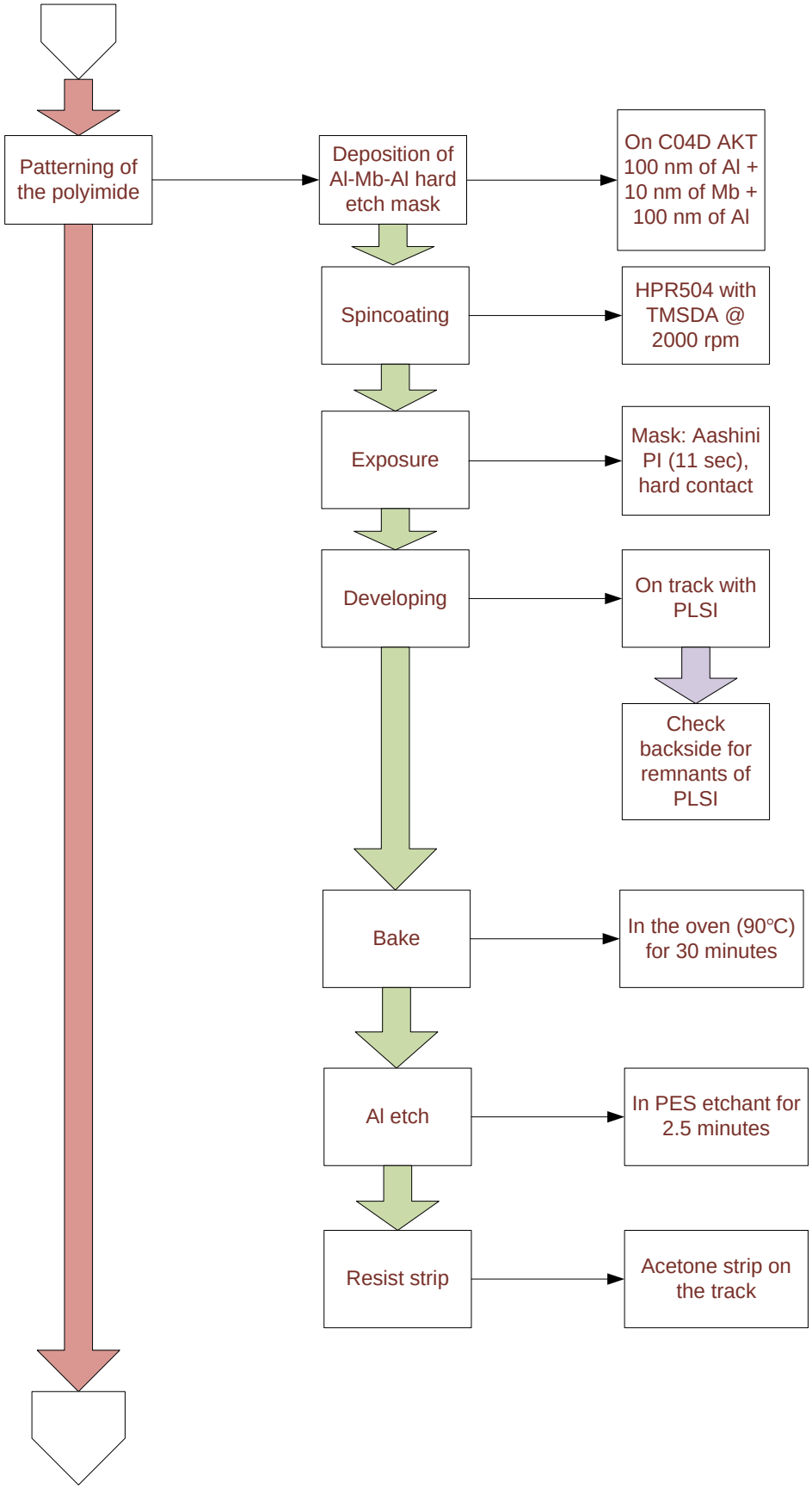
Patterning of the polyimide
Deposition of Al-Mb-Al hard etch mask
On C04D AKT 100 nm of Al + 10 nm of Mb + 100 nm of Al
Spincoating
HPR504 with TMSDA @ 2000 rpm
Exposure
Mask: Aashini PI (11 sec), hard contact
Developing
On track with PLSI
Check backside for remnants of PLSI
Bake
In the oven (90°C) for 30 minutes
Al etch
In PES etchant for 2.5 minutes
Resist strip
Acetone strip on the track

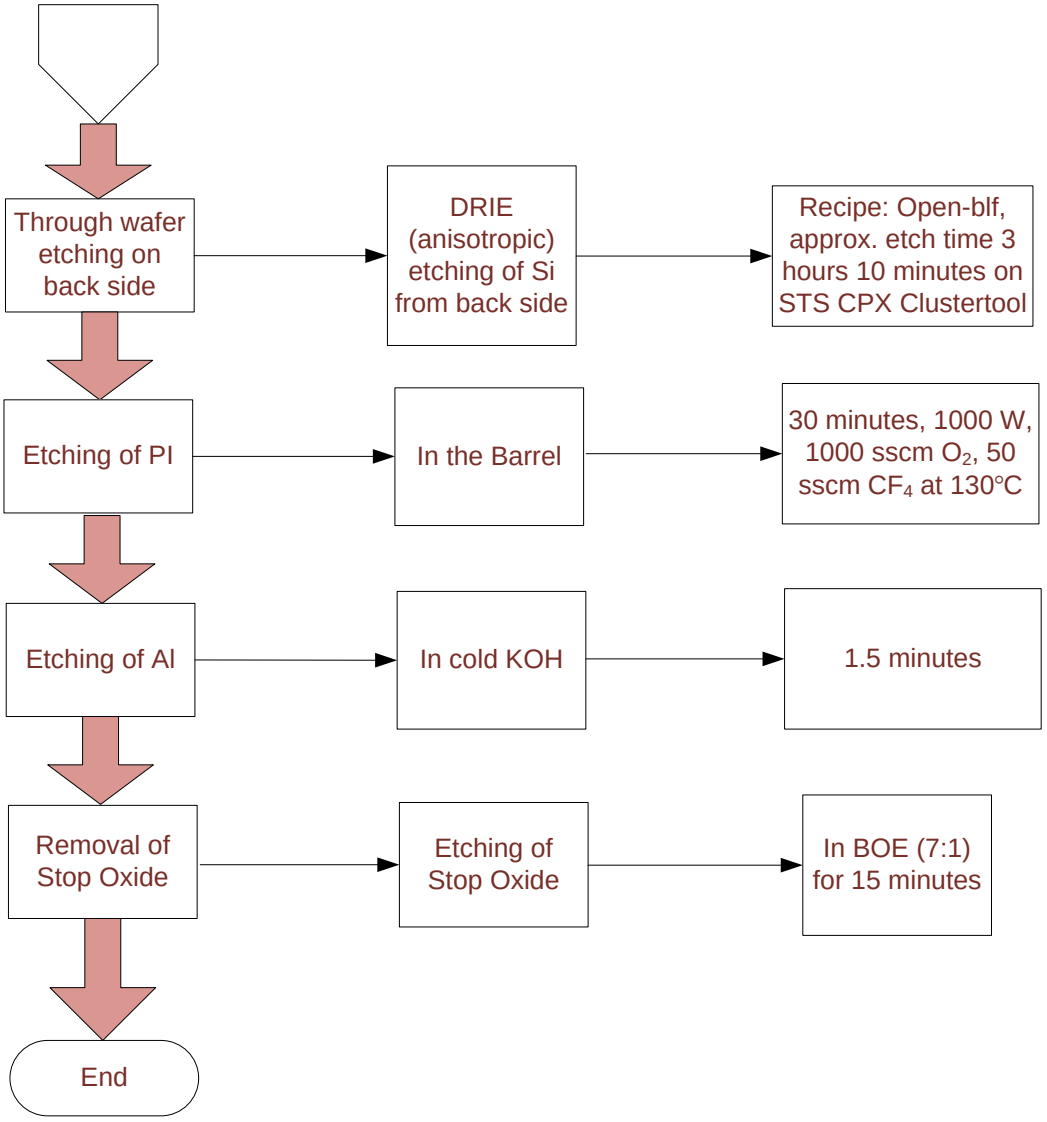
Through wafer etching on back side
DRIE (anisotropic) etching of Si from back side
Recipe: Open-blf, approx. etch time 3 hours 10 minutes on STS CPX Clustertool
Etching of PI
In the Barrel
30 minutes, 1000 W, 1000 sscm O_2, 50 sscm CF_4 at 130°C
Etching of Al
In cold KOH
1.5 minutes
Removal of Stop Oxide
Etching of Stop Oxide
In BOE (7:1) for 15 minutes
End

Acknowledgement

Dedication, hard work, and an unremitting devotion towards one's goals are the prerequisites for any success. This thesis could not have been a success without the contribution of Dr. Ronald Dekker, who encouraged and challenged me throughout the course of my work. He patiently guided me through the proceedings, never accepting less than my best efforts. He has been my guide, inspiration, advisor and a moral support. I am thankful to him for being the father figure that he is for me.

I am humbled by the generous help provided by numerous people at Philips Research, Eindhoven. I would specially like to mention Eric van den Heuvel, Harold Roosen, Pascal de Graaf, and Vincent Henneken for their inputs and help.

I would like to thank Dr. Paul Breedveld, Arjan Knulst and Dr. Jan van Meurs for providing me with an insight into the topic.

I am grateful to Saeed Khoshfetrat Pakazad, Ting Yan and Angel Savov who helped me and motivated me at every step of my work. All of my office mates deserve a mention for creating the best environment at work. You are all like a second family to me now.

I am thankful to my parents and my sister without whose unconditional support I would not have had the ability to rise above my failures.

I would also like to thank Göktürk, Seema, Arnica and Zeng for standing by me through thick and thin. I cannot imagine having to get through this without you all.